Hydrogenation of Unsaturated Polymers in Latex Form

by

Xingwang Lin

A thesis
presented to the University of Waterloo
in fulfillment of the
thesis requirement for the degree of
Doctor of Philosophy
in
Chemical Engineering

Waterloo, Ontario, Canada, 2005

AUTHOR'S DECLARATION FOR ELECTRONIC SUBMISSION OF A THESIS

I hereby declare that I am the sole author of this thesis. This is a true copy of the thesis, including any required final revisions, as accepted by my examiners.

I understand that my thesis may be made electronically available to the public.

Abstract

Diimide generated from the hydrazine/hydrogen peroxide/catalyst system can be used to hydrogenate unsaturated polymers in latex form. As an economical and environmentally benign alternative to the commercial processes based on hydrogen/transition metal catalysts, this method is of special interest to industry. This thesis provides a detailed description of the diimide hydrogenation process. Reaction kinetics, catalysts and gel formation mechanism have been investigated.

Four main reactions and a mass transfer process form three parallel processes in this system: diimide is generated at the interface of the latex particles; diimide diffuses into the organic phase to saturate carbon-carbon double bonds; diimide may be consumed at the interface by hydrogen peroxide, and may also be consumed by the disproportionation reaction in the organic phase. The two side reactions contribute to the low hydrogenation efficiency of hydrogen peroxide. Slowing down hydrogen peroxide addition and using stable interfacial catalysts may totally suppress the side reaction in the aqueous phase. The actual catalytic activity of metal ions in the latex depends on the hydrogen peroxide concentration and the addition procedure of reactants. Cupric ion provides better selectivity for hydrogenation than ferric ion and silver ion do. Boric acid as a promoter provides improved selectivity for hydrogenation and faster diimide generation rate. The side reaction in the rubber phase results in low efficiency and gel formation. The rate constants of the four reactions in this system are estimated.

It is shown that the hydrogenation of nitrile rubber latex with an average particle diameter of 72 nm is mainly a reaction-controlled process. Diimide diffusion presents limitation upon hydrogenation at high hydrogenation degree range. Antioxidants can not effectively inhibit gel formation during hydrogenation. Hydrogenation of a core-shell latex with NBR as the shell layer should be able to achieve a higher efficiency, a higher degree of hydrogenation and a lower level of crosslinking.

Acknowledgements

At the time I am finishing my Ph. D. thesis, I would like to gratefully acknowledge the following people:

Dr. G. L. Rempel and Dr. Q. Pan, for their insight, understanding and assistance as my supervisors.

Dr. N. McManus, for his helpful discussion and his help in improving the English writing of Chapters 5 and 9 of this thesis.

My friends and lab mates, L. Zhang, Z. Wei, G. He, C. Mouli, D. Fang, C. Gan, J. Wu, and J. Liu, for the time we shared together in our laboratories.

My parents, my wife and my sons, for their encouragement and understanding during these years.

I also gratefully acknowledge the financial support of the Natural Sciences and Engineering Research Council and Bayer Inc.

.

Table of Contents

Abstract iii
Acknowledgements iv
Table of Contents v
List of Figures ix
List of Tables xiv
Chapter 1 Introduction 1
1.1 : Objectives 2
1.2 : Research outline 3
Chapter 2 Literature review 4
2.1 : Diimide hydrogenation fundamentals 4
2.2 : Homogeneous hydrogenation by diimide 4
2.3 : Hydrogenation of polymer latex by diimide 6
2.4 : Crosslinking in diimide hydrogenation process 10
2.5 : Summary 10
Chapter 3 Research approaches 11
Chapter 4 Hydrogenation of NBR latex 13
4.1 : Experimental 13
4.2 : Results and discussion 13
4.2.1 : Efficiency of hydrogenation and selectivity of catalysts 14
4.2.2 : Selectivity over carbon-carbon double bonds 19
4.2.3 : Stabilization of catalysts in latex 20
4.2.4 : Effect of radical scavengers and radical transfer agents 21
4.2.5 : Effect of hydrazine concentration 22
4.2.6 : Effect of hydrogen peroxide addition rate 23
4.2.7 : Hydrogenation performance with fresh latex addition during the reaction 24
4.2.8 : Effect of solvent addition 25
4.2.9 : Effect of aging time upon the hydrogenation behavior of NBR latex 26
4.2.10 : Hydrogenation performance of latex with low residual *C*=*C* 26
4.2.11 : Crosslinking of polymer during hydrogenation 27
4.3 : Summary 28
Chapter 5 Reaction kinetics of hydrazine and hydrogen peroxide 29
5.1 : Introduction 29
5.2 : Experimental 30

5.3 : Results and discussion 31
5.3.1 : The significance of the side reactions 31
5.3.2 : Catalytic behavior 33
5.3.3 : Effect of $[N_2H_4]$ 36
5.3.4 : Effect of boric acid 37
5.3.5 : Activation energy 38
5.4 : Summary 40
Chapter 6 Reaction of hydrazine and hydrogen peroxide in NBR latex 41
6.1 : Experimental 41
6.2 : Reaction course and its interpretation 41
6.3 : Results and discussion: diimide production rate 44
6.3.1 : Reproducibility of the experiments 44
6.3.2 : Catalysis for the reaction 46
6.3.3 : Effect of $[H_3BO_3]$ on diimide production rate 48
6.3.4 : Effect of $[N_2H_4]$ on diimide production rate 49
6.3.5 : Effect of $[H_2O_2]_0$ on diimide production rate 50
6.3.6 : Effect of solid content on diimide production rate 52
6.3.7 : Effect of temperature on diimide production rate 52
6.3.8 : Summary 54
6.4 : Results and understanding: hydrogenation efficiency 55
6.4.1 : HE for different catalysts 55
6.4.2 : HE at different $[H_3BO_3]$ 56
6.4.3 : HE at different $[N_2H_4]$ 57
6.4.4 : HE at different $[H_2O_2]_0$ 57
6.4.5 : HE at different temperatures 58
6.4.6 : HE at different solid contents 58
6.4.7 : HE at different HD levels 58
6.4.8 : Summary 60
6.5 : Comparison of the redox reaction in aqueous solution and in NBR latex 60
Chapter 7 Hydrogenation of *C*=*C*s by Diimide 61
7.1 : Results from the literature 61
7.2 : Experimental 61
7.3 : Analysis methods 62
7.3.1 : The rationale for the kinetic analysis 62

7.3.2 : Measurement of *C*=*C* conversion by ^{1}H-NMR spectrum 63
7.3.3 : Measurement of *C*=*C* conversion by FT-IR spectrum 64
7.4 : Results and discussion 64
7.4.1 : Rate comparison of diimide hydrogenation in a homogeneous system 64
7.4.2 : Rate comparison of diimide hydrogenation in the latex system 66
7.5 : Summary 69
7.6 : Analysis of the effect of diimide diffusion upon the diimide hydrogenation process 69
Chapter 8 Crosslinking mechanism of diimide hydrogenation reaction 71
8.1 : Experimental 71
8.2 : Results and discussion 72
8.2.1 : Effect of the individual chemicals on gel formation 72
8.2.2 : Analysis of the possibility of crosslinking from aqueous radicals 73
8.2.3 : Analysis of the possibility of crosslinking from oxygen 74
8.2.4 : Analysis of the possibility of crosslinking from the side reactions of diimide hydrogenation 75
8.3 : Summary 76
Chapter 9 Simulation of diimide hydrogenation process 77
9.1 : Process simulation 77
9.2 : Simulation of reaction-controlled processes 80
9.2.1 : Simulation of the pressure-buildup experiment 81
9.2.2 : Simulation of the semi-batch hydrogenation process 84
9.3 : Simulation of diffusion-interfered hydrogenation process 87
9.3.1 : Parameter presetting and simulation 87
9.3.2 : Limitation of this simulation 98
9.4 Summary 99
Chapter 10 Gel formation reduction 100
10.1 : Effects of antioxidants upon gel formation 101
10.2 : Two-step hydrogenation 102
10.2.1 : Summary of research on thiol addition in the literature 103
10.2.2 : Thiol addition experiment 104
10.2.3 : Thiol addition of diimide-partially-saturated NBR latex 106
10.2.4 : Analysis 107
10.3 : Recommendations 108
Appendix A Nomenclature 109

Appendix B Matlab program-simulation of a semibatch hydrogenation process with the assumption of reaction control 112
Appendix C Matlab program-Simulation of the diimide hydrogenation of NBR latex 115
Appendix D Comparison of manufacturing costs of two hydrogenation processes 118
D.1 : Homogeneous solution hydrogenation process 118
D.1.1 : Process description 118
D.1.2 : Estimating manufacturing costs 119
D.2 : Diimide hydrogenation process 121
D.2.1 : Process description 121
D.2.2 : Estimating manufacturing costs 122
D.3 : Comparison 123
D.4 : Process flow diagrams of the two processes 125
Bibliography 129

List of Figures

Figure 1-1: HNBR production process [16] 2
Figure 2-1: Proposed mechanism for diimide hydrogenation by Parker [31] 7
Figure 2-2: Two models for the distribution of double bonds in hydrogenated SBR latex particle: (a) layer model; (b): uniform model [36] 8
Figure 2-3: Effect of mixed inhibitors on the hydrogenation degree and gel content; ($N_2H_4/C=C$) = 1.4 molar ratios, H_2O_2/N_2H_4 = 1.25; 52 ˚C [37] 9
Figure 4-1: Comparison of the actual hydrogenation curve to the ideal hydrogenation curve (boric acid/NBR - 10.0 wt%; 40ºC, ($N_2H_4/C=C$) =2.0; H_2O_2/N_2H_4 =0.75; addition over 6.3hr) 14
Figure 4-2: Comparison of the actual hydrogenation curve to the ideal hydrogenation curve (no added catalyst; 40ºC, ($N_2H_4/C=C$) =2.0; H_2O_2/N_2H_4 =0.75; addition over 6.0 hr) 15
Figure 4-3: Effect of ferrous ion as a catalyst on hydrogenation (ferrous sulphate: 7.03×10^{-7} mole/g of NBR; 45ºC, ($N_2H_4/C=C$) =1.5; H_2O_2/N_2H_4 =1.0; H_2O_2 addition over 8.5hrs, total NBR: 15.0g) 16
Figure 4-4: Comparison of the actual hydrogenation curve to the ideal hydrogenation curve (silver nitrate: 9.20×10^{-6} mole/g of NBR; 40ºC, ($N_2H_4/C=C$) =2.0; H_2O_2/N_2H_4 =0.75; addition over 6.5 hrs) 16
Figure 4-5: Comparison of the actual hydrogenation curve to the ideal hydrogenation curve (cupric sulphate: 6.98×10^{-7} mole/g of NBR; 40ºC, ($N_2H_4/C=C$) =2.0; H_2O_2/N_2H_4 =0.75; addition over 6.5 hrs) 17
Figure 4-6: Effect of addition rate of hydrogen peroxide upon hydrogenation efficiency (catalyst: silver nitrate: 9.20×10^{-6} mole/g of NBR; 40ºC, ($N_2H_4/C=C$) =2.0; H_2O_2/N_2H_4 =0.75) 18
Figure 4-7: Effect of addition rate of hydrogen peroxide upon hydrogenation efficiency (catalyst: boric acid: 10.0 wt% of NBR; 40ºC, ($N_2H_4/C=C$) =1.5; H_2O_2/N_2H_4 =1.0) 19
Figure 4-8: FT-IR spectra of partially hydrogenated NBR at different HD (Catalyst: boric acid - 10.0 wt% of NBR; 40ºC, ($N_2H_4/C=C$) =1.5; H_2O_2/N_2H_4 =1.0; addition over 10.5 hrs) 20
Figure 4-9: Hydrogenation comparison with/without ammonium hydroxide (catalyst: cupric sulphate: 7.51×10^{-7} mole/g of NBR; 40ºC, ($N_2H_4/C=C$) = 1.5; H_2O_2/N_2H_4 =1.0; addition over 8.5hrs, total NBR: 15.0g) 21
Figure 4-10: Effect of benzoquinone on hydrogenation (catalyst: boric acid - 10.0 wt% of NBR; 45ºC, $N_2H_4/C=C$ =1.5; H_2O_2/N_2H_4 =1.0; H_2O_2 addition over 8.5hrs, total NBR: 15.0g) 22
Figure 4-11: Effect of initial concentration of hydrazine upon hydrogenation (catalyst: boric acid - 10.0 wt% of NBR; 45ºC; H_2O_2/N_2H_4 =1.0; H_2O_2 addition over 7.3hrs) 23

Figure 4-12: Hydrogenation comparison with/without hydrazine addition during the reaction (catalyst: boric acid - 10.0 wt% of NBR; 45ºC, $N_2H_4/C=C$ =1.5; H_2O_2/N_2H_4 =1.0; H_2O_2 addition over 8.5hrs; hydrazine hydrate added in case B: 0.5 moles per mole of $C=C$ initial, added at 4.0 hours) 23
Figure 4-13: comparison of hydrogenation curves at different addition rates of hydrogen peroxide (catalyst: boric acid - 10.0 wt% of NBR; 40ºC, ($N_2H_4/C=C$) =2.0; H_2O_2/N_2H_4= 0.8 for Case A, 0.75 for Case B) 24
Figure 4-14: Hydrogenation curve with fresh latex addition during the reaction (Part one: 50.0 mL of NBR latex, 1.50g of boric acid, 20.0g of $N_2H_4 \cdot H_2O$, 0.07mol of H_2O_2 added over 4.0 hours; Part two: 50.0 mL of fresh NBR latex added, 0.14 mol of H_2O_2 added over 4.0 hours, 40ºC).....25
Figure 4-15: Hydrogenation comparison with/without solvent addition (catalyst: boric acid - 10.0 wt% of NBR; 45ºC, ($N_2H_4/C=C$) =1.5; N_2H_4/H_2O_2 =1.0; H_2O_2 addition over 8.5hrs; 15.0 g of NBR in the system in total).....25
Figure 4-16: Hydrogenation comparison with/without cupric ion at the catalyst (catalyst: A: boric acid - 10.0 wt% of NBR + cupric sulphate: 6.98×10^{-7} mole/g of dry polymer; B: boric acid - 10.0 wt% of NBR; 45ºC, ($N_2H_4/C=C$) =1.5; N_2H_4/H_2O_2 =1.0; H_2O_2 addition over 7.3hrs) 26
Figure 4-17: Hydrogenation of latex partially saturated by diimide (catalyst: boric acid - 10.0 wt% of NBR; 45ºC, ($N_2H_4/C=C$) = 7.0 (new added); ($H_2O_2/C=C$) = 1.5; H_2O_2 addition over 8.0hrs. $[C=C]_0$ =1.67M) 27
Figure 5-1: Schematic diagram of the pressure build-up instrumental setup.....31
Figure 5-2: Pressure build-up curve for the reaction between hydrazine and hydrogen peroxide without catalyst ($[N_2H_4]$ =1.49 M, $[H_2O_2]_0$= 0.027 M, T=25.0 °C).....33
Figure 5-3: Pressure build-up curve for the reaction between hydrazine and hydrogen peroxide catalyzed by Cu^{2+}-EDTA and its first-order fitting ($[N_2H_4]$=1.41±0.06 M, $[H_2O_2]_0$= 0.027M, T=25.0 ºC, $[Cu^{2+}\text{-EDTA}]$ =1.72×10^{-5} M).....35
Figure 5-4: Effect of $[N_2H_4]$ on the reaction between hydrazine and hydrogen peroxide ($[H_3BO_3]$ = 0.06 M, $[H_2O_2]_0$=0.03 M, T=25 °C).....37
Figure 5-5: $k_m/[N_2H_4]$ versus $[N_2H_4]$ for the reaction between hydrazine and hydrogen peroxide as catalyzed by boric acid ($[H_3BO_3]$=0.06 M, $[H_2O_2]_0$=0.03 M, T=25 ºC) 37
Figure 5-6: Effect of boric acid on the reaction between hydrazine and hydrogen peroxide ($[H_2O_2]_0$=0.03 M, T=25 ºC) 38

Figure 5-7: Activation energy of the reaction between hydrazine and hydrogen peroxide catalyzed by Cu^{2+}-EDTA (5.0g of gelatin in 200mLof reactants; [Cu^{2+}-EDTA] = 6.89×10^{-6} M, [N_2H_4] = 1.27-1.43 M, $[H_2O_2]_0$= 0.027-0.03M) 39
Figure 5-8: Activation energy of the reaction of hydrazine and hydrogen peroxide catalyzed by boric acid ([H_3BO_3] = 0.059 M, [N_2H_4] = 1.9 M, $[H_2O_2]_0$ = 0.027-0.03 M) 39
Figure 6-1: Nitrogen generation curve and its first-order interpretation of NBR hydrogenation without catalyst ([N_2H_4] = 1.10 M, $[H_2O_2]_0$ = 0.0832 M, T = 25.0 ºC, NBR content: 3.8 wt%).....42
Figure 6-2: Nitrogen generation curve and its first-order interpretation catalyzed by Cu-EDTA ([N_2H_4] = 1.66 M, $[H_2O_2]_0$= 0.0297 M, T= 25 ºC, NBR content: 3.8 wt%) 43
Figure 6-3: Nitrogen generation curve and its first-order interpretation catalyzed by aqueous Cu^{2+} ([N_2H_4] = 1.66 M, $[H_2O_2]_0$= 0.0297 M, T= 25.0 ºC, NBR content: 3.8wt%).....43
Figure 6-4: Nitrogen generation curve and its first-order fitting of the hydrogenation reaction catalyzed by boric acid ([N_2H_4] = 2.35~2.19 M, [H_3BO_3] = 0.066 M, NBR content: 3.8 wt%, T = 25.0 ºC) 44
Figure 6-5: The promotion effect of boric acid at different concentrations (25ºC, solid content= 13.2wt%, $[H_2O_2]_0 \approx$ 0.05 M for A; $[H_2O_2]_0 \approx$ 0.006 M for B) 49
Figure 6-6: The effect of [N_2H_4] on the rate of the reaction between hydrazine and hydrogen peroxide (25.0ºC, solid content= 13.2wt%, $[H_2O_2]_0 \approx$ 0.05 M) 50
Figure 6-7: Comparison of nitrogen generation rate at different solid content levels (25.0 ºC).....52
Figure 6-8: Effect of temperature on the reaction rate of the hydrogenation reaction ([N_2H_4]= 1.8~2.2M, [H_2O_2] =0.03M; [H_3BO_3] = 0.059M, NBR content: 3.8 wt%) 54
Figure 6-9: HE at different [H_3BO_3] levels ($[H_2O_2]_0 \approx$ 0.025 M, [N_2H_4] = 2.2±0.1 M, T=25.0ºC)....56
Figure 6-10: HE at different $[H_2O_2]_0$ ([N_2H_4] = 2.2 M, [H_3BO_3] = 0.060 M, T = 25.0ºC) 57
Figure 6-11: Decrease of HE at increasing HD ($[H_2O_2]_0 \approx$ 0.025M, [N_2H_4]=2.23±0.12M, [H_3BO_3]=0.24M, T=25.0ºC) 59
Figure 6-12: HE versus HD at high HD range ($[H_2O_2]_0 \approx$ 0.18M, [N_2H_4]=1.7±0.5M, [H_3BO_3]=0.20M, T=25.0ºC) 60
Figure 7-1: Hydrogenation course of vinyl group in NBR by diimide and its first-order fitting (132ºC, TSH/[*C*=*C*] = 2.0, chlorobenzene as the solvent).....65
Figure 7-2: Hydrogenation course of *trans*- *C*=*C* group in NBR by diimide and its first-order fitting (132ºC, TSH/[*C*=*C*] = 2.0, chlorobenzene as the solvent) 66

Figure 7-3: Hydrogenation course of vinyl group in NBR latex by diimide and its first-order fitting (40ºC, $[N_2H_4]/[C=C]$ = 3.0, $[H_3BO_3]/[C=C]$ = 0.076, $[N_2H_4]/[H_2O_2]$ = 1.0, H_2O_2 (30.47% aqueous solution) added over 6.5 hours) 68
Figure 7-4: Hydrogenation course of *trans*- *C=C* group in NBR latex by diimide and its first-order fitting (40ºC, $[N_2H_4]/[C=C]$ = 3.0, $[H_3BO_3]/[C=C]$ = 0.076, $[N_2H_4]/[H_2O_2]$ = 1.0, H_2O_2 (30.47% aqueous solution) added over 6.5 hours) 68
Figure 9-1: Diagram of a latex particle and reaction locations for diimide hydrogenation 78
Figure 9-2: Comparison of nitrogen generation curve with the first-order approximation 82
Figure 9-3: HE at different $[H_2O_2]_0$ ($[N_2H_4]$ ~ 2.2M, T=25.0ºC, $[H_3BO_3]$ ~ 0.063M, solid content=3.8wt%)....84
Figure 9-4: Simulation of HD curve at different k_4 values (k_2=0.1 $(sM)^{-1}$, k_3=1.47 $(sM)^{-1}$, V_p=0.015L, V_s=0.0015L, k_4 in $(sM)^{-1}$) 86
Figure 9-5: Simulation of HD curve at different k_3 values (k_2=0.1 $(sM)^{-1}$, k_4=1.8 $(sM)^{-1}$, V_p=0.015L, V_s=0.0015L, k_3 in $(sM)^{-1}$) 86
Figure 9-6: $[H_2O_2]$ dynamics for the semi-batch hydrogenation process described in section 9.2.2....88
Figure 9-7: HD, HE, HE_{aqu}, and HE_{org} curve for the case with $k_2=2\times10^3$ $(sM)^{-1}$; $k_3=2\times10^5$ $(sM)^{-1}$; and $k_4=3.2\times10^{10}$ $(sM)^{-1}$ 89
Figure 9-8: Development of crosslinking, $[N_2H_2]$ at the surface, $[N_2H_2]$ distribution in the particle, and the residual *C=C* distribution curves for the case with $k_2=2\times10^3$ $(sM)^{-1}$; $k_3=2\times10^5$ $(sM)^{-1}$; and $k_4=3.2\times10^{10}$ $(sM)^{-1}$....90
Figure 9-9: HD, HE, HE_{aqu}, and HE_{org} curve for the case with k_2=20 $(sM)^{-1}$, k_3 = 4000 $(sM)^{-1}$, and $k_4=3.2\times10^6$ $(sM)^{-1}$ 91
Figure 9-10: The development of crosslinking, $[N_2H_2]$ at the surface, $[N_2H_2]$ distribution in the particle, and the residual *C=C* distribution curves for the case with k_2=20 $(sM)^{-1}$, k_3=4000 $(sM)^{-1}$, and $k_4=3.2\times10^6$ $(sM)^{-1}$ 92
Figure 9-11: HD, HE, HE_{aqu}, and HE_{org} curves for the case with k_2=800 $(sM)^{-1}$, $k_3=1.6\times10^5$ $(sM)^{-1}$, $k_4=5.12\times10^9$ $(sM)^{-1}$, and R=115 nm 93
Figure 9-12: HD, HE, HE_{aqu}, and HE_{org} curves for the case with k_2=800 $(sM)^{-1}$, $k_3=1.6\times10^5$ $(sM)^{-1}$, $k_4=5.12\times10^9$ $(sM)^{-1}$, and R=36 nm 94
Figure 9-13: HD, HE, HE_{aqu}, and HE_{org} curves for the case with k_2=800 $(sM)^{-1}$, $k_3=1.6\times10^5$ $(sM)^{-1}$, $k_4=5.12\times10^9$ $(sM)^{-1}$, and R=25 nm 95
Figure 9-14: Development of crosslinking, $[N_2H_2]$ at the surface, $[N_2H_2]$ distribution in the particle, and the residual *C=C* distribution curves for the case with k_2 = 800 $(sM)^{-1}$, $k_3 = 1.6\times10^5$ $(sM)^{-1}$, $k_4 = 5.12\times10^9$ $(sM)^{-1}$, and R = 115 nm 96

Figure 9-15: Development of crosslinking, [N_2H_2] at the surface, [N_2H_2] distribution in the particle, and the residual *C=C* distribution curves for the case with $k_2 = 800\ (sM)^{-1}$, $k_3 = 1.6\times10^5\ (sM)^{-1}$, $k_4 = 5.12\times10^9\ (sM)^{-1}$, and R=36 nm 97
Figure 9-16: Development of crosslinking, [N_2H_2] at the surface, [N_2H_2] distribution in the particle, and the residual *C=C* distribution curves for the case with $k_2 = 800\ (sM)^{-1}$, $k_3 = 1.6\times10^5\ (sM)^{-1}$, $k_4 = 5.12\times10^9\ (sM)^{-1}$, and R=25 nm 98
Figure 10-1: Aging of Therban in air at 160°C: influence of RDB on relative loss of elongation at break [61] 100
Figure 10-2: General accepted degradation scheme for polymers, originally developed for natural rubber [64] 102
Figure 10-3: FT-IR Spectra of SBS and thiol-saturated SBS 105
Figure 10-4: FT-IR spectra of NBR and thiol partially saturated NBR 105
Figure D- 1: PFD of the solution hydrogenation process……125
Figure D- 2: PFD of the diimide hydrogenation process……....127

List of Tables

Table 1-1: Commercial products for hydrogenated rubbers 1
Table 2-1: Hydrogenation of polymers in the presence of diimide [29] 5
Table 2-2: Polymer hydrogenation conditions and results using diimide 9
Table 5-1: H_2O_2 and N_2H_4 decomposition rate comparison [48] 30
Table 5-2: Decomposition rate of hydrazine 32
Table 5-3: Decomposition rate of hydrogen peroxide 32
Table 5-4: Reaction rate between hydrazine and hydrogen peroxide 34
Table 5-5: Effect of adding hydrazine on the reaction between hydrazine and hydrogen peroxide as catalyzed by boric acid 36
Table 6-1: Nitrogen generation rate from the reaction between hydrazine and hydrogen peroxide in NBR latex (T=25.0 ^{o} C, Solid content = 0.04wt%, $[H_3BO_3]$ = 0.067 M) 45
Table 6-2: Nitrogen generation rate from the same NBR latex (without added catalyst, T=25.0^{o} C, Solid content = 13.2 wt%) 46
Table 6-3: Comparison of nitrogen generation from the reaction between hydrazine and hydrogen peroxide with different catalysts (Solid content = 0.04wt%, T=25.0ºC) 47
Table 6-4: Diimide production rate with different concentrations of boric acid (25.0ºC, solid content= 13.2wt%, $[H_2O_2]_0 \approx 0.05$ M) 48
Table 6-5: Diimide production rate with different concentrations of boric acid (25.0ºC, solid content: 13.2wt%, $[H_2O_2]_0 \approx 0.006$M) 49
Table 6-6: Diimide production rate at different $[N_2H_4]$ catalyzed by boric acid (25ºC) 50
Table 6-7: Comparison of k_m at different $[H_2O_2]_0$ (25.0ºC) 51
Table 6-8: Comparison of nitrogen generation rate at different solid content levels (T=25.0 ºC) 53
Table 6-9: Nitrogen generation rate observed at different temperatures ($[H_3BO_3]$= 0.062M) 53
Table 6-10: HE at different $[H_2O_2]_0$ ($[N_2H_4]$=2.2M, $[H_3BO_3]$ = 0.060M, T=25.0ºC) 57
Table 7-1: Conversion of *C*=*C*s in NBR (132ºC, TSH/[*C*=*C*] = 2.0, chlorobenzene as the solvent) 65
Table 7-2: Rate ratio of *C*=*C*s to diimide in the homogeneous hydrogenation system 66
Table 7-3: Conversion of *C*=*C*s in NBR (40ºC, $[N_2H_4]$/[*C*=*C*] = 3.0, $[H_3BO_3]$/[*C*=*C*] = 0.076, $[N_2H_4]/[H_2O_2]$ = 1.0, H_2O_2 (30.47% aqueous solution) added over 6.5 hours) 67
Table 7-4: Hydrogenation rate ratio of vinyl to *trans*-*C*=*C* observed in the diimide hydrogenation of NBR latex 69
Table 8-1: Effects of individual chemicals on gel formation during NBR hydrogenation 73

Table 8-2: Initiation of styrene polymerization by substances in diimide hydrogenation (reaction for 8.0hrs at 40.0ºC) 73
Table 8-3: Experiments with oxygen crosslinking (reaction for 8.0hrs at 40.0ºC)....75
Table 9-1: Comparing (9-30) with (9-32) by numerical method 83
Table 10-1: Thiol addition experiments....106
Table 10-2: Glass transition temperature of polymers....107
Table D- 1: Calculation of raw materials costs (C_{RM}) of the solution hydrogenation process 119
Table D- 2: Estimation of C_{UT} (The cost of electricity is $0.06/kwh, the heater efficiency is 90%) of the solution hydrogenation process....120
Table D- 3: Calculation of operation labor cost (C_{OL}) of the solution hydrogenation process....120
Table D- 4: Estimating manufacturing cost- Solution hydrogenation process 121
Table D- 5: Calculation of raw materials costs (C_{RM}) of the diimide hydrogenation process 122
Table D- 6: Estimation of utility costs (C_{UT}) of the diimide hydrogenation process....122
Table D- 7: Estimating manufacturing cost- diimide hydrogenation process....123
Table D- 8: Comparison of manufacturing costs of the two processes....123
Table D- 9: Flow summary table for the solution hydrogenation process....126
Table D- 10: Flow summary table for the diimide hydrogenation process....128

Chapter 1
Introduction

Hydrogenation with respect to organic materials, by definition, is a reaction in which hydrogen adds across a double or triple bond. Hydrogenation of diene-based rubbers helps to improve the thermal and oxidative stability of these polymers when the radical-susceptive *C*=*C*s are replaced by saturated hydrocarbon bonds. In particular, the hydrogenation of styrene-butadiene-styrene block copolymer (SBS) and acrylonitrile-butadiene rubber (NBR) has received considerable attention in industry [1] (Table 1-1). The hydrogenated NBR (HNBR), in particular, is widely known for its physical strength and retention of properties after long-term exposure to heat, oil, and chemicals, which makes HNBR an ideal material for under-the-hood rubber components in the automobile industry [2].

Table 1-1: Commercial products for hydrogenated rubbers

Rubber	Brands	Major applications
HNBR	Therban®, Zetpol®	Automotive (seals, gaskets, host and belts), mechanical engineering (seals, rolls), and oil industries
HEBS	Kraton® Dynasol®	Adhesives/Sealants, Asphalt Modification, Polymer modification, Compounding

Selective hydrogenation of NBR by molecular hydrogen under catalysis as presented in (1-1) is practically the most important hydrogenation method nowadays, which saturates *C*=*C*s and leaves the CN triple bond untouched.

$$\begin{aligned} &-(CH_2{-}CH{=}CH{-}CH_2)_m-(CH_2{-}CH(CH{=}CH_2))_n-(CH_2{-}CH(CN))_p- \quad + H_2 \\ &\xrightarrow{cat}(CH_2)_{4m}-(CH_2{-}CH(CH_2{-}CH_3))_n-(CH_2{-}CH(CN))_p- \end{aligned} \tag{1-1}$$

There are two routes in practice commercially for HNBR production, the homogeneous-catalysis process used by LANXESS Inc. and the heterogeneous-catalysis process used by Zeon Chemicals. In the homogeneous-catalysis process, a specially designed complex transition-metal catalyst (as an example, Wilkinson's catalyst, $RhCl(P(C_6H_5)_3)_3$) is dissolved in an organic solution of NBR. NBR is hydrogenated selectively under high pressure of hydrogen at elevated temperature [3-11]. In the heterogeneous-catalysis process, transition metals are supported on C, Al_2O_3 or SiO_2, and mixed with the NBR solution [12,13]. High pressure of hydrogen is also needed to ensure the performance of this process. The two processes also work for SBR [14] and SBS [15]. A typical catalytic hydrogenation process is shown in Figure 1-1.

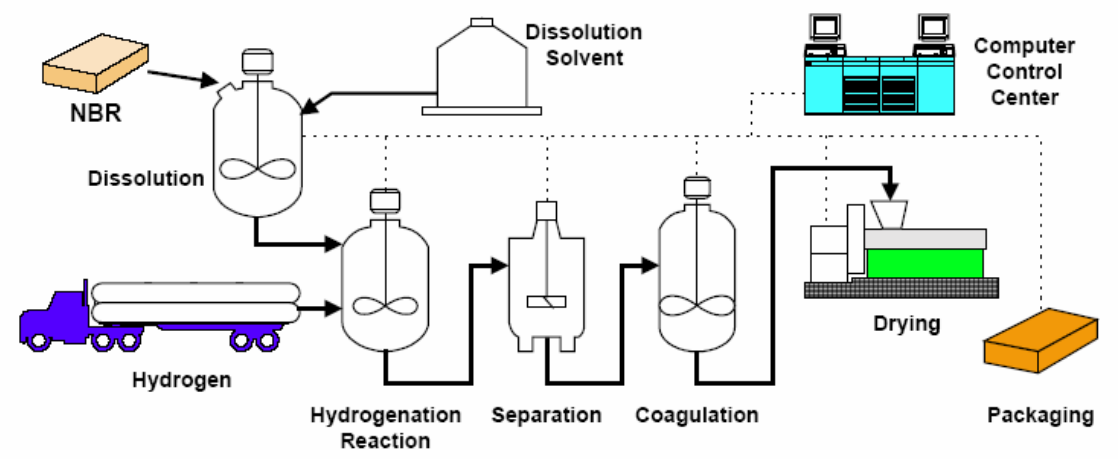

Figure 1-1: HNBR production process [16]

There are two major drawbacks in this hydrogenation process; the use of solvents and the difficulties in catalyst separation. Environmentally benign processes with higher efficiency are desired. One direction is to carry out the hydrogenation of NBR in aqueous latex form rather than in organic solution form. NBR is produced exclusively by emulsion polymerization in practice. The advantages of direct latex hydrogenation are obvious. The dissolution and separation of solvents from rubbers would be omitted from the improved process, which makes this process energy favorable over the solution hydrogenation processes. Furthermore, this process will make it possible to provide hydrogenated rubbery materials in latex form.

In order to hydrogenate unsaturated polymers in latex form, three routes are of interest:

1) Biphasic catalysis may serve this purpose. However, a previous report regarding the potential use of biphasic catalysis identified a number of problems [17],

2) Using the catalysts for the solution hydrogenation process directly in the latex system [11],

3) Diimide hydrogenation process [18].

The diimide hydrogenation process is much more attractive because precious metal catalysts are not needed for the actual hydrogenation step. Both the organic solvent and the catalyst separation problems are eliminated, which makes the diimide hydrogenation preferred over the other two routes. The diimide hydrogenation process would be much more economical when compared to the conventional methods (Appendix E). Therefore, the diimide hydrogenation process is the focus of this research.

1.1 : Objectives

Research on the topic of "Hydrogenation of unsaturated polymers in latex form" was initiated at The Goodyear Tire & Rubber Company in 1980s [18]. The clever invention by Wideman [18] brought the old, practically ignored diimide hydrogenation method into consideration for industrial practice and provided this method as a potentially successful hydrogenation route with several advantages.

However, the subsequent research has not been able to lead this invention into industrial success. There were limited research activities in this area in the following 20 years. The recent progresses made by DSM N.V. reactivated the research and imagination on this topic. An economic and highly efficient process together with hydrogenated rubber products comparable to the commercialized products is expected on this diimide technology.

Therefore, this project aims to fully reveal the advantages and limitations of the diimide hydrogenation process. A systematic description of reactions involved in the diimide hydrogenation process would help to identify problems in this process, to identify origins of these problems, and to optimize this process.

1.2 : Research outline

This research began with the semi-batch process set by Wideman [18]. The redox reaction between hydrazine and hydrogen peroxide was used as the hydrogen source. NBR latex from LANXESS Inc. was used as the model system. Different catalytic systems have been investigated.

Semi-batch hydrogenation experiments revealed that two problems, low efficiency of diimide utilization and gel formation, existed in the diimide hydrogenation process. The kinetics of the redox reaction between hydrazine and hydrogen peroxide in aqueous solution was investigated by following the nitrogen generation curve from this reaction. This work provided the diimide generation kinetics, and revealed the effects of different catalysts on this reaction. Similar kinetic investigation was conducted on the same reaction in NBR latex, which revealed how diimide was generated and utilized in latex. Comparison of the two reaction kinetics would provide insight into how to modulate the interface and catalyst to improve the diimide utilization efficiency. Kinetic investigation also showed that both the problems with this process were related to diimide accumulation in the rubber phase. The reaction rates of different *C*=*C*s with diimide have been compared using FT-IR and ^{1}H NMR spectra to follow reaction courses.

Radical generation from reactions in the aqueous phase and in the organic phase was analyzed. The chance for these radicals to initiate gel formation in rubber was investigated. The radical source for gel formation during hydrogenation has been identified.

Based on the kinetics, a systematic simulation of this process was conducted, which took into account three parallel processes and provided reasonable estimates for rate constants for all the reactions in this system. The effect of diimide diffusion upon hydrogenation was analyzed. An optimized process would be available from this research.

Chapter 2
Literature review

Diimide is quite active and unstable, which makes it difficult to modulate the reactions of diimide, and also confines its utilization. Diimide has only been tried on *C*=*C*s as recorded in the literature. The work on diimide chemistry, the utilization of diimide to saturate *C*=*C*s in organic solvents and in polymer latex, and the proposed gel formation mechanism for the diimide hydrogenation process, was reviewed in this chapter.

2.1 : Diimide hydrogenation fundamentals

The use of diimide to hydrogenate carbon-carbon double bonds is well known in the organic chemistry literature [19]. Diimide is believed to be the intermediate when hydrazine or a derivative of it is used as a reducing agent to saturate unsaturated bonds [20]. The reaction is:

$$NH = NH + -CH = CH- \rightarrow N_2 + -CH_2 - CH_2 - \qquad (2\text{-}1)$$

The existence of *cis*-diimide has been shown by IR, NMR and mass spectra [21]. Normally, *p*-toluenesulfonylhydrizide (*p*-TSH)[22,23] has been used as the source for diimide in the organic phase (other methods to produce diimide were summarized by E.E.Van Tamelen [20]). The redox reactions between hydrazine and oxidants were used to produce diimide in the aqueous phase. The reaction of hydroxylamine with ethyl acetate was also used to provide diimide [24].

Diimide can selectively hydrogenate symmetrical multiple bonds, such as *C*=*C*, *C*≡*C*, *N*=*N* and *O*=*O*, whereas reactions of more polar functions, such as *C*≡*N, S*=*O, S*-*C*-*S* and *C*=*O* are more difficult. The hydrogenation of nitrile by diimide was not observed [19]. Based on the observed phenomena, it was suggested that "the transition state for diimide reduction should be largely uncharged and involve simultaneous transfer of neutral hydrogen to the substrate" [20], which led to the assumption that *cis*-diimide was the only active form of diimide, and *trans*-diimide was expected not to be active for hydrogenation. However, calculations on diimide systems conducted by Pasto, et al [25] showed that the energy barrier for the conversion of *trans*-diimide to *cis*-diimide was 46.3- 60.0 kcal/mol. Thus, any mechanism requiring this inter-conversion was "untenable" considering the rapid rates of hydrogenation normally observed [25]. Consequently, *cis*- N_2H_2 is unlikely to be the only species involved in hydrogenation. A two-stage, hydrogen atom transfer process proceeding via N_2H and N_2H_3 radicals was considered to be an energetically feasible process for the disproportionation reaction [26].

2.2 : Homogeneous hydrogenation by diimide

Diimide reactions were carried out in organic solutions initially. Unsaturated molecules were dissolved in solvents, and diimide was generated in situ, as the best example, from *p*-TSH

thermolysis. Different *C=C* showed different activities toward diimide. The major factors that contributed to the observed reactivity difference were torsional strain, bond angle bending strain, and α -alkyl substitution effects [26].

Ratnayake, et al [27] compared the relative reduction rates of double bonds at different positions of fatty acids. The terminal ethylenic bond was the most reactive, and among the others, reactivity was greater nearer the ends of the chain than in the center. Also, the ethylenic bonds closer to a carboxyl end of a chain showed greater reactivity than those closer to a methyl end of the chain. Differences in reactivity among the centrally located double bonds were not significant. The terminal ethylenic bond reacted with diimide 5.8 times faster than the centrally located double bonds.

Diimide had been used to hydrogenate polymers, such as polybutadiene (PBD), *cis*-polyisoprene, SBR and SBS, etc [22,28,29]. Hahn [22] observed that a molar ratio of *p*-TSH to *C=C* of approximately 2:1 was necessary to achieve complete hydrogenation of SBS and PBD. Polyisoprene could not be fully hydrogenated even when five times of *p*-TSH was used. The efficiency of hydrogenation appeared to decrease at solid loadings above 2%. High molecular weight components appeared in the GPC curves when the loading was 5%.

The hydrogenation reaction of different polymers with diimide was compared by Harwood, et al [29]. See in Table 2-1.

Table 2-1: Hydrogenation of polymers in the presence of diimide [29]

Polymer	Conversion (%) calculated from		
	Elemental analysis	FT-IR spectra	NMR Spectra
trans- 1.4 –polybutadiene	73.5	100	
cis- 1.4-polybutadiene	90.0	100	
SBS	100	100	
Styrene-butadiene random copolymer	93.5	98	
Polycyclohexadiene	89.0	97	100
cis- polyisoprene	94.0	100	100
Poly-2,3- dimethylbutadiene	62.5		47
poly-2.5-dimethyl-2.4-hexadiene	22.5		
poly-2-chlorobutadiene	11.0		

Steric effects were believed to be the major one upon the difference in reaction activity. Double bonds containing mono-, di- and tri-substitution were more readily hydrogenated by diimide. Further substitution reduced the effectiveness of diimide hydrogenation. Mango and Lenz [28] showed that the relative rates of hydrogenation for *cis*-, *trans*- and vinyl butadiene units were $k_{cis} \sim k_{trans} < k_{vinyl}$.

Nang, et al [30] observed that the rate of hydrogenation of polyisoprene by diimide obeyed the rate law: Rate of hydrogenation = rate constant [polymer] [TSH].

Some side-reactions also occurred with the hydrogenation reaction when TSH was used to hydrogenate unsaturated polymers. The phenomena observed included crosslinking, chain decomposition and attachment of *p*-toluenesulfonate to the rubber. Amines and pyridine were used to reduce these side-reactions. For example, 2 mol of *tri*-n-propyl amine [22] respect to 1 mol of *C=C* could suppress the cleavage of backbones during the diimide hydrogenation reaction.

2.3 : Hydrogenation of polymer latex by diimide

The use of diimide to saturate polymers in latex form is relatively new idea. In 1984, Wideman of The Goodyear Tire & Rubber Company [18] introduced the diimide hydrogenation method to hydrogenate NBR latex. The hydrazine hydrate/ hydrogen peroxide (or oxygen) redox system was used to produce diimide in situ. Cupric ion (or ferric sulfonate) was used as a catalyst. 80% of hydrogenation was attained. Based on the patent by Wideman [18], Parker provided more refined results [31] and detailed a process for the preparation of highly saturated nitrile rubber latex [31]. A mechanism for the hydrogenation reactions was proposed (Figure 2-1). The anionic soap was indispensable for hydrogenation because the soap helped to keep the catalytic cupric ions at the surface of the rubber particles.

Schiessl of Olin Corporation [32] in 1991 suggested that maintaining a large excess of hydrazine helped to reduce crosslinking. They claimed that gel-free HNBR with a hydrogenation degree of 90% was attained in the process.

After 1998, Belt, et al (DSM N.V.) filed several patents [33], in which, boric acid was used as a catalyst. It was claimed that a compound was added before, during or after the hydrogenation to break crosslinks formed during the hydrogenation. The compound can be chosen from primary or secondary amines, hydroxylamine, imines, azines, hydrazones, and oximes. The emulsion form of N-1,4-dimethylphenyl (N'-phenyl)-*p*-phenylenediamine was also suggested to reduce gel formation [33].

Zhang et al [34] further proved that dropwise addition of hydrogen peroxide with post reaction at ambient temperature was the most effective way of conducting diimide hydrogenation. The hydrogenated nitrile latex with a hydrogenation degree over 90% was obtained. In suppressing gel formation, it was suggested that hydroquinone be added during the hydrogenation [35]. The mass fraction of gel in the hydrogenated product was significantly reduced by adding hydroquinone. The hydrogenated NBR with a hydrogenation degree of 80% and a gel mass fraction of 3.1% was obtained.

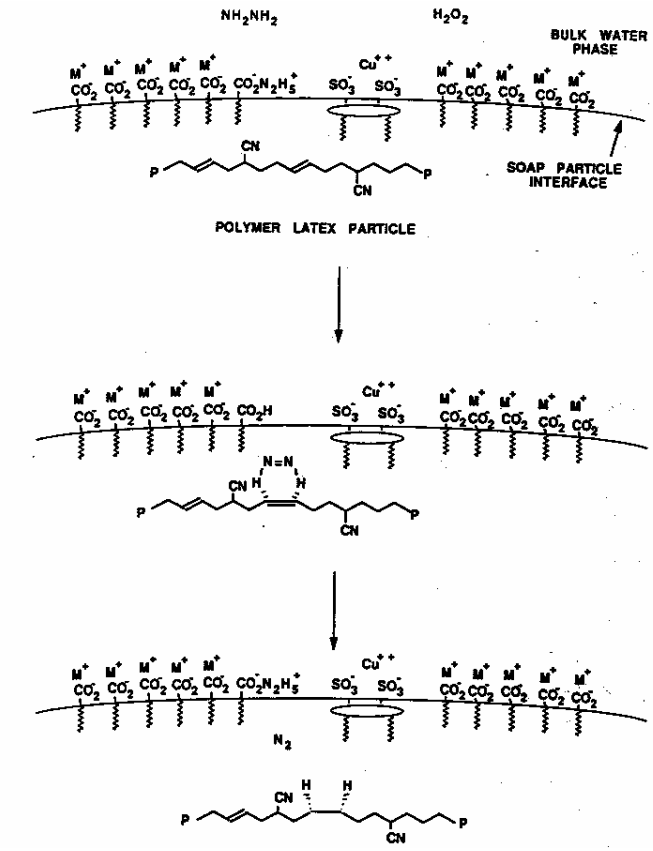

Figure 2-1: Proposed mechanism for diimide hydrogenation by Parker [31]

El-Aasser et al [36] compared the hydrogenation of latex with respect to different particle sizes. SBR latex with a diameter of 50 nm could be hydrogenated to 91% using 1 mol of hydrazine and 1 mole of hydrogen peroxide per mole of double bond. For the latex with a diameter of 230 nm, the hydrogenation degree was only 42%. A "Layer model" was proposed for hydrogenation of latex with a relatively large particle size (for example, a diameter of 230 nm) (Figure 2-2). The catalyst, cupric ion, was postulated as staying at the surface of latex particles. By modulating the concentration of cupric ions at the particle surface, a higher degree of hydrogenation could be attained.

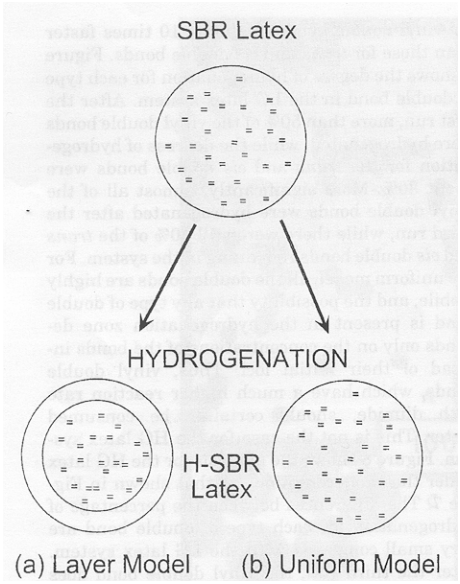

Figure 2-2: Two models for the distribution of double bonds in hydrogenated SBR latex particle: (a) layer model; (b): uniform model [36]

Xie, et al [37] measured the effect of reaction conditions on both hydrogenation and crosslinking. The use of inhibitors both in the rubber phase and in the aqueous phase was suggested to reduce crosslinking. By using sodium N,N-dimethyldithiocarbonate and *p*-tert-butylpyrocatechol as the inhibitors, the gel content in the final rubber could be reduced to 5% (Figure 2-3). Similar results were also presented by Sarkar [38].

Xie et al[39] showed that under the following optimum conditions: using 0.8% sodium dodecyl benzene sulfonate as emulsifier and 0.0025 mmol/g of $CuSO_4$ as catalyst, mole ratio of $N_2H_4/C{=}C$ at 1.8, mole ratio of H_2O_2/N_2H_4 at 1.4, hydrogenation temperature at 55°C, hydrogenation time at 7 hours, hydrogenated styrene butadiene rubber with a hydrogenation degree of 98% and a gel content less than 0.6% could be obtained (this result is the best claim appearing in the published literature). However, the publication regarding the method of determining the degree of hydrogenation of HSBR raises some doubts regarding the claim. Iodometry method was used by the group to check the degree of hydrogenation.

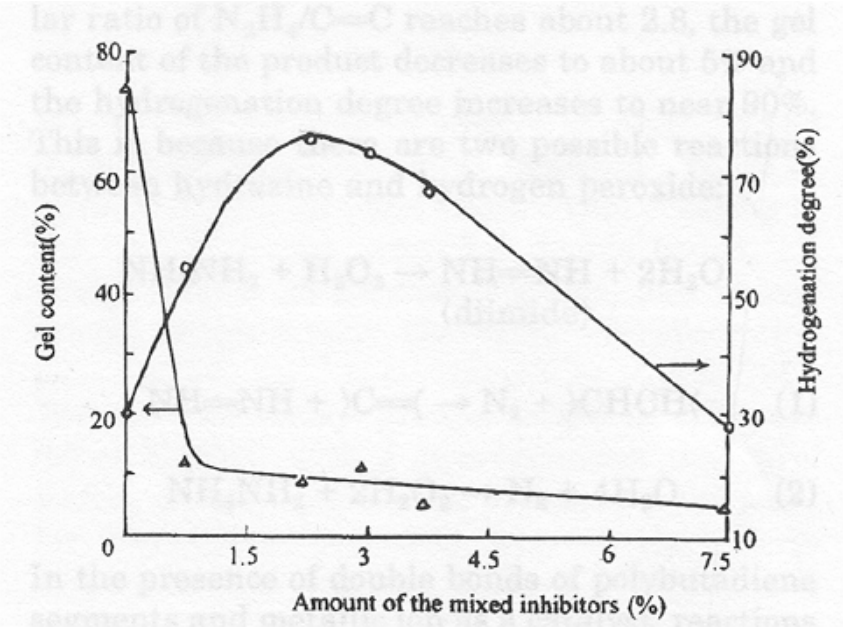

Figure 2-3: Effect of mixed inhibitors on the hydrogenation degree and gel content; (N_2H_4/*C=C*) = 1.4 molar ratios, H_2O_2/N_2H_4 = 1.25; 52 °C [37]

Results from the studies introduced above are summarized in Table 2-2.

Table 2-2: Polymer hydrogenation conditions and results using diimide

Latex details, particle size D, solid cont.	Catalyst	Catalyst: ppm of rubber	N_2H_4/*C=C*, H_2O_2/*C=C*	T(ºC) / t (hr)	Degree of hydrogenation	Reference
SBR:50nm, 20%	$CuSO_4$	100	1:1, 1:1	50 /7	90%	[36]
SBR,230nm, 20%		10			40%	
SBR, ?, ?	$CuSO_4$	5.5	1.44, 1.87	45 / 4	94%	[38]
SBR, ?, 54%	$FeSO_4$	270	1.4, 1.75	52	91%	[37]
NBR, ?, 25%	$CuSO_4$	480	1.1, 1.4	47/ 7	94.6%	[31]
NBR, ?, 35%	$B(OH)_3$	10%	1.5, 1.5	40/6	91%	[33]
NBR, ?, 29%	$CuSO_4$	1724	4.0, 0.5	50-55/2.5	97%	[30]
NBR,72.4nm, 39.7%,	$CuSO_4$	440	1.0, 1.0	40-50/6	85-90%	[31]
NBR,?, 35%	none	0	10, 2.5	35/long	>96%	[32]

2.4 : Crosslinking in diimide hydrogenation process

Gel formation is generally observed for the diimide hydrogenation both for the homogeneous process and for the latex system. The mechanism for crosslink bond formation has not been clearly identified. The disproportionation of diimide may cause the crosslinking of rubber backbones [24].

$$2N_2H_2 \rightarrow N_2H\bullet + N_2H_3\bullet \qquad (2\text{-}2)$$

Generally, gel content increases together with the reduction in unsaturation, which deteriorates the mechanical properties of the rubbers. Further increase in gel content would render the rubber useless. On the other hand, in order to improve the oxidation resistance of a rubber, the saturation of the polymer must be elevated to a level that the residual unsaturation is only enough for vulcanization. To deal with this puzzle, Parker, et al [40] tried to hydrogenate a rubber emulsion to a moderate level of saturation, and then used antioxidants to balance the performance of the material over the degree of crosslinking and oxidation resistance. It was shown that HSBRs containing a bound amine-type antioxidant and moderate hydrogenation levels can greatly outperform HSBRs with similar saturation levels without the bound antioxidant with regard to aged property retention under thermal and photolytic conditions, and that the HSBRs with a bound antioxidant and a modest hydrogenation level can approach the thermal resistance of highly saturated HSBR without antioxidant. The other route suggested by Parker, et al [41] comprised treating the resulting mixture from hydrogenation with ozone to react with residual polymer unsaturation to form ozonated latex, and then treating the ozonated latex with hydroxylamine to convert aldehyde end groups to oxime end groups to form oximated polymer latex. This treatment of the resultant latex from diimide hydrogenation generated a soluble, hydrogenated elastomeric polymer in latex form with a reduced level of residual hydrazine therein.

Belt, et al [42] suggested using a metal compound containing a metal atom in an oxidation state of at least 4 to overcome the problem. This suggestion has proven unsuccessful in the present work.

2.5 : Summary

The industry is quite interested in the diimide hydrogenation process. Around 40 patents have been filed on this subject. However, this method has not been used successfully in industry. Research needs to be done to further improve this process.

Chapter 3
Research approaches

Based on the knowledge of this system accumulated till now, there are possibly four major reactions in this process. The diimide hydrogenation reaction:

$$N_2H_4 + H_2O_2 + R_1HC = CHR_2 \longrightarrow N_2 + R_1H_2C - CH_2R_2 + 2H_2O \quad (3\text{-}1)$$

is achieved by two steps: (1) the reaction between hydrazine and hydrogen peroxide to produce diimide and (2) the reaction between diimide and carbon-carbon double bonds to form hydrogenated polymer, as given by the following equations:

$$N_2H_4 + H_2O_2 \longrightarrow N_2H_2 + 2H_2O \quad (3\text{-}2)$$

$$N_2H_2 + R_1HC = CHR_2 \longrightarrow N_2 + R_1H_2C - CH_2R_2 \quad (3\text{-}3)$$

However, according to the reactivity of diimide, two side reactions possibly accompany the diimide hydrogenation reaction. One is the further reaction of diimide with hydrogen peroxide to generate nitrogen (3-4), which most likely occurs on the interface as the hydrogen peroxide resides in the water phase. The other side reaction (3-5) is the reaction between two diimide molecules to produce one molecule of hydrazine and to release one nitrogen molecule, which most likely occurs in the rubber phase.

$$N_2H_2 + H_2O_2 \longrightarrow N_2 + 2H_2O \quad (3\text{-}4)$$

$$2N_2H_2 \longrightarrow N_2H_4 + N_2 \quad (3\text{-}5)$$

The four reactions represented by (3-2), (3-3), (3-4), and (3-5) comprise the framework of the diimide hydrogenation process. (3-2) may occur at the interface of rubber particles and also at the bulk aqueous phase. Diimide may get consumed according to (3-4) either at the interface or in the aqueous phase before it actually diffuses into the rubber particles. Reaction (3-5) is the radical source for crosslinking.

There are three competing parallel processes in this kinetic framework:

1) The reaction (3-2) may occur at the interface and also in the bulk aqueous phase. Diimide generated in the aqueous phase would not be available for the hydrogenation reaction in the organic phase, generally speaking. This competition influences the efficiency of the diimide utilization in the aqueous phase.

2) The reaction (3-4) competes with the diimide diffusion process for diimide before it diffuses into the rubber particles. This competition influences the efficiency of diimide utilization at the interface.

3) Reactions (3-5) competes with (3-2) for diimide. This competition influences the diimide utilization efficiency in the rubber phase, and also sets up the platform for radical generation and crosslinking.

The research was designed based on this understanding. Four items were investigated: kinetics, crosslinking mechanism, process analysis and simulation and improved hydrogenation process.

Kinetics investigation was conducted on the four reactions. The reaction in (3-2) was investigated both in the aqueous system and in the latex system to obtain the catalytic behavior of different catalysts, kinetic rate equation and parameters, as well as the difference between the aqueous system and the latex system (Chapter 5 and Chapter 6). The other three reactions, (3-3), (3-4), and (3-5) all involve the unstable intermediate diimide. This research can not provide a direct measurement of diimide. Therefore, the reaction rates are compared rather than measured directly. Comparing the kinetics of reactions (3-4) and (3-2) without the interference of other reactions would be able to quantify reaction (3-4). Similarly, comparing the kinetics of reactions (3-5) and (3-2) would provide kinetic understanding of both reactions (Chapter 6). Reaction (3-3) was investigated in both the homogeneous system and the latex system (Chapter 7).

Crosslinking mechanism (Chapter 8) research was conducted based on the well-accepted free radical crosslinking mechanism. The purpose of this investigation is to define the free radical generation kinetics.

A process simulation would be carried out based on the kinetic observations (Chapter 9). This simulation aims to provide reasonable estimates for those rate constants.

Methods to optimize this hydrogenation process (better efficiency of reactants and better quality of the final rubber product) will be discussed in Chapter 10.

Chapter 4
Hydrogenation of NBR latex

In the research, NBR latex is used as a representative for the diene-based polymers. As the outset of this project, hydrogenation of NBR latex was conducted to accumulate knowledge of this diimide hydrogenation process. The hydrogenation studies tried to reveal the effects of reaction conditions upon hydrogenation performance.

4.1 : Experimental

The hydrogenation process was designed based on the procedure adopted by Belt, et al [33], although some modifications were applied. The experiments were conducted in a semi-batch operation mode. Normally, 100.0 g of the latex was put into a three-neck round-bottom flask, in which an over-head agitator was mounted. 0.100 g of sodium dodecyl sulfate (SDS) was used to ensure the stability of the latex. 5 drops of mineral oil was added to reduce foaming. 0.265 mol of hydrazine hydrate (1.5 mole ratio to *C*=*C*s initially present) and a certain amount of catalyst(s) were added into the flask. A water bath was used to maintain the temperature at 40 ± 0.1 ºC. 0.265 mol of H_2O_2, which was supplied as a 30 wt% aqueous solution, was added dropwise with a pump at a preset addition rate. The latex was aged for an additional period of three hours after the last addition of H_2O_2. Samples were taken over a definite time period. The samples were coagulated with ethanol. After being washed with ethanol and water, and being dried by squeezing between two pieces of filter paper, the samples were then re-dissolved in acetone for analysis of hydrogenation degree (HD). HD was measured by FT-IR spectroscopy following the ASTM D3616-95 method. The crosslinking was checked by visual observation of the solubility of rubber samples. The concentration of aqueous hydrogen peroxide was measured following ISO7157.

The NBR latex with a solid content of 15.0wt% was provided by LANXESS Inc. (Sarnia, Canada). Hydrazine hydrate (~99.0%) and aqueous hydrogen peroxide (29.0~32.0 wt%) were purchased from VWR Scientific Products (West Chester, PA); boric acid was provided by J. T. Baker Company Co. (Phillipsburg, N. J.); and SDS (~99%) was purchased from Aldrich chemical Company, Inc. (Milwaukee, MI).

This experimental operation is named as semi-batch hydrogenation in this thesis.

4.2 : Results and discussion

To facilitate the description which follows, two parameters, hydrogenation degree (HD) and hydrogenation efficiency (HE) are defined here as follows:

$$HD = 1 - \frac{[C=C]_t}{[C=C]_0} \tag{4-1}$$

where $[C=C]_t$ is the double bond concentration at the reaction time t and $[C=C]_0$ is the initial double bond concentration.

$$HE = \frac{Number\ of\ moles\ of\ hydrogen\ peroxide\ utilized\ for\ hydrogenation}{Number\ of\ moles\ of\ hydrogen\ peroxide\ reacted} = \frac{Number\ of\ moles\ of\ C=C\ hydrogenated}{Number\ of\ moles\ of\ hydrogen\ peroxide\ reacted} \quad (4\text{-}2)$$

HE characterizes how much hydrogen peroxide is efficiently used for the purpose of polymer hydrogenation. When HE is much lower than 1, the side reactions dominate the overall reaction.

The experimental results of HD and HE can help to understand the hydrogenation mechanism and the effect of side reactions on the hydrogenation can be revealed.

4.2.1 : Efficiency of hydrogenation and selectivity of catalysts

The experimental data indicated that HD of the NBR did not increase detectably during the aging period following the final H_2O_2 addition, which suggests that hydrogen peroxide was consumed immediately when added into the system. The accumulation of hydrogen peroxide is not significant in the semi-batch operation as long as a suitable addition rate of hydrogen peroxide is chosen. Thus, the number of moles of hydrogen peroxide reacted can be considered to be equal to the added hydrogen peroxide amount. Under an ideal condition, H_2O_2 is used 100% for hydrogenation; the amount of H_2O_2 added divided by $[C=C]_0$ would be the highest HD that can be achieved by this process. Therefore, an ideal HD line is constructed based on the addition rate of H_2O_2.

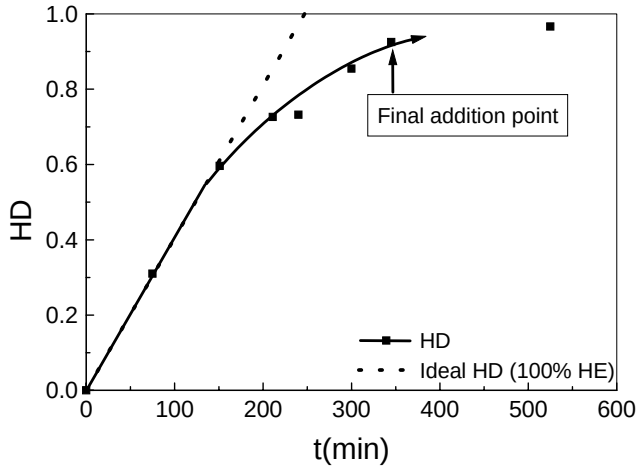

Figure 4-1: Comparison of the actual hydrogenation curve to the ideal hydrogenation curve (boric acid/NBR - 10.0 wt%; 40°C, (N_2H_4/*C*=*C*) =2.0; H_2O_2/N_2H_4 =0.75; addition over 6.3hr)

When 10.0wt% of boric acid relative to the dry polymer was used, HE was virtually 100% until the HD reached about 60%, after which it decreased very quickly (Figure 4-1). The phenomenon shown in Figure 4-1 suggests (1) boric acid promotes this reaction with a high selectivity; (2) the side reactions of diimide become significant when HD rises above 60%.

Without the addition of alien catalysts, HE was always lower than 100% even at the beginning of the reaction. The accumulation of hydrogen peroxide is not significant as shown in Figure 4-2 (The HD curve flattens beyond the point of final addition). Therefore the lower HE in this case suggests that the inherent catalytic system has lower selectivity for hydrogenation than the system with boric acid.

Ferrous sulfate is normally used in the recipe for producing NBR latex in industrial processes. The concentration could be as high as 0.2wt% of the latex. Therefore, ferric ion may be the catalyst in the case when no alien catalyst is added. However, when ferrous ion was added into the reaction system as a catalyst, the hydrogenation performance was even worse. HE was much lower than that without the addition of ferrous ion (Figure 4-3).

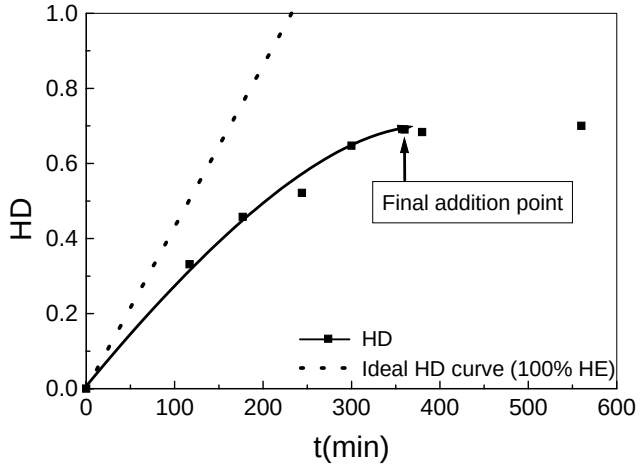

Figure 4-2: Comparison of the actual hydrogenation curve to the ideal hydrogenation curve (no added catalyst; 40ºC, (N_2H_4/*C*=*C*) =2.0; H_2O_2/N_2H_4 =0.75; addition over 6.0 hr)

Silver ion as a catalyst (Figure 4-4) also shows a poorer performance compared to the result in Figure 4-2.

Cupric ion (6.98×10^{-7} mole/g of polymer) provides a similar catalytic effect to boric acid (1.6×10^{-3} mole/g polymer) (Figure 4-5). Further increasing the amount of cupric ion tends to cause coagulation of the NBR latex, and shows no beneficial effect upon improving HE. On the other hand, cupric ion at a lower concentration tends to get lower HE (Figure 4-5).

Among the above five catalytic systems, the reaction with boric acid gives the best HE, although it has to be used at a much higher concentration than the conventional concentration range for a catalyst.

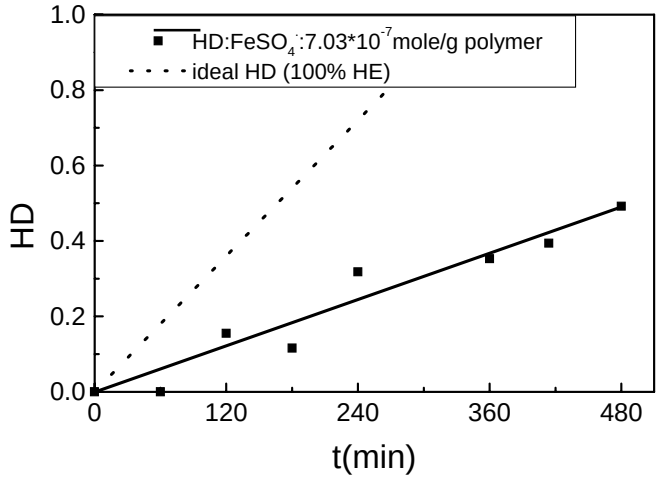

Figure 4-3: Effect of ferrous ion as a catalyst on hydrogenation (ferrous sulphate: 7.03×10^{-7} mole/g of NBR; 45ºC, ($N_2H_4/C=C$) =1.5; H_2O_2/N_2H_4 =1.0; H_2O_2 addition over 8.5hrs, total NBR: 15.0g)

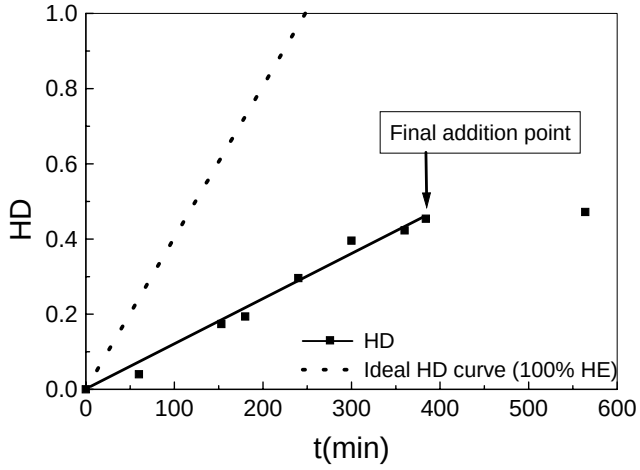

Figure 4-4: Comparison of the actual hydrogenation curve to the ideal hydrogenation curve (silver nitrate: 9.20×10^{-6} mole/g of NBR; 40ºC, ($N_2H_4/C=C$) =2.0; H_2O_2/N_2H_4 =0.75; addition over 6.5 hrs)

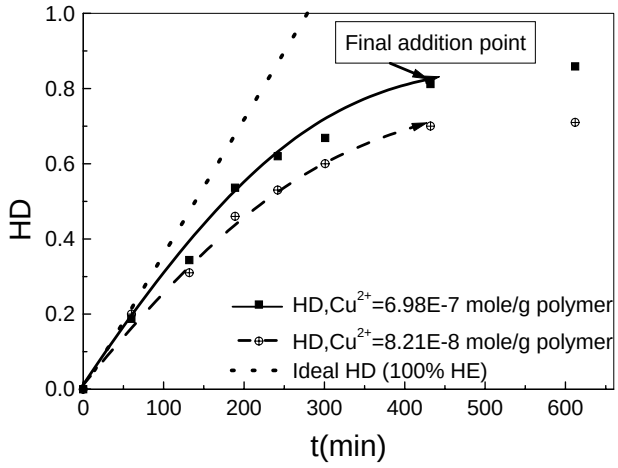

Figure 4-5: Comparison of the actual hydrogenation curve to the ideal hydrogenation curve (cupric sulphate: 6.98×10^{-7} mole/g of NBR; 40ºC, (N_2H_4/*C*=*C*) =2.0; H_2O_2/N_2H_4 =0.75; addition over 6.5 hrs)

Comparing the results for the four catalysts studied, it can be seen that HE is modulated not only by the catalyst, but also by the HD range. Different catalysts obviously provide different levels of HE. Over the low HD range, HD increases linearly with the addition of hydrogen peroxide, which means HE remains at the same level during this period. Among all the catalysts tested, boric acid was found to be the best one for higher HE. When HD reaches more than 60%, HE decreases quickly. This phenomenon is shared by all of the catalysts tested except silver ions (For silver ions, since the HD is at a low level throughout the process, it can not be distinguished as to whether there are two different stages for HD). Therefore, this decrease in HE should be related to high HD rather than the type of a catalyst.

It is reasonable to postulate that the decrease in HE at high HD range results mainly from the reaction (3-5). High HD means low [*C*=*C*]. A low [*C*=*C*] will definitely slow down the hydrogenation reaction and reduce the utilization efficiency of diimide. HE decreases as a result. In the low HD range, HE is modulated by the competition between the diimide production reaction (3-2) and the side reaction (3-4) at the interface. The catalysts provide catalytic effect only for reaction (3-2). The selectivity of the catalysts, related to the rate ratio of reaction (3-2) and (3-4), is determined by the catalytic activity of the catalyst upon reaction (3-2).

The mechanism for the catalytic effect provided by boric acid is quite interesting. Boric acid, which is not a transition metal ion, would not be expected to provide catalytic effects upon the reactions. It was proposed once that boric acid may provide a buffer effect upon which the hydrogenation reaction is promoted. However, the use of sodiumdihydrogen phosphate (NaH_2PO_4) which provides similar buffer effect to boric acid failed to provide the same promotion effect upon the hydrogenation reaction. Boric acid is capable of forming hydrogen-bonds with hydrogen peroxide. This formation of hydrogen-bonds stabilizes hydrogen peroxide and reduces the activity of hydrogen peroxide in this system. As a result, the side reaction (3-4) is retarded. The high efficiency in the case of boric acid benefits actually from the low concentration of hydrogen peroxide which is

available for diimide. The explanation would lead to the conclusion that a lower concentration of hydrogen peroxide (or a slower addition rate) gives higher efficiency of hydrogenation. In this sense, boric acid functions more like a promoter, rather than a catalyst.

Some comparative experiments were carried out to check the HE at different addition rates (Figure 4-6 and Figure 4-7). Although Case B in Figure 4-6 had a faster addition rate for hydrogen peroxide than Case A, it showed a similar hydrogenation curve to Case A, which implied that HE in Case A was higher than that in Case B. A similar phenomenon was observed for the experiments in which boric acid was used (Figure 4-7). Over the low HD range, HE was 100% in both cases. However, the decrease in HE in the range of high HD was less in Case B (Figure 4-7) in which a slower addition rate was applied. Therefore, the overall efficiency in case B was higher than that of case A. These comparisons demonstrate that a faster addition rate of hydrogen peroxide tends to give lower HE, which is consistent with the postulated mechanism above.

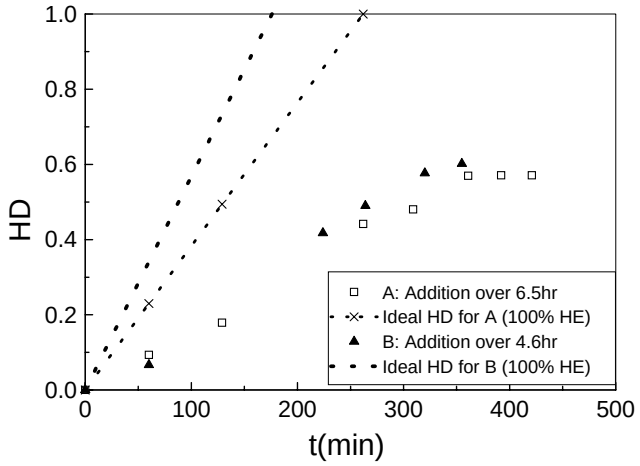

Figure 4-6: Effect of addition rate of hydrogen peroxide upon hydrogenation efficiency (catalyst: silver nitrate: 9.20×10^{-6} mole/g of NBR; 40ºC, (N_2H_4/*C*=*C*) =2.0; H_2O_2/N_2H_4 =0.75)

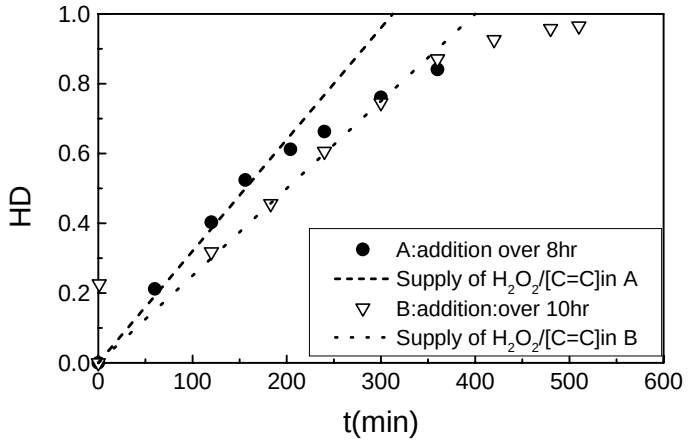

Figure 4-7: Effect of addition rate of hydrogen peroxide upon hydrogenation efficiency (catalyst: boric acid: 10.0 wt% of NBR; 40ºC, (N_2H_4/*C=C*) =1.5; H_2O_2/N_2H_4 =1.0)

4.2.2 : Selectivity over carbon-carbon double bonds

In the FT-IR spectrum of partially-hydrogenated NBR (Figure 4-8), the peak at 970 cm^{-1} is representative of the *trans*- 1, 4-butadiene unit; and the peak at 917 cm^{-1} of the 1, 2-vinyl butadiene unit [38, 43]. Figure 4-8 shows that the vinyl group is saturated at a faster rate than t*rans*-*C=C*. This phenomenon was also observed in the diimide hydrogenation of styrene-butadiene latex [36]. This phenomenon is similar to the catalytic hydrogenation of *C=C*s using molecular hydrogen [44]. The vinyl group is more active towards diimide than internal double bonds, as observed by Mango, et al. [27] and Tachiev et al. [45] for the homogeneous hydrogenation of *C=C*s within organic solvents. This selectivity is the result of the different steric resistance in the coordination step of diimide with different types of *C=C*s.

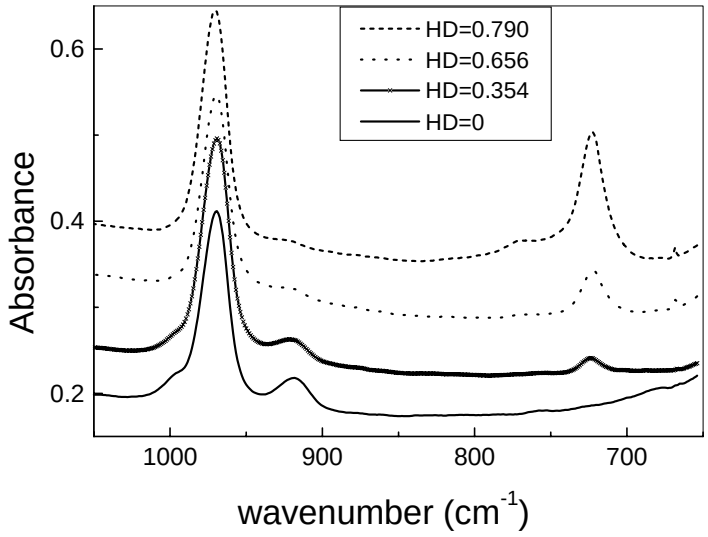

Figure 4-8: FT-IR spectra of partially hydrogenated NBR at different HD (Catalyst: boric acid - 10.0 wt% of NBR; 40ºC, (N_2H_4/*C*=*C*) =1.5; H_2O_2/N_2H_4 =1.0; addition over 10.5 hrs)

4.2.3 : Stabilization of catalysts in latex

It was observed that transition metal ions could precipitate out of hydrazine solution. Consequently, ligands were introduced into the system to stabilize the catalysts. Ammonia is a common ligand for cupric ions. The effect of ammonium hydroxide was checked by using Cu^{2+} together with ammonium hydroxide. Figure 4-9 shows the effect of ammonium hydroxide as a ligand significantly activates the cupric ion catalyst. HE at low HD improves greatly when cupric ion is used together with ammonium hydroxide. The use of ammonium hydroxide here probably modified the dissolving capacity of the cupric ions so that they could have a higher concentration in the latex with a pH above 10. High concentration of catalyst would accelerate the diimide production reaction and reduce [H_2O_2], and HE at low HD increases as a result. It is hard to believe that the ligand would benefit the activity of cupric ions. The ligand here probably only functions as a carrier to transfer cupric ion to the interface of the particles. Hydrogen peroxide is a much stronger ligand which will definitely substitute ammonium hydroxide. This observation suggested that cupric ion at low concentration together with a suitable ligand should be a good alternative to boric acid.

A similar effect was not observed with iron ion when EDTA or ethylene diamine (EDA) was used as a ligand. Both EDTA and EDA showed an inhibiting effect upon the catalytic activity of iron.

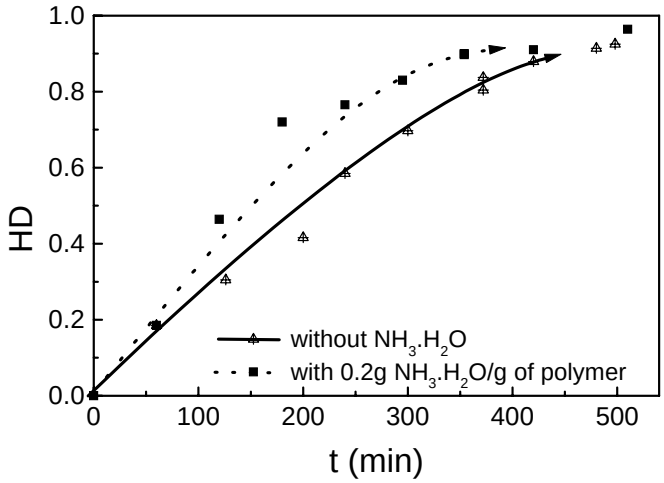

Figure 4-9: Hydrogenation comparison with/without ammonium hydroxide (catalyst: cupric sulphate: 7.51×10^{-7} mole/g of NBR; 40ºC, (N_2H_4/*C*=*C*) = 1.5; H_2O_2/N_2H_4 =1.0; addition over 8.5hrs, total NBR: 15.0g)

4.2.4 : Effect of radical scavengers and radical transfer agents

The role of radicals in the hydrogenation process is not fully understood. Normally it is believed that crosslinking is caused by radical reactions. The effect of radical scavengers upon hydrogenation and gel formation was studied in the present investigation. Hydroquinone and 1,4-benzoquinone showed adverse effects upon hydrogenation, even if the adverse effect was marginal. HE was reduced on the addition of benzoquinone (Figure 4-10). On the other hand, 2,2' methylene-bis (4-methyl 6-tertiary butyl phenol)(BKF) showed no effect upon hydrogenation (experiments showed the HD increased the same way for both cases with and without BKF). It is reasonable to believe that aqueous-borne antioxidants interfere with the diimide production reaction and reduce HE while organic-borne antioxidants do not. 1,4-benzoquinone reacts with hydrazine to form hydroquinone and thus becomes aqueous-borne.

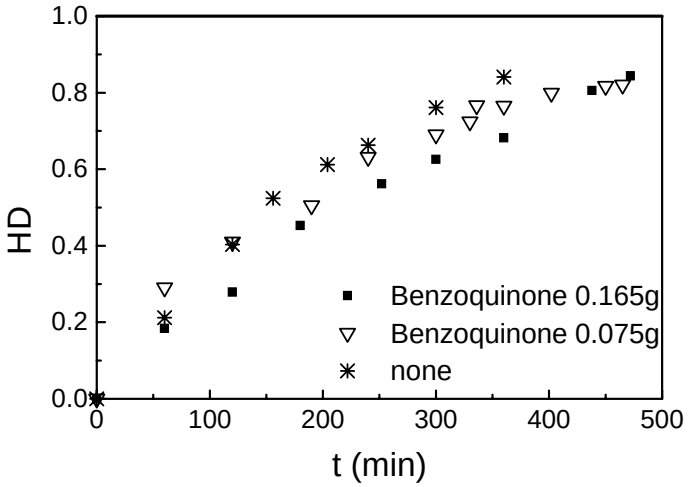

Figure 4-10: Effect of benzoquinone on hydrogenation (catalyst: boric acid - 10.0 wt% of NBR; 45ºC, N_2H_4/*C*=*C* =1.5; H_2O_2/N_2H_4 =1.0; H_2O_2 addition over 8.5hrs, total NBR: 15.0g)

4.2.5 : Effect of hydrazine concentration

The hydrogenation performance at different concentrations of hydrazine was compared in Figure 4-11. When the initial concentration of hydrazine is lower, the HE tends to go below 100% at lower HD.

The supplement of hydrazine during the reaction was also compared as shown in Figure 4-12. The hydrogenation curve with hydrazine addition during the reaction is the same as that without hydrazine addition during the reaction, which means it is ineffective to keep [N_2H_4] at a high level all through the reaction.

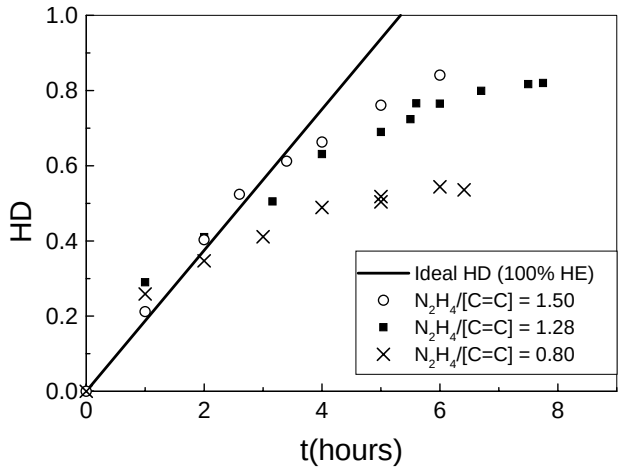

Figure 4-11: Effect of initial concentration of hydrazine upon hydrogenation (catalyst: boric acid - 10.0 wt% of NBR; 45ºC; H_2O_2/N_2H_4 =1.0; H_2O_2 addition over 7.3hrs)

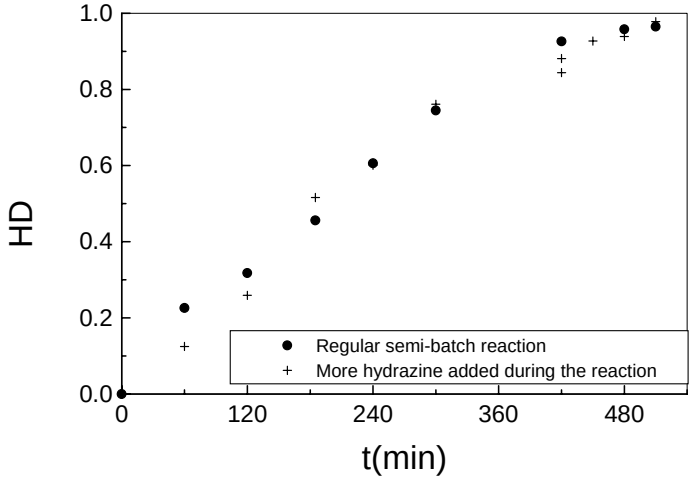

Figure 4-12: Hydrogenation comparison with/without hydrazine addition during the reaction (catalyst: boric acid - 10.0 wt% of NBR; 45ºC, $N_2H_4/C=C$ =1.5; H_2O_2/N_2H_4 =1.0; H_2O_2 addition over 8.5hrs; hydrazine hydrate added in case B: 0.5 moles per mole of *C=C* initial, added at 4.0 hours)

4.2.6 : Effect of hydrogen peroxide addition rate

The addition rate of hydrogen peroxide is crucial in this semi-batch hydrogenation experiment. It was observed that a slower addition of hydrogen peroxide tended to give a higher HD with the same amount of hydrogen peroxide. This effect is clearly shown in Figure 4-13.

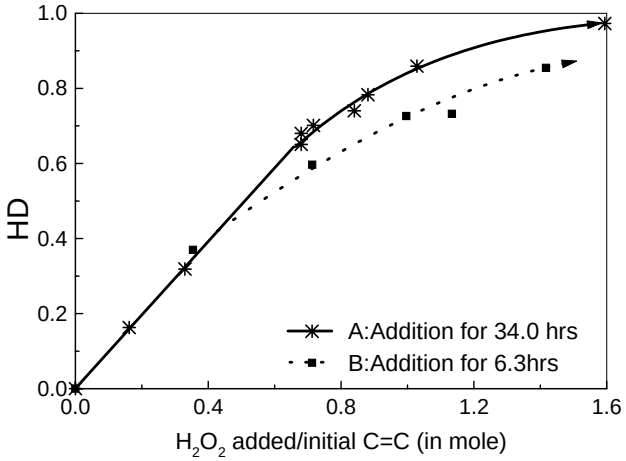

Figure 4-13: comparison of hydrogenation curves at different addition rates of hydrogen peroxide (catalyst: boric acid - 10.0 wt% of NBR; 40°C, (N_2H_4/*C=C*) =2.0; H_2O_2/N_2H_4= 0.8 for Case A, 0.75 for Case B)

The hydrogenation experiment in Case A (addition over 34.0hrs) gave totally soluble rubber when HD was as high as 86.0%; while for the experiment with a faster addition rate in Case B (addition over 6.3hrs), the rubber was not soluble when HD reached 82.0%. Therefore, slow addition can raise the gel point of HD by at least 4.0%.

4.2.7 : Hydrogenation performance with fresh latex addition during the reaction

It was wondered if the deactivation of the catalyst during the reaction might play a role in this process. An experiment was carried out to check whether the addition of fresh latex would help to improve the efficiency. In the first part of this reaction, only half of the latex (50.0 mL instead of 100.0 mL) was added into the reactor. 0.07 mol of hydrogen peroxide was added over 4.0 hours. HD reached 62.0% when the first part of hydrogenation was done. In the second part of this experiment, 50.0 mL of fresh NBR latex was added into the partially hydrogenated NBR latex. When the content was mixed well, hydrogen peroxide addition was resumed at a double rate. The hydrogenation results were presented in Figure 4-14. Basically, this hydrogenation curve is quite similar to that shown in Figure 4-1. The addition of fresh latex does not benefit hydrogenation. And it was also found that gel was formed at a lower HD (69.1%), which was actually from the rubber added initially.

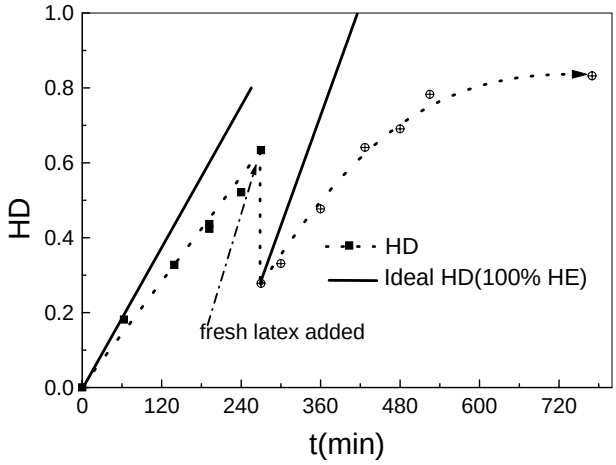

Figure 4-14: Hydrogenation curve with fresh latex addition during the reaction (Part one: 50.0 mL of NBR latex, 1.50g of boric acid, 20.0g of $N_2H_4 \cdot H_2O$, 0.07mol of H_2O_2 added over 4.0 hours; Part two: 50.0 mL of fresh NBR latex added, 0.14 mol of H_2O_2 added over 4.0 hours, 40ºC)

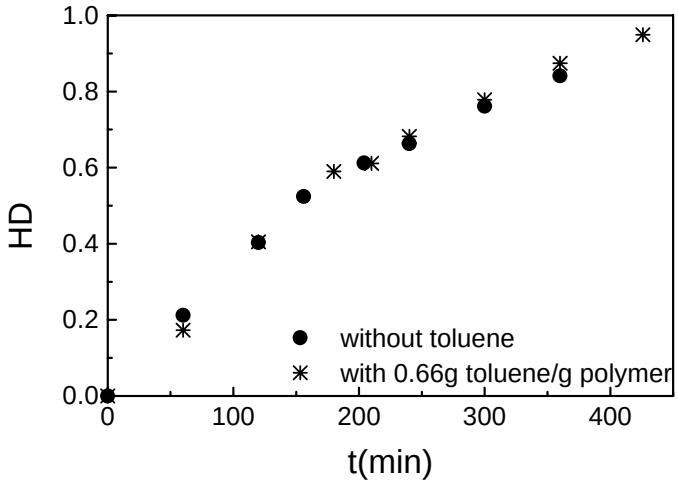

Figure 4-15: Hydrogenation comparison with/without solvent addition (catalyst: boric acid - 10.0 wt% of NBR; 45ºC, (N_2H_4/*C*=*C*) =1.5; N_2H_4/H_2O_2 =1.0; H_2O_2 addition over 8.5hrs; 15.0 g of NBR in the system in total)

4.2.8 : Effect of solvent addition

The effect of solvent addition was checked by adding 10.0 wt% of toluene into NBR latex. The mixture was mixed for 10 hours. Toluene diffused into latex particles quickly and the separate organic phase disappeared thereafter. The hydrogenation of the solvent-soaked NBR latex was carried

out following the same procedure as described in Section 4.1. The result was presented in Figure 4-15. The expectation on HE improvement at higher HD based on the solvent-aided diffusion of diimide did not show up. At least, the improvement on diimide diffusion is not enough for a better hydrogenation performance.

4.2.9 : Effect of aging time upon the hydrogenation behavior of NBR latex

When the NBR latex was stored for more than two months, the hydrogenation performance actually got worse. HE was lower even if boric acid was used as catalyst. It was thought that this worse hydrogenation behavior might be the result of catalyst loss during storage. Upon added cupric ion together with boric acid as the catalyst, HE was improved to the level of the fresh latex. See in Figure 4-16. This experiment showed that boric acid was not the actual catalytic substance. Transition metal ions provide the actual catalytic activity.

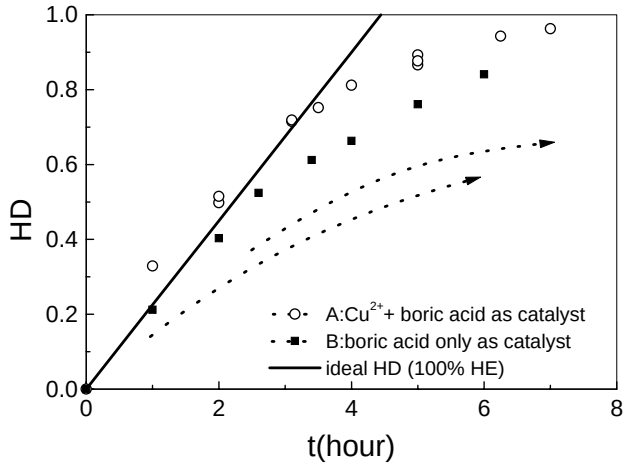

Figure 4-16: Hydrogenation comparison with/without cupric ion at the catalyst (catalyst: A: boric acid - 10.0 wt% of NBR + cupric sulphate: 6.98×10^{-7} mole/g of dry polymer; B: boric acid - 10.0 wt% of NBR; 45°C, (N_2H_4/*C=C*) =1.5; N_2H_4/H_2O_2 =1.0; H_2O_2 addition over 7.3hrs)

4.2.10 : Hydrogenation performance of latex with low residual *C=C*

In this experiment, the NBR latex was hydrogenated to 85.6% (HD) in the first step. The residual [*C=C*] was 1.67 M. The resultant latex was aged over 24 hours. No hydrogen peroxide would be left in the latex. After supplementing of 8.7g of hydrazine hydrate, the reaction was resumed at the same addition rate of hydrogen peroxide aqueous solution which was diluted by a factor of 7. The hydrogenation curve is presented in Figure 4-17. HE is much lower than that in the first step. However, the shape of the HD increase curve is quite similar to that of the first step. This

similarity of hydrogenation curves between latex with different $[C=C]_0$ would suggest that hydrogenation reaction is generally a first-order reaction.

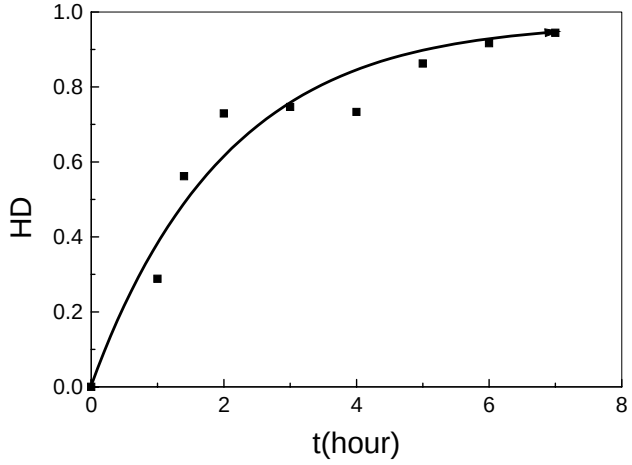

Figure 4-17: Hydrogenation of latex partially saturated by diimide (catalyst: boric acid - 10.0 wt% of NBR; 45ºC, (N_2H_4/*C*=*C*) = 7.0 (new added); (H_2O_2/*C*=*C*) = 1.5; H_2O_2 addition over 8.0hrs. $[C=C]_0$ =1.67M)

4.2.11 : Crosslinking of polymer during hydrogenation

It was hard to quantify the gel content especially when the gel content kept increasing after the samples were precipitated. The general observed phenomena of crosslinking are listed below:

1) Gel was observed when HD reached more than 60%, as companying the decrease of HE. Gel content increased very fast when HD went up further;

2) Slower addition of hydrogen peroxide tended to produce less gel at the same level of HD;

3) The process with boric acid gave less gel when compared to the process with cupric ion;

4) Normally, the hydrogenated NBR was insoluble when HD reached more than 80%.

There was no detectable effect on gel formation when the three antioxidants (hydroquinone, 1,4-benzoquinone and 2,2' methylene-bis (4-methyl 6 tertiary butyl phenol)) were examined. This observation is in contradiction with that observed and reported by Johannes W. Belt, et al [33] and Shuqin Zhou, et al [43]. The use of antioxidants may reduce the radical concentration in the system. However the low HE in the high HD range suggests the radical production rate is substantial. Antioxidants can not stop radicals from transferring to the polymer backbone efficiently when the concentration is high. On the other hand, crosslinking bonds even at a very low concentration are enough to render the polymer insoluble. Therefore, the ineffectiveness of radical scavengers,

antioxidants and transfer agents to suppress gel formation results from the less than 100% radical-capture efficiency with respect to the high efficiency of crosslinking bonds to form gels.

4.3 : Summary

From these hydrogenation results, two major problems associated with the diimide hydrogenation process were identified, the gel formation problem and the low efficiency of reactants (HE).

Side reactions can affect significantly HE in the diimide process. Over the low HD range (<60%), the decrease in HE mainly results from side reactions at the interface. Active catalysts can accelerate the diimide production rate, resulting in a decrease in the $[H_2O_2]$ in the system, and as a result, a higher HE can be achieved. With a promoter, such as boric acid, the HE can be significantly improved. When the HD goes beyond 60% the HE decreases quickly with an increase in HD, which is related to the side reactions of diimide in the organic phase. Both a high supply rate of diimide and the low [*C=C*] are attributed to the decrease in HE within the high HD range.

Radical scavengers are not efficient in suppressing gel-formation to a detectable extent and they may even decrease the activity of hydrazine.

Remarks: A major part of content here has been published in Reference [46].

Chapter 5
Reaction kinetics of hydrazine and hydrogen peroxide

In order to facilitate the investigation of the reaction between hydrazine and hydrogen peroxide, this reaction was carried out in aqueous solution. By doing so, this reaction is separated from the hydrogenation reaction. The effects of different catalysts upon diimide generation and the reaction kinetics can be observed directly.

5.1 : Introduction

The reaction between hydrazine and hydrogen peroxide has been thoroughly investigated in the literature. Hans Erlenmeyer, et al [47] and D.P. Graham, et al [48] established the stoichiometry of the reaction as:

$$N_2H_4 + 2H_2O_2 \longrightarrow N_2 + 4H_2O \qquad (5\text{-}1)$$

Rolf Griesser and Helmut Sigel [49, 50] investigated the kinetics of the reaction between hydrogen peroxide and hydrazine catalyzed by Cu^{2+}-2,2'-bipyridyl complex. The reaction followed the rate law:

$$-\frac{d[H_2O_2]}{dt} = k_{Cu}\frac{[Cubipyl][H_2O_2][N_2H_5^+]}{[H^+]} \qquad (5\text{-}2)$$

for the experimental range of pH = 5.2~7, $[N_2H_4]$ = 0.004~0.016 M, $[H_2O_2]$ = 0.002 ~0.032 M; k_{Cu}=0.00342 *M/s* (25ºC) when the pH is 7. It has been found [47] that this reaction proceeds at a very slow rate in the absence of catalysts, and shows a first-order reaction with respect to hydrazine and hydrogen peroxide, respectively. The reaction rate could become seven orders of magnitude higher when catalyzed by metal ions [51]. The reaction rate is significantly influenced by the pH value: at a pH<8 it is very slow; when the pH exceeds 8, the reaction rate increases dramatically; and at pH=10, the reaction rate reaches its maximum [51]. However, a kinetic expression for the normal ranges used for the diimide hydrogenation operation (e.g. pH >10.0, $[N_2H_4]$ = 0.05-3.0 M) is still not available.

Accompanying the redox reaction between hydrazine and hydrogen peroxide, the decomposition of hydrogen peroxide occurs as the following (5-3).

$$2H_2O_2 \longrightarrow O_2 + 2H_2O \qquad (5\text{-}3)$$

D.P. Graham, et al [48] measured gas production from the mixture of hydrazine with an excess amount of hydrogen peroxide. The oxygen production represented hydrogen peroxide decomposition according to (5-3). The nitrogen production represented hydrazine oxidation according to (5-1). The rate of hydrogen peroxide decomposition was always faster than that of the hydrazine oxidation (Table 5-1). Cupric sulfate was more effective than ferric sulfate for both reactions; using both cupric and ferric ions as catalysts had a promoter effect.

Table 5-1: H_2O_2 and N_2H_4 decomposition rate comparison [48]

Cupric sulfate as catalyst							
[Cu], mM	0.05	0.100	0.150	0.20	0.30	0.50	0.70
$10^4 k_{H2O2}$	0.443	0.865	1.59	2.88	5.60	14.2	25.6
$10^4 k_{N2H4}$	0.320	0.71		1.96	4.05		
Ferric sulfate as catalyst							
[Fe], mM	0.20	0.40	0.50	0.70	1.00	1.50	2.00
10^4 k_{H2O2}	0.39	0.61	0.74	0.90	1.19	1.62	2.4
10^4 k_{N2H4}	0.20		0.35		0.52	0.78	

The generally accepted mechanism of reaction (5-1) includes two steps:

$$N_2H_4 + H_2O_2 \xrightarrow{k_1} N_2H_2 + 2H_2O \qquad (5\text{-}4)$$

$$N_2H_2 + H_2O_2 \longrightarrow N_2 + 2H_2O \qquad (5\text{-}5)$$

Diimide is the unstable and active intermediate. The rate of reaction (5-5) is much faster than that of reaction (5-4). The overall reaction given by (5-1) is controlled by reaction (5-4). The reaction kinetics of (5-1) is identical to that of (5-4), which enables the investigation of diimide production simply by working on reaction (5-1).

In fact, hydrazine may also decompose by way of **(5-6)**, which makes the kinetic investigation even more complicated.

$$3N_2H_4 \longrightarrow 4NH_3 + N_2 \qquad (5\text{-}6)$$

The kinetic behavior of reactions (5-1), (5-3) and (5-6) was examined in this investigation and reported in this chapter.

5.2 : Experimental

Cupric sulfate hydrate (analytical grade from BDH Chemicals) and EDTA (disodium salt crystal from J. T. Baker Chemical) in 1:1 mole ratio was used as a representative complexed metal ion. Hydrogen peroxide, hydrazine hydrate (> 99%), sodium n-dodecyl sulfate (SDS) (99%), and boric acid are supplied from sources detailed in Chapter 4. Gelatin was purchased from J. T. Baker Chemical Co. (Phillipsburg, N. J.).

The kinetic investigation was carried out based on the stoichiometric relationship between the reactant consumption and the gas production from reaction (5-1), (5-3) and (5-6). The reactions were carried out in a 300ml Parr high-pressure reactor equipped with a pressure transducer (See in Figure

5-1). Initially, hydrazine, deionized water and additives were charged into the reactor. The total volume of the liquid was controlled at about 200 mL. The gas volume around was about 80 mL. After degassing and saturating the content of the reactor with nitrogen, hydrogen peroxide was added using a syringe. Then the reactor was closed and the pressure in the reactor was recorded automatically by an interfaced computer. An excess of hydrazine (> 95%) was used in all the experiments. The concentration range of hydrazine was 0.62-3.07 M; the corresponding pH value of the reactant solution is in the range of 10.86-11.21 and remains unchanged over one experiment because of the large excess of hydrazine. The amount of hydrogen peroxide was measured by weighing the syringe before and after hydrogen peroxide addition. Temperature was controlled at 25.0±1.0ºC. Each run was repeated 3-5 times by adding hydrogen peroxide solution to the same batch of hydrazine and additives solution. The concentration of the stock hydrogen peroxide was measured following ISO7157.

To understand the effect of the side reactions, the decomposition of hydrazine and hydrogen peroxide were also investigated, respectively. The relevant experimental procedures were similar to that described above. Hydrazine or hydrogen peroxide was added into the reactor together with water and catalysts. The pressure change was recorded to follow the reaction course.

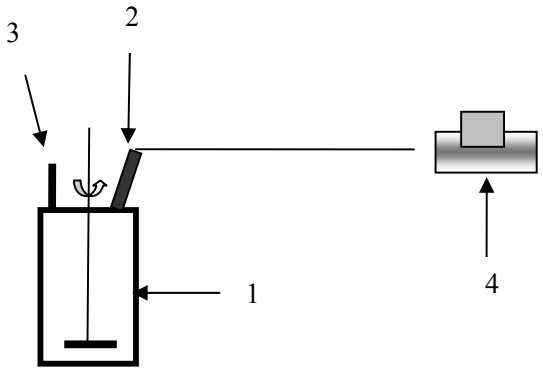

Figure 5-1: Schematic diagram of the pressure build-up instrumental setup

1: high-pressure reactor, Parr Instrument Company;

2: Pressure sensor, 0-500 psi

3: Hydrogen peroxide addition port with valve;

4: computer

5.3 : Results and discussion

5.3.1 : The significance of the side reactions

In order to correlate the nitrogen production with the reactions, the kinetics of the side reactions ((5-3) and (5-6)) were examined respectively before the detailed experiments were carried

out for the kinetic performance of the reaction (5-1). The gas production rates of reaction (5-3) and (5-6) can be expressed as:

$$r_{N_2H_4de} = \frac{d[N_2]}{dt} = -\frac{1}{3}\cdot\frac{d[N_2H_4]}{dt} = k_{N_2H_4de}\cdot f_{N_2H_4de}([cat],[N_2H_4]) \quad (5\text{-}7)$$

$$r_{H_2O_2de} = \frac{d[O_2]}{dt} = -\frac{1}{2}\cdot\frac{d[H_2O_2]}{dt} = k_{H_2O_2de}\cdot f_{H_2O_2de}([cat]),[H_2O_2]) \quad (5\text{-}8)$$

The experimental conditions and the reaction rate ($r_{N_2H_4de}$) for (5-6) are summarized in Table 5-2.

Table 5-2: Decomposition rate of hydrazine

$[N_2H_4]$ (M)	**Catalyst**	**[Cat] (10^{-5}M)**	$r_{N_2H_4de}$ **(10^{-8}M/s)**
2.70	None	0.00	0.880
2.70	aqu-Cu^{2+}	22.7	4.22
3.20	Cu^{2+}-EDTA	4.05	1.76
3.07	Cu^{2+}-EDTA, + Fe^{2+}-EDTA	3.89 5.07	1.54
2.75	Fe^{2+}-EDTA	6.85	2.22

The decomposition of hydrogen peroxide is first-order with respect to $[H_2O_2]$ as seen from the oxygen generation curve. The first order rate constant ($k_{H_2O_2de}$) and half-life ($t_{1/2}$) of reaction (5-3) are shown in Table 5-3. The results indicate that reaction (5-3) and (5-6) are very slow under the experimental conditions employed in the present study.

Table 5-3: Decomposition rate of hydrogen peroxide

Catalyst (T= 40 ºC)	$k_{H_2O_2de}$ **(s^{-1})**	**$t_{1/2}$ (hr)**
None	1.950×10^{-6}	98.7
1.067×10^{-5} M of Cu^{2+}-EDTA	4.819×10^{-6}	40.0

It will be confirmed from the data below that the rates for reaction (5-3) and (5-6) are negligible when compared with that of the reaction (5-1). The stoichiometry observed follows (5-1) very well for all the experiments, i.e. 2 mol of H_2O_2 produce 1 mol of N_2.

5.3.2 : Catalytic behavior

Experiments were run with different levels of [N_2H_4] and [catalyst]. Assuming reaction (5-3) and (5-6) are negligible; reaction (5-1) shows first-order behavior with respect to [H_2O_2] in all the runs. Figure 5-2 provides a typical nitrogen production curve and its first-order fitting. The kinetic equation for this process can be described by:

$$r_1 = -\frac{d[H_2O_2]}{2dt} = \frac{d[N_2]}{dt} = k_1 \cdot f([Cat],[N_2H_4]) \cdot [H_2O_2] \propto k_m \cdot (P_{N_2T} - P_{N_2}) \qquad (5\text{-}9)$$

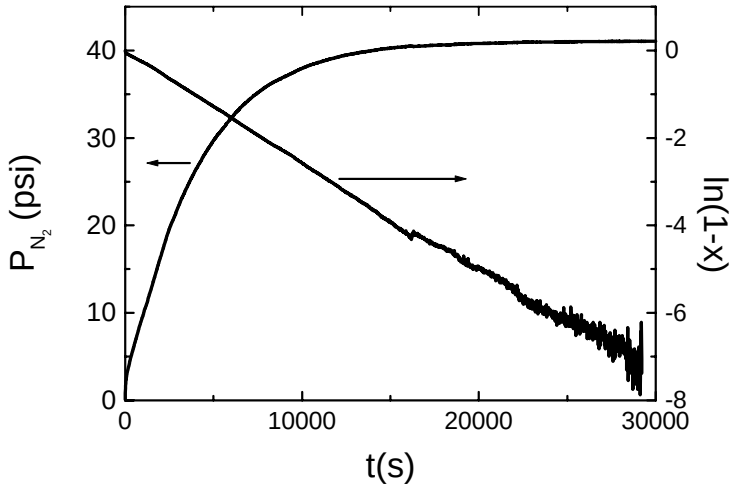

Figure 5-2: Pressure build-up curve for the reaction between hydrazine and hydrogen peroxide without catalyst ([N_2H_4] =1.49 M, [H_2O_2]$_0$= 0.027 M, T=25.0 °C)

The combined experimental rate constant k_m is used in formulating the reaction rate. A detailed investigation has been carried out and the obtained k_m values for various catalytic systems used are listed in Table 5-4. The k_m in Table 5-4 is much higher than the corresponding kinetic constants in Table 5-2 and Table 5-3; therefore, the assumption that reaction (5-3) and (5-6) are negligible is valid.

The data in Table 5-4 indicate that [Cu^{2+}-EDTA] is quite active as a catalyst. However, Cu^{2+} is unstable during the course of the reaction and is readily reduced by hydrazine to Cu^0. Cu^0 can form aggregates and results in a loss of catalytic activity. Although the aggregation process cannot be observed when the concentration of cupric ion is in the normal catalytic range used in the experiments, it can be clearly observed at higher concentration range of cupric ion [52]. Even a 1:1 mole ratio of EDTA/ Cu^{2+} cannot protect cupric ion from being reduced by hydrazine. Hydrogen peroxide helps to remove the ligand (as hydrogen peroxide is stronger than EDTA as a ligand [52]). The addition of hydrogen peroxide recovers part of the activity by oxidizing and solubilizing the catalyst. Higher [H_2O_2] gives higher k_m (refer to No. 3a, b, c in Table 5-4). k_m tends to be larger at the beginning of the reaction (see Figure 5-3). Because of the instability of this catalyst, the kinetics cannot be measured accurately. Therefore $t_{1/2}$ is used as an approximate indication of the reaction rate.

Table 5-4: Reaction rate between hydrazine and hydrogen peroxide

No.	$[N_2H_4]_0$ (M)	$[H_2O_2]_0$ (M)	Catalyst	[cat] (M)	k_m (10^{-3} s^{-1})	$t_{1/2}$ (s)
5-1	1.57±0.08	0.027	None	0	0.1735	4000
5-2	1.59±0.03	0.029~0.06	Cu^{2+}-EDTA	1.54×10^{-5}	not available (N/A)	~70
5-3a	1.47	0.027		1.72×10^{-5}	N/A	~70
5-3b	1.41	0.073		1.72×10^{-5}	N/A	~60
5-3c	1.35	0.110		1.72×10^{-5}	N/A	~40
5-4	1.47	0.028	Cu^{2+}-EDTA + SDS (0.5g/200ml)	2.01×10^{-5}	5.94	117
5-5	1.50	0.028	Cu^{2+}-EDTA + Gelatin 1.1g/200ml	1.37×10^{-5}	1.30	533
5-6	1.48	0.027	Cu^{2+}-EDTA + Gelatin 5.0g/200ml	7.0×10^{-6}	1.4	495
5-7	1.82±0.09	0.027	Boric acid	0.0606	3.80	182
5-8	1.07±0.05	0.028		0.0607	1.62	427
5-9	0.878± 0. 09	0.028		0.0594	2.20	315
5-10	0.620	0.029		0.0628	1.1	660
5-11	1.81±0.04	0.029		0.00479	2.25	308
5-12	1.83±0.07	0.028		0.0225	2.57	270
5-13	1.05	0.0269	NaH_2PO_4	0.0513	0.058	11880

The present kinetic investigation was aimed at understanding hydrogenation behavior of the reaction on polymer latex. The effect of surfactants which were normally present in latex was therefore also examined. The data (nos. 3a and 4 in Table 5-4) show that the use of the anionic surfactant SDS does not reduce the activity of cupric ion.

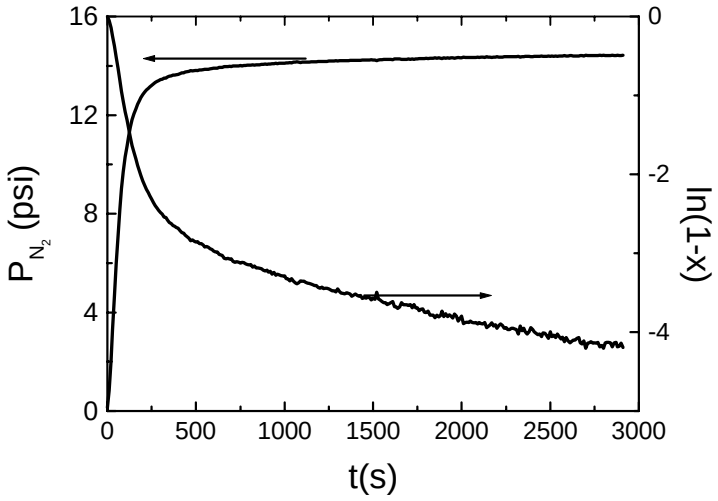

Figure 5-3: Pressure build-up curve for the reaction between hydrazine and hydrogen peroxide catalyzed by Cu^{2+}-EDTA and its first-order fitting ($[N_2H_4]$=1.41±0.06 M, $[H_2O_2]_0$= 0.027M, T=25.0 °C, $[Cu^{2+}\text{-EDTA}] = 1.72\times10^{-5}$ M)

Gelatin was normally selected to inhibit the catalytic effect of trace amount metal ions on hydrazine oxidation by oxidant reactants in the hydrazine production process [43]. The amino group in gelatin is highly active as a ligand to stabilize cupric ion. The stabilized cupric ions show a steady activity over the course of the reaction and the results showed good reproducibility (nos. 5 and 6). On the other hand, gelatin may reduce the availability of coordinate sites on cupric ions by complexing and therefore reduce the turn-over rate of the catalyst.

Boric acid promotes the reaction according to the results shown in Table 5-4. The underlying mechanism for this phenomenon is unclear. Hydrazinium ion ($N_2H_5^+$) was formerly proposed as the reactive form of hydrazine for the oxidation of hydrazine [53]. The present investigation does not support this mechanism. Following this mechanism, sodium orthophosphate should behave in a similar manner as boric acid in promoting the disassociation of hydrazine (5-10) and accelerating reaction (5-1), which is contradicted by the result of Run 13. The result implies that the promoting ability of boric acid is unique, and is not shared with other weak acids. This comparison suggests that $N_2H_5^+$ may not be the reactive form of hydrazine, or that it is not involved in the rate-determining step of reaction (5-1).

$$N_2H_4 + H_2O \longrightarrow N_2H_5^+ + OH^- \qquad (5\text{-}10)$$

Similar to the case of "without catalyst", the reaction with boric acid did not reproduce very well when different batches of reactants were used. However, reasonable reproducibility was observed in the case of the cupric-ion-catalyzed reactions. This phenomenon suggests that the real form of catalyst in the two cases is metal ion residual in the reaction system. However, the catalytic effect of the metal residuals is not significant compared with the relatively large amount of cupric ion added. Without added cupric ion, the trace amount of metal ion provides all the activation centers for the reaction. The introduction of any impurities may cause significant rate fluctuations.

5.3.3 : Effect of $[N_2H_4]$

Reaction (5-1) is faster at higher levels of $[N_2H_4]$, as shown by the results provided in Figure 5-4. $k_m/[N_2H_4]$ is approximately constant at different levels of $[N_2H_4]$ (see Figure 5-5), i.e. reaction (5-1) is first-order with respect to $[N_2H_4]$. As an example, the reaction rate is

$$r_{redox} = 0.001881[N_2H_4][H_2O_2], \quad ([H_3BO_3] = 0.0604M, T = 25.0^\circ C) \tag{5-11}$$

However, when hydrazine was further added to the reaction system which had been run once for the reaction, the reaction rate did not change as shown by the results provided in Table 5-5. Run 15 in Table 5-5 was carried out wherein further hydrazine was added to the remains from run 14. The same procedure was followed for runs16 and 17. Additional hydrazine did not increase the reaction rate. The observed phenomenon is considered to be the overall result of the balance between higher $[N_2H_4]$ and lower concentration of the catalytic entity. The real form of catalyst appears to be the trace amount of metal ions soluble in the solution. As more hydrazine is added, the solubility of the catalytic substances decreases.

Table 5-5: Effect of adding hydrazine on the reaction between hydrazine and hydrogen peroxide as catalyzed by boric acid

No.	$[N_2H_4]_0$ (M)	$[H_2O_2]_0$ (M)	$[H_3BO_3]$ (M)	k_m (10^{-3} s^{-1})	$t_{1/2}$ (sec)
5-14	0.961	0.0282	0.207	1.56	444
5-15	1.69	0.0278	0.195	1.52	456
5-16	0.64	0.0283	0.0626	1.15	603
5-17	1.24	0.0276	0.0603	1.03	673

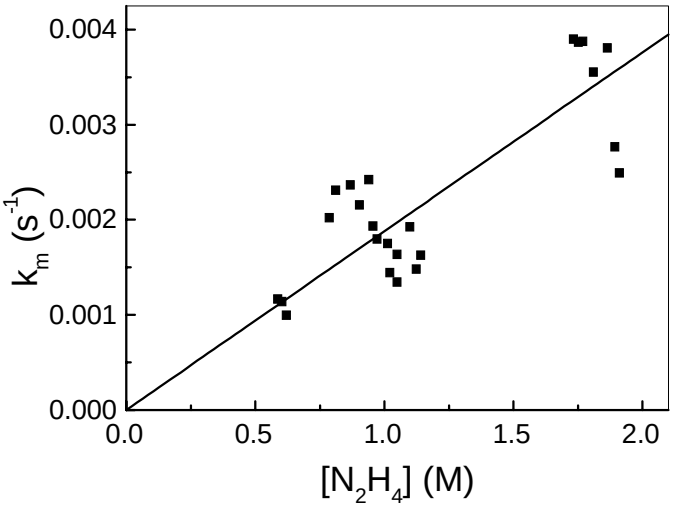

Figure 5-4: Effect of $[N_2H_4]$ on the reaction between hydrazine and hydrogen peroxide ($[H_3BO_3]$ = 0.06 M, $[H_2O_2]_0$=0.03 M, T=25 °C)

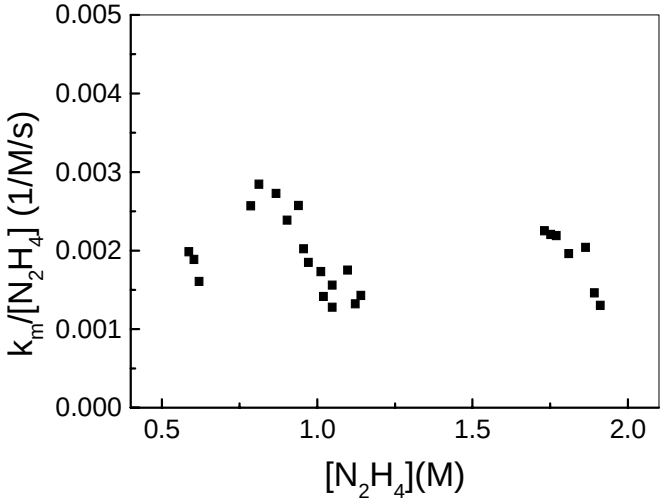

Figure 5-5: $k_m/[N_2H_4]$ versus $[N_2H_4]$ for the reaction between hydrazine and hydrogen peroxide as catalyzed by boric acid ($[H_3BO_3]$=0.06 M, $[H_2O_2]_0$=0.03 M, T=25 ° C)

5.3.4 : Effect of boric acid

The effect of boric acid on the reaction was examined using the same procedure as that for $[N_2H_4]$. The results are provided in Table 5-4 (nos. 7, 11, 12). The results shown in Figure 5-6

indicate that the addition of boric acid promotes the reaction. However, there is no proportional relation between $[H_3BO_3]$ and k_m as illustrated in Figure 5-6. The addition of a small amount of boric acid accelerates the reaction by 10 times (compare nos. 1 and 11 in Table 5-4). The increase in reaction rate by a further increase in boric acid concentration fell within the error range of this measurement. Therefore, it appears that the reaction rate is not directly related to $[H_3BO_3]$ (0.005 M~0.023 M).

5.3.5 : Activation energy

Gelatin helps to stabilize cupric ion, which makes the kinetic investigation possible for cupric ion. The nitrogen production curves fit a first-order behavior very well when gelatin is used to stabilize the cupric catalyst. The activation energy of cupric-catalyzed reaction was measured by using gelatin and Cu^{2+}-EDTA together as the catalyst (Figure 5-7). The calculated activation energy is 65.05±2.74 kJ/mol (95% confidence). The activation energy of the boric acid promoted reaction is 35.86±0.75 kJ/mol (95% confidence; Figure 5-8). This difference in activation energy shows clearly that boric acid provides promoting effect and is actually involved in the rate-determining step.

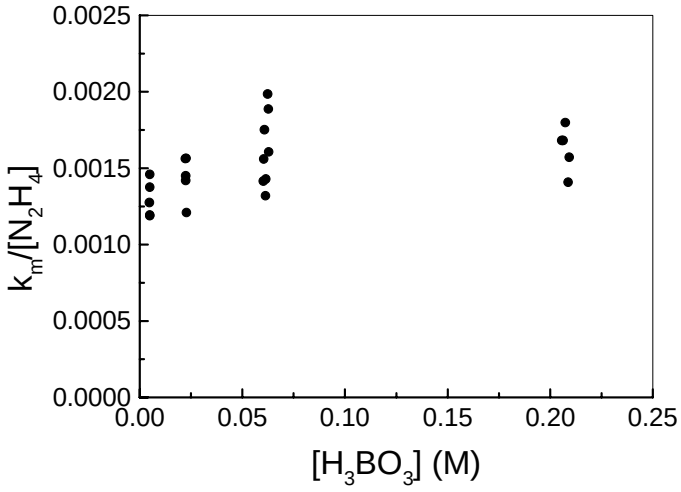

Figure 5-6: Effect of boric acid on the reaction between hydrazine and hydrogen peroxide ($[H_2O_2]_0$=0.03 M, T=25 °C)

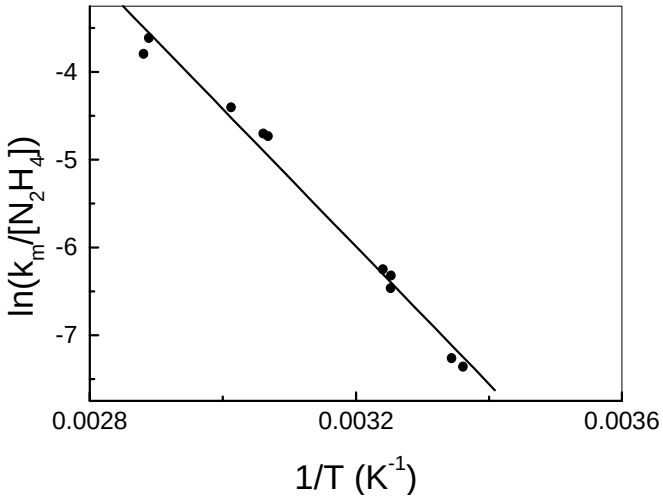

Figure 5-7: Activation energy of the reaction between hydrazine and hydrogen peroxide catalyzed by Cu^{2+}-EDTA (5.0g of gelatin in 200mLof reactants; [Cu^{2+}-EDTA] = 6.89×10^{-6} M, [N_2H_4] = 1.27-1.43 M, $[H_2O_2]_0$= 0.027-0.03M)

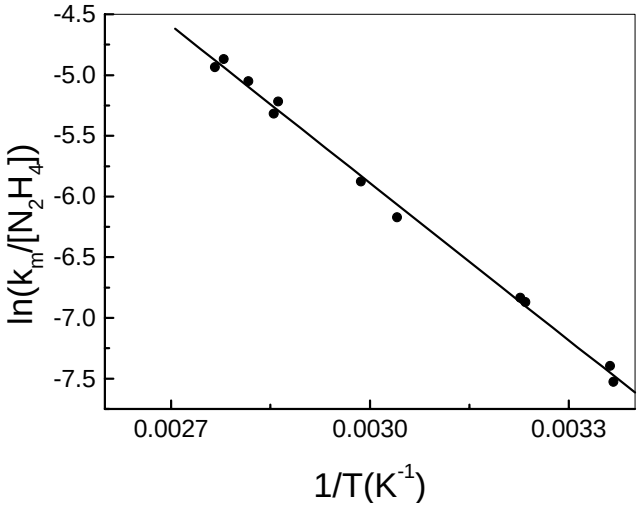

Figure 5-8: Activation energy of the reaction of hydrazine and hydrogen peroxide catalyzed by boric acid ([H_3BO_3] = 0.059 M, [N_2H_4] = 1.9 M, $[H_2O_2]_0$ = 0.027-0.03 M)

5.4 : Summary

The kinetic study provided in this investigation suggests that the redox reaction between hydrazine and hydrogen peroxide is first-order with respect to both reactants over the concentration range investigated ($[N_2H_4]$=0.04-2.0 M, $[H_2O_2]_0$= 0.027-0.6M, 25-75 ºC). Cupric ion is a highly active catalyst; however, since it is not stable in hydrazine, the reaction is difficult to control. Gelatin reduces the catalytic activity of cupric ions possibly by complexing with cupric ions and reducing the efficiency of the cupric ions for catalyzing the reaction. Without an added catalyst, the reaction is believed to be catalyzed by trace amount of residual metal ions in the reaction mixture. Boric acid provides unidentified promoting effects and is involved in the rate-determining step. However, even in the presence of boric acid the actual catalyst should be the trace amount of metal ions. The effect of boric acid and gelatin is significant when they are added at a low level. Further increase in the amount of them does not provide any better control of the reaction rate. The activation energy of the reaction as catalyzed by gelatin complexed cupric ion is 65.05±2.74kJ/mol; When the reaction is promoted with boric acid, the activation energy is 35.86±0.75kJ/mol. Hydrazinium ion does not appear to be the active form of hydrazine in the redox reaction, and does not appear to be involved in the rate-determining step of the reaction.

Remark: A major part of content in this chapter has been published in Ref.[54]

Chapter 6

Reaction of hydrazine and hydrogen peroxide in NBR latex

The kinetics of the reaction between hydrazine and hydrogen peroxide in aqueous solution can be represented as:

$$-\frac{d[N_2H_4]}{dt} = -\frac{1}{2}\frac{d[H_2O_2]}{dt} = k_1[Cat]\bullet[N_2H_4]\bullet[H_2O_2] = k_1 f[H_2O_2] = \frac{d[N_2H_2]}{dt} \qquad (6\text{-}1)$$

It has been shown in Chapter 5 that (6-1) also provides the diimide production kinetics.

In the work described in this chapter, the nitrogen generation rate from the reaction between hydrazine and hydrogen peroxide in NBR latex was investigated. Combining the diimide production kinetics given by (6-1) with the nitrogen generation rate as observed in NBR latex, this investigation aimed to build an understanding of how diimide was utilized in the heterogeneous latex system. Two key parameters were calculated from the nitrogen generation curve, the apparent rate constant (k_m) for nitrogen generation and the percentage of hydrogen peroxide used for saturation of *C*=*C*s (HE).

6.1 : Experimental

An investigation of the reaction kinetics was carried out following the procedure described in Chapter 5. The reaction medium was NBR latex instead of water. The NBR latex provided by LANXESS Inc.(Sarnia, Canada) was used with no modification, except that coagulated rubber mass was removed. The other chemicals used were the same as described in Chapter 5.

The reaction was investigated by batch operation. Controlled amount of NBR latex, catalyst(s) and hydrazine were added into the reactor. After removing oxygen from the reactor and saturating the contents of the reactor by nitrogen, an accurately measured amount of hydrogen peroxide solution was added into the reactor using a syringe. Hydrazine and *C*=*C* were supplied in large excess when compared to hydrogen peroxide so that the changes in [N_2H_4] and [*C*=*C*] would be negligible through the reaction. Therefore, the reaction could be simply repeated by adding another batch of hydrogen peroxide solution into the same batch of initial mixture of hydrazine, latex and catalyst(s). Normally, the same reaction was repeated three times on the same batch of initial mixture by sequentially adding three batches of hydrogen peroxide solution.

6.2 : Reaction course and its interpretation

According to the proposed mechanism for NBR latex hydrogenation (Refer to Chapter 3), if diimide is 100% efficiently used for hydrogenation, the overall hydrogenation reaction would be:

$$N_2H_4 + H_2O_2 + R_1HC = CHR_2 \longrightarrow N_2 + R_1H_2C - CH_2R_2 + 2H_2O \qquad (6\text{-}2)$$

The nitrogen generation curve can be fitted by a first-order kinetic equation since the reaction is first-order with respect to $[H_2O_2]$:

$$P_{N_2} = P_{N_{2T}}(1 - e^{-k_m t}) \quad \text{or} \quad n_{N_2} = n_{N_2 T}(1 - e^{-k_m t}) \tag{6-3}$$

$$x = \frac{n_{N_2}}{n_{N_T}}, \quad \text{and} \quad \ln(1 - x) = -k_m t \tag{6-4}$$

(P_{N2}: the pressure of nitrogen at time t; P_{N2T}: the highest pressure of nitrogen reached by the reaction; k_m: the apparent rate constant; n_{N2}: the amount of nitrogen in mole at time t; n_{N2T}: the total amount of nitrogen generated from the reaction in mole)

Experiments showed that the hydrogenation efficiency was quite high (~ 90%) for the hydrogenation of fresh NBR latex under relatively low levels of $[H_2O_2]$ (<0.03M) (Table 6-3). The overall hydrogenation reaction (some proportion of side reactions may also occur) under similar conditions, therefore, would not depart much from the simplified hydrogenation reaction given by (6-2).

The reaction courses with different catalytic systems were examined by recording the nitrogen generation and fitting it by (6-4). The results are presented below. Without added catalyst, the nitrogen generation curve of the reaction fits first-order kinetics well (as defined by (6-4)) over a major part of the conversion range (Figure 6-1). Cu^{2+}-EDTA and aqueous Cu^{2+} perform similarly as a catalyst for the reaction as seen from the nitrogen generation curves (Figure 6-2 and Figure 6-3). The reaction follows the first-order kinetics fairly well. When boric acid is used as catalyst, the nitrogen generation curve fits the first order kinetics quite well as seen in Figure 6-4.

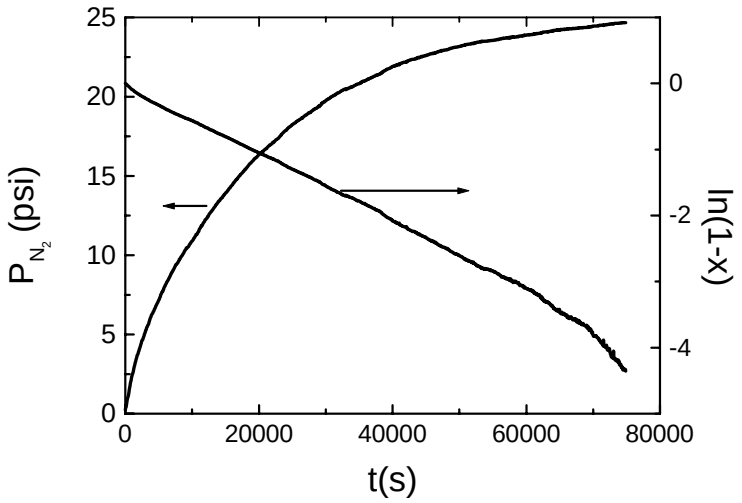

Figure 6-1: Nitrogen generation curve and its first-order interpretation of NBR hydrogenation without catalyst ($[N_2H_4]$ = 1.10 M, $[H_2O_2]_0$ = 0.0832 M, T = 25.0 °C, NBR content: 3.8 wt%)

The experimental results shown above suggest that the nitrogen generation reaction could be represented very well by first-order kinetics under all the catalytic conditions examined. Therefore, first-order rate constants were determined from regression. The apparent rate constants (k_m) were collected as a key parameter for the reaction.

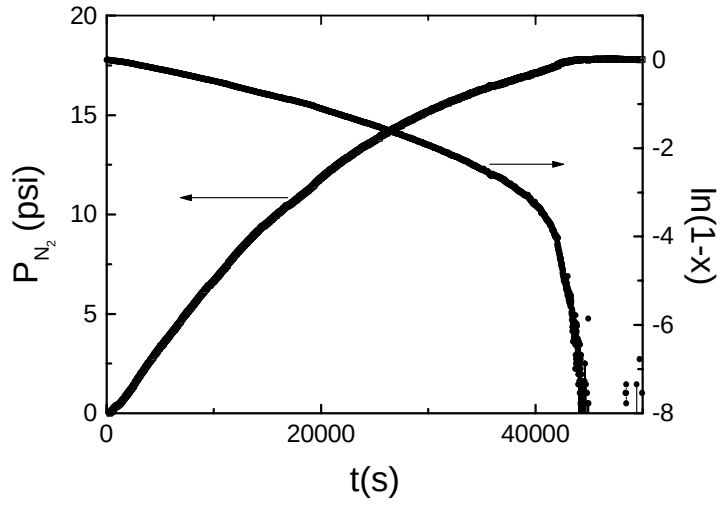

Figure 6-2: Nitrogen generation curve and its first-order interpretation catalyzed by Cu-EDTA ($[N_2H_4]$ = 1.66 M, $[H_2O_2]_0$= 0.0297 M, T= 25 ° C, NBR content: 3.8 wt%)

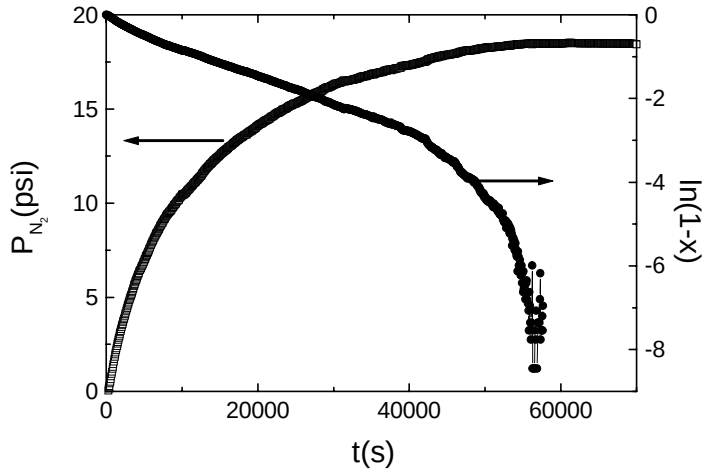

Figure 6-3: Nitrogen generation curve and its first-order interpretation catalyzed by aqueous Cu^{2+} ($[N_2H_4]$ = 1.66 M, $[H_2O_2]_0$= 0.0297 M, T= 25.0 ° C, NBR content: 3.8wt%)

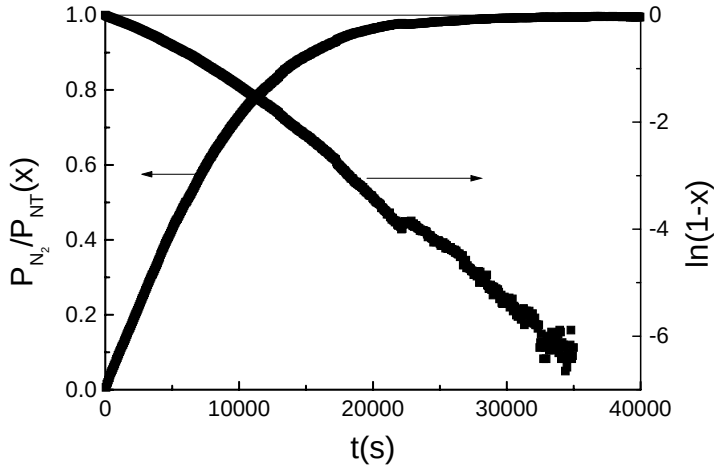

Figure 6-4: Nitrogen generation curve and its first-order fitting of the hydrogenation reaction catalyzed by boric acid ($[N_2H_4]$ = 2.35~2.19 M, $[H_3BO_3]$ = 0.066 M, NBR content: 3.8 wt%, T = 25.0 ºC)

6.3 : Results and discussion: diimide production rate

This investigation began with a single factor examination since preliminary experiments had shown the lack of reproducibility. The experiments were designed to examine the effect of every single factor on k_m by keeping all the other factors at the same level except the factor under examination. The factors examined include: catalyst, catalyst concentration [Cat], initial hydrogen peroxide concentration ($[H_2O_2]_0$), hydrazine concentration ($[N_2H_4]$), solid content, temperature, batches of the latex, and the time the catalyst stays inside the reactant mixture before the reaction.

6.3.1 : Reproducibility of the experiments

As the first step, the reproducibility of the experiment was examined. Two types of reproducibility were checked, the reproducibility of kinetics for runs on the same batch of hydrazine, latex and catalyst(s) mixture and the reproducibility of kinetics for runs on different batches of the mixture with the same composition.

It was found that the kinetics for runs on the same batch of the mixture reproduced very well in each other. However, the kinetics for runs on different batches of the mixture with the same recipe did not reproduce very well. It has been shown in Chapter 4 that the reaction of hydrazine and hydrogen peroxide is very sensitive to catalysis by transition metal ions. The impurities from deionized water and possible contamination at the inner surface of the container used for the reaction were believed to contribute to the rate difference between so called reproducible experiments. Therefore, the following experiments were conducted with a standard rinsing procedure of the reactor and a standard addition sequence. Moreover, experiments were repeated at least once on the same

mixture to minimize experiment error. Reactants were poured directly from the storage bottle to the reaction containers to minimize chemical transfer which may introduce experiment error. Hydrogen peroxide aqueous solution was taken out of the container, measured quickly and added into the reactor immediately. However, the quality of deionized water, especially transition metal ion concentrations, could not be followed in the series of experiments. The agitator was used without being covered, thus the metal surface was still in contact with reactants.

From the results shown in Table 6-1 and Table 6-2 the apparent rate constant, k_m, measured for different batches may vary from each other by as much as 100%. The first run of a batch normally presents higher k_m. Consistent rate readouts have not been achieved. Therefore, this relatively large error range of k_m has to be kept in mind when the reaction rates are compared. This investigation has revealed that the way hydrogen peroxide and catalyst solution were added and dispersed into the system has a strong impact upon catalyst activity. It is believed that this inconsistency in dispersion results in the large error range for k_m.

Table 6-1: Nitrogen generation rate from the reaction between hydrazine and hydrogen peroxide in NBR latex (T=25.0 °C, Solid content = 0.04wt%, $[H_3BO_3]$ = 0.067 M)

No.	Run	$[N_2H_4]$ (M)	$[H_2O_4]$ (M)	HE	k_m (s^{-1})
6-1*	Run 1	1.943	0.0494	0.562	1.721×10^{-4}
	Run 2		0.0472	0.549	1.788×10^{-4}
	Run 3		0.0536	0.481	1.702×10^{-4}
6-2	Run 1	1.981	0.0508	0.514	1.158×10^{-4}
	Run 2		0.0485	0.549	1.074×10^{-4}
6-3	Run 1	1.936	0.0511	0.447	2.532×10^{-4}
	Run 2		0.0601	0.505	1.223×10^{-4}
	Run 3		0.0557	0.490	1.123×10^{-4}
6-4	Run 1	1.967	0.0502	0.564	2.588×10^{-4}
	Run 2		0.0500	0.448	2.198×10^{-4}
	Run 3		0.0574	0.484	2.357×10^{-4}
Average	**$k_m = (1\pm0.46)\times1.77\times10^{-4}$ (s^{-1})**				

* Three runs were carried out on the same fill for all the experiments

Table 6-2: Nitrogen generation rate from the same NBR latex (without added catalyst, T=25.0° C, Solid content = 13.2 wt%)

No.	Run	$[N_2H_4]$ (M)	$[H_2O_4]$ (M)	HE	k_m (s^{-1})
6-5	Run 1	2.068	0.0525	0.349	8.168×10^{-5}
	Run 2		0.0549	0.346	5.500×10^{-5}
	Run 3		0.0535	0.355	4.700×10^{-5}
6-6	Run 1	2.071	0.0545	0.332	9.173×10^{-5}
	Run 2		0.0479	0.356	5.140×10^{-5}
	Run 4		0.0528	0.367	4.318×10^{-5}
Average	$k_m = (1\pm0.49)\times5.97\times10^{-5}(s^{-1})$				

6.3.2 : Catalysis for the reaction

The catalytic conditions compared include: no added catalyst, aqueous Cu^{2+}, Cu^{2+}-EDTA, Cu^{2+}-EDTA plus gelatin, solid cupric oxide, and boric acid. The interference from impurities introduced from sources other than the latex was carefully controlled. k_m and HE are summarized in Table 6-3.

Without added catalyst, the diimide production rate constant k_m ($[N_2H_4] \approx 2.2M$) for the latex reaction is much lower than $k_1 f\ [N_2H_4]$ for the aqueous solution ($4.502\times10^{-5}\ s^{-1}$ in the latex versus $2.43\times10^{-4}\ s^{-1}$ in the aqueous solution). This rate difference sums up the difference in residual catalyst concentration and the difference of reaction volume. The virtually 100% efficiency of diimide to conduct hydrogenation as reported in Chapter 4 firmly supported that diimide could not be generated in the aqueous phase. The diimide generation reaction appears to occur in the interfacial area. It has been mentioned by D. K. Parker, et al [31] that anion surfactants help to keep metal ions at the interface. Hydrogenation of latex with anion surfactants showed improved HE over latex with nonionic surfactants. This observation also suggests that diimide has to be generated at the interface. Catalytic sites concentrate at the interface; their concentration in the aqueous phase would be very low. The total volume of the interfacial area should be much less than the aqueous phase volume.

Table 6-3: Comparison of nitrogen generation from the reaction between hydrazine and hydrogen peroxide with different catalysts (Solid content = 0.04wt%, T=25.0°C)

No.	**Catalyst**	**[Cat] (M)**	**$[N_2H_4]$(M)**	**$[H_2O_2]_0$(M)**	**k_m (10^{-5} s^{-1})**	**HE**
6-7	No alien	0	2.27	0.027	4.50	0.773
6-8	Aqu. Cu^{2+}	1.97E-5	2.27	0.032	8.29	0.725
6-9	Aqu. Cu^{2+}	1.57E-3	2.28	0.027	7.43	0.723
6-10	Cu^{2+}-EDTA	1.52E-5	2.18	0.030	6.06	0.753
6-11	Cu^{2+}-EDTA + gelatin	1.79E-5	2.24	0.029	21.1	0.762
6-12	CuO(s)	N/A	2.06	0.0270	33.2	0.262
6-13	H_3BO_3	0.06068	2.24	0.0296	26.0	0.827

The use of aqueous Cu^{2+} and Cu^{2+}-EDTA did not accelerate the diimide production rate to the same extent as observed in the aqueous system. Basically, aqueous Cu^{2+} and Cu^{2+}-EDTA are ineffective in the latex system, which suggests that the added metal ions are not available for catalysis in the latex system. Coagulation of latex was generally observed with the use of cupric ions. Gelatin helps to retain part of the added metal ions from particle coagulation. Therefore, the use of gelatin together with cupric ion presents a moderate level of catalysis. Solid cupric oxide presented high catalytic activity. But the hydrogenation efficiency was much lower. The combination of a fast reaction rate and a low efficiency suggests diimide is mainly produced at the oxide surface rather than at the rubber particle surface. In this case, diimide would get consumed before it diffuses into the rubber particles. This extremely low efficiency in this case also supports that diimide is generated at the interface for other catalytic conditions which give rise to higher efficiency.

When cupric ion was added after the addition of hydrazine, cupric ion showed a catalytic effect upon the reaction, even though the catalytic activity dropped very quickly. Conversely, when cupric ion was added before the addition of hydrazine, the catalytic effect of cupric ion upon the reaction was totally lost. This phenomenon has not been fully understood. However, it may suggest that the loss of catalyst is probably by way of cupric ion. Hydrazine may complex with cupric ion to solublize it; hydrazine may also reduce Cu^{2+} to Cu^{+} or further to Cu^{0} and make it less likely for cupric ions to coagulate latex particles, since ions with higher valence tend to be more efficient to coagulate latex particles. It is reasonable to conclude here that the coagulation of latex particles tends to cover high valence metal ions and makes them ineffective for catalysis.

We have seen that boric acid provides a higher and more stable rate for the reaction, which makes boric acid the most suitable choice in the latex system for promoting diimide formation. However, how boric acid achieves this promoting effect is still beyond our understanding.

It has been established that boric acid is a promoter rather than the real form of catalyst, and the reaction is catalyzed by transition metal ions. The reaction is very sensitive to catalysis. However,

the addition of transition metal ions in the latex is not as effective as it should be (compare no. 6-8, 6-9 with 6-7 in Table 6-3). Therefore, it was deduced as discussed above that at least part of the added metal ions must be isolated from the reaction by some unknown mechanism. Considering the poor hydrogenation performance of aged NBR latex and coagulation effect of metal ions upon latex, it is believed that a good catalyst for diimide hydrogenation should not cause any reduction of surface area of latex particles and stay in the surface. In case of poor hydrogenation performance, a minimum amount of cupric ion can be added into the latex at very low concentration. Otherwise, the use of boric acid will ensure the best hydrogenation performance.

6.3.3 : Effect of $[H_3BO_3]$ on diimide production rate

As discussed above, the use of boric acid gives rise to the best hydrogenation performance. This promoting effect of boric acid at different concentrations was examined in the latex system (Table 6-4 and Table 6-5).

Table 6-4: Diimide production rate with different concentrations of boric acid (25.0°C, solid content= 13.2wt%, $[H_2O_2]_0 \approx 0.05$ M)

No.	$[H_3BO_3]$(M)	$[H_2O_2]_0$(M)	$[N_2H_4]$ (M)	HE	k_m (s^{-1})
6-6-1	0	0.0545	2.071	0.332	9.173×10^{-5}
6-6-2		0.0479		0.356	5.140×10^{-5}
6-6-4		0.0528		0.367	4.318×10^{-5}
6-14-1	0.065	0.0583	1.974	0.513	2.853×10^{-4}
6-14-2		0.0500		0.595	4.018×10^{-4}
6-14-3		0.0557		0.626	4.854×10^{-4}
6-14-4		0.0438		0.613	5.211×10^{-4}
6-15-1	0.129	0.0507	2.067	0.579	6.153×10^{-4}
6-15-2		0.0547		0.591	7.756×10^{-4}
6-15-4		0.0537		0.584	6.659×10^{-4}
6-16-1	0.218	0.0540	2.014	0.562	5.466×10^{-4}
6-16-2		0.0519		0.591	4.936×10^{-4}
6-16-3		0.0470		0.623	5.036×10^{-4}

Table 6-5: Diimide production rate with different concentrations of boric acid (25.0ºC, solid content: 13.2wt%, $[H_2O_2]_0 \approx 0.006$M)

No.	$[H_3BO_3]$(M)	$[H_2O_2]_0$(M)	$[N_2H_4]$(M)	HE	k_m (s^{-1})
6-6-3	0.000	0.0062	2.071	0.817	4.791×10^{-5}
6-14-5	0.065	0.0062	1.974	1.006	1.908×10^{-4}
6-15-3	0.129	0.0068	2.067	1.010	2.050×10^{-4}
6-16-4	0.218	0.0059	2.014	1.017	1.208×10^{-4}

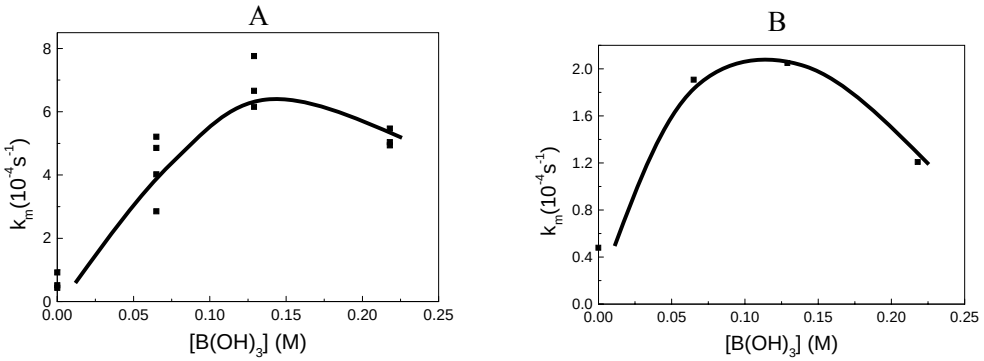

Figure 6-5: The promotion effect of boric acid at different concentrations (25ºC, solid content= 13.2wt%, $[H_2O_2]_0 \approx 0.05$ M for A; $[H_2O_2]_0 \approx 0.006$ M for B)

Based on Figure 6-5, the preferred $[H_3BO_3]$ range would fall into the range of 0.08-0.15M. Further increase in the amount of boric acid would result in the coagulation of latex, and a less effective catalysis would be expected.

6.3.4 : Effect of $[N_2H_4]$ on diimide production rate

It has been shown in Section 6.3.2 that the actual catalyst is only the part that is soluble and therefore accessible metal ions. Hydrazine concentration would have an effect upon the reaction, which was shown to be first-order in Chapter 5. At the same time, the concentration of hydrazine would affect the catalyst concentration. Both effects are summed up together into k_m.

The first order dependence on $[N_2H_4]$ is observed from the results provided in Figure 6-6.

Table 6-6: Diimide production rate at different $[N_2H_4]$ catalyzed by boric acid (25ºC)

	$[H_2O_2]$ (M)	$[N_2H_4]$(M)	$[H_3BO_3]$(M)	Solid content	HE	k_m ($\times 10^{-4} s^{-1}$)
6-17-1	0.0544	5.17	0.067	0.108	0.542	10.14
6-17-2	0.0541				0.549	9.218
6-17-3	0.0545				0.563	1.091
6-18-1	0.0554	3.76	0.066	0.107	0.565	8.970
6-18-2	0.0507				0.549	7.420
6-18-3	0.0553				0.535	7.900
6-19-1	0.0456	2.23	0.070	0.113	0.550	3.243
6-19-2	0.0511				0.589	4.146
6-19-3	0.0544				0.589	2.369
6-20-1	0.0581	1.01	0.066	0.107	0.516	2.045
6-20-2	0.0462				0.584	2.145

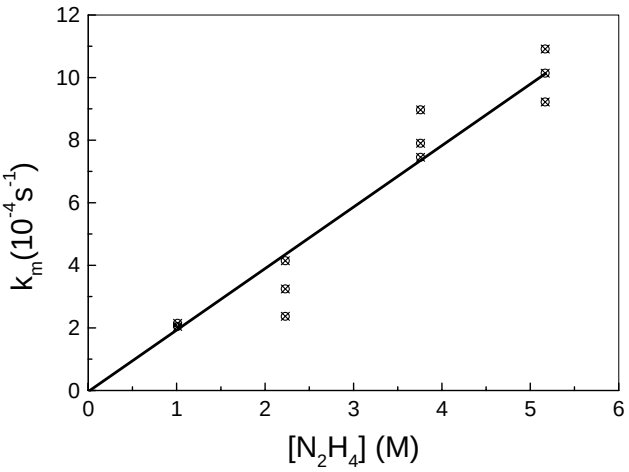

Figure 6-6: The effect of $[N_2H_4]$ on the rate of the reaction between hydrazine and hydrogen peroxide (25.0ºC, solid content= 13.2wt%, $[H_2O_2]_0 \approx 0.05$ M)

6.3.5 : Effect of $[H_2O_2]_0$ on diimide production rate

The effect of $[H_2O_2]_0$ on nitrogen generation rate was examined for the case of the boric-acid-promoted reaction. The nitrogen generation curve fits well to the first-order kinetics as described by (6-3) for a batch reaction, which is observed under different $[H_2O_2]_0$ (Section 6.2). The fitting to first-order kinetics suggests the diimide production is first-order with respect to $[H_2O_2]$. However, the apparent rate constants (k_m) were different at different $[H_2O_2]_0$. In case of the boric acid catalyzed

reaction, the measured k_m is lower when $[H_2O_2]_0$ is lower. Whereas in the case of no added catalyst, k_m is similar at different $[H_2O_2]_0$. In Table 6-7, the ratio of the k_m($[H_2O_2]_0$~0.052M) to the k_m ($[H_2O_2]_0$~0.0061M), defined as $R_{H/L}$, was compared. This ratio $R_{H/L}$ is around 2.2 when $[H_3BO_3]$ = 0.067M, regardless of the solid content and $[N_2H_4]$. The ratio $R_{H/L}$ goes up when $[H_3BO_3]$ goes up.

This comparison supports the postulation about the role of boric acid in this reaction made in Chapter 5, where it was suggested that boric acid served to lower the concentration of hydrogen peroxide. The equilibrium below was proposed:

$$H_3BO_3 + H_2O_2 \Leftrightarrow H_3BO_3 \cdots H_2O_2 \tag{6-5}$$

The formation of hydrogen bonds may increase the activity of hydrogen peroxide toward hydrazine oxidation. The much lower activation energy for the boric acid promoted hydrogenation (Refer to Section 6.3.7) suggests that boric acid should be involved in the rate-determining step which involves coordination of reactants to the catalytic site. At the same time, hydrogen bonds help to reduce the activity of hydrogen peroxide, or to reserve part of hydrogen peroxide from the reaction with hydrazine, which would reduce the chance for hydrogen peroxide molecules to collide with diimide molecules. High HE can then be achieved as a result. This promoting effect would be stronger when $[H_3BO_3]$/ $[H_2O_2]$ is higher.

Table 6-7: Comparison of k_m at different $[H_2O_2]_0$ (25.0ºC)

	$[H_2O_2]_0$ (M)	$[N_2H_4]$ (M)	$[H_3BO_3]$(M)	Solid content	HE	k_m ($\times 10^{-4} s^{-1}$)	$R_{H/L}$
6-5	0.0537	2.068	0.000	0.132	0.347	0.6834	0.9
	0.0107				0.771	0.7804	
6-6	0.0518	2.071	0.000	0.132	0.352	0.6210	1.3
	0.0062				0.817	0.4791	
6-14	0.0520	1.974	0.065	0.132	0.587	4.234	2.2
	0.0062				1.006	1.908	
6-15	0.0530	2.067	0.129	0.131	0.585	6.856	3.3
	0.0068				0.851	2.050	
6-16	0.0510	2.014	0.218	0.130	0.592	5.146	4.3
	0.0059				1.017	1.208	
6-17	0.0543	5.168	0.067	0.108	0.551	10.09	2.1
	0.0065				0.999	5.221	
6-19	0.0504	2.229	0.070	0.113	0.576	3.253	2.1
	0.0064				1.020	1.143	
6-18	0.0538	3.759	0.066	0.107	0.550	11.20	2.4
	0.0067				1.000	5.268	
6-20	0.0522	1.011	0.066	0.107	0.550	2.095	2.4
	0.0067				0.840	0.8901	

6.3.6 : Effect of solid content on diimide production rate

It was suggested that the transition metal residual in the NBR latex is actually the catalyst in this system with boric acid. The nitrogen generation rate at different solid contents (mass percentage of NBR in the reaction system) was measured to test this assumption.

In this comparison, [H_3BO_3] was kept at the same level of 0.067M. k_m was measured at different solid contents when the concentrations of hydrazine and hydrogen peroxide were kept at the same level (See in Table 6-8). According to Figure 6-7, k_m is proportional to the solid content of the reaction system. A rough regression conducted for the data shown in Figure 6-7 gave:

$$k_m = 3.26 \times 10^{-3} \bullet solid\ content\ (s^{-1}) \quad ([H_3BO_3] = 0.067M) \tag{6-6}$$

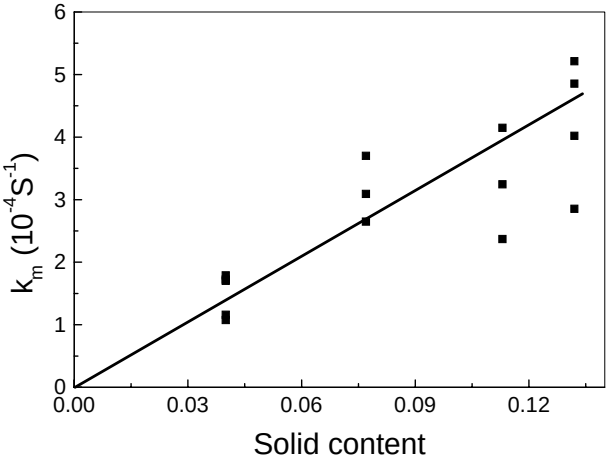

Figure 6-7: Comparison of nitrogen generation rate at different solid content levels (25.0 ºC)

6.3.7 : Effect of temperature on diimide production rate

The effect of temperature on the diimide production rate (see in Table 6-9) was checked by fitting the kinetic data at different temperatures according to the Arrhenius equation. The activation energy embodied in k_m is 64.48 $\pm$2.56 kJ/mol (95% confidence) from fitting (Figure 6-8). k_m includes the effect from [N_2H_4] which is independent of temperature, and also the effect of [Cat] which would not change significantly with temperature. Therefore, the activation energy estimated here is actually the activation energy for the rate constant for the diimide generation reaction. This value is very close to the activation energy measured for gelatin-complexed cupric ion catalyzed diimide production reaction (65.05±2.74 kJ/mol) in the aqueous system, but far different from the activation energy measured for boric-acid-promoted reaction (35.86 ± 0.75 kJ/mol). This inconsistence between the aqueous system and the latex system has not been well explained.

Table 6-8: Comparison of nitrogen generation rate at different solid content levels (T=25.0 ºC)

	$[N_2H_4]$(M)	$[B(OH)_3]$(M)	Solid content	$[H_2O_2]$ (M)	HE	k_m ($\times 10^{-4}$ s^{-1})
6-1-1	1.943	0.066	0.040	0.0494	0.562	1.721
6-1-2				0.0472	0.549	1.788
6-1-3				0.0536	0.481	1.702
6-2-1	1.981	0.067	0.040	0.0508	0.514	1.158
6-2-2				0.0485	0.549	1.074
6-3-1	1.981	0.067	0.040	0.0508	0.514	1.158
6-3-2				0.0485	0.549	1.074
6-4-1	1.967	0.067	0.040	0.0502	0.564	2.588
6-4-2				0.0500	0.448	2.198
6-4-3				0.0574	0.484	2.357
6-21-1	1.901	0.066	0.077	0.0481	0.377	3.700
6-21-2				0.0448	0.551	2.649
6-21-3				0.0512	0.552	3.091
6-19-1	2.229	0.070	0.113	0.0456	0.550	3.243
6-19-2				0.0511	0.589	4.146
6-19-3				0.0544	0.589	2.369
6-14-1	1.974	0.065	0.132	0.0583	0.513	2.853
6-14-2				0.0500	0.595	4.018
6-14-3				0.0557	0.626	4.854
6-14-4			0.132	0.0438	0.613	5.211

Table 6-9: Nitrogen generation rate observed at different temperatures ($[H_3BO_3]$= 0.062M)

No.	$[H_2O_2]_0$(M)	$[N_2H_4]$ (M)	T (ºC)	k_m(s^{-1})	HE (%)
6-22-a	0.028	1.99	22.86	0.000156	91.3
6-22-g	0.029	1.80	23.35	0.00015	84.7
6-23-h	0.026	1.76	23.31	5.91E-05	86.8
6-23-a	0.029	2.24	47.49	0.002042	89.9
6-23-b	0.028	2.21	48.86	0.002195	78.5
6-23-c	0.027	2.17	48.08	0.001849	83.6
6-24-a	0.029	2.05	69.13	0.007122	95.1
6-24-b	0.029	2.02	65.45	0.006111	78.9
6-24-c	0.029	1.98	65.25	0.004885	76.8
6-25-a	0.027	1.95	87.15	0.01011	59.0
6-25-b	0.029	1.91	86.84	0.01785	70.0
6-25-c	0.028	1.88	86.94	0.01685	68.9

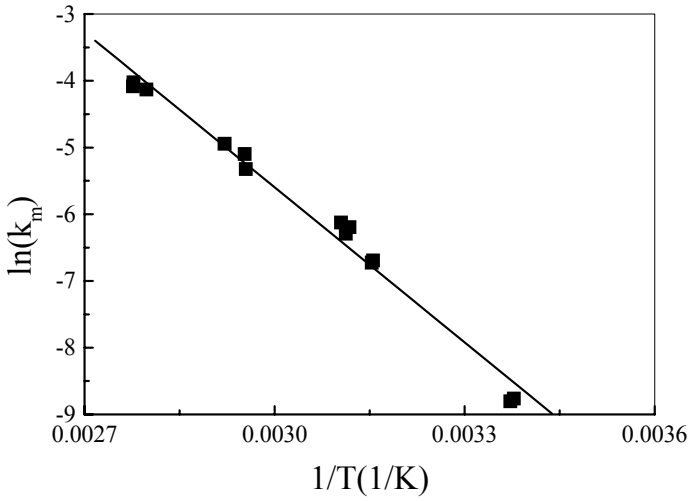

Figure 6-8: Effect of temperature on the reaction rate of the hydrogenation reaction ($[N_2H_4]$= 1.8~2.2M, $[H_2O_2]$ =0.03M; $[H_3BO_3]$ = 0.059M, NBR content: 3.8 wt%)

6.3.8 : Summary

The kinetic investigation provided clarification of the kinetic behavior for the reaction between hydrazine and hydrogen peroxide in NBR latex. The reaction behaves the same in the aqueous system as in the latex system. The diimide generation rate is first order with respect to $[N_2H_4]$ and $[H_2O_2]$ respectively. Generally, transition metal ions are not effective as a catalyst in the latex system, because the metal ions may be isolated from the reactants in the aqueous phase. However, boric acid works efficiently in both systems.

The apparent rate constant for nitrogen generation in NBR latex, k_m, sums up the effects from $[N_2H_4]$, temperature, $[H_3BO_3]$, $[H_2O_2]_0$, solid content, and catalyst. The expression for k_m is given as:

$$k_m = k_1 \bullet f_1(T) \bullet f_2([Cat]) \bullet f_3([H_3BO_3]) \bullet f_4([H_2O_2]_0) \bullet f_5(Solid\ content) \bullet f_6([N_2H_4]) \quad (6\text{-}7)$$

Because boric acid has two functions upon this reaction: the promoting effect on catalysis and the complexing effect upon hydrogen peroxide, this investigation failed to give an accurate and simplified form for (6-7). Calculation of k_m would have to consider the complication of $[H_3BO_3]$ and $[H_2O_2]_0$. The effects from temperature, $[N_2H_4]$ and $[H_2O_2]$ are well documented by this investigation.

6.4 : Results and understanding: hydrogenation efficiency

Hydrogenation efficiency (HE) is defined as the percentage of hydrogen peroxide which is actually used for hydrogenation in the diimide hydrogenation process (refer to Chapter 4). When hydrogen peroxide is totally used for hydrogenation, 1 mol of hydrogen peroxide releases 1 mol of nitrogen. While without hydrogenation, 1 mol of hydrogen peroxide releases 0.5 mol of nitrogen. Therefore, the stoichiometric ratio of H_2O_2 and N_2 can be used to calculate **HE** using:

$$HE = 2 \bullet \frac{mole\_number\_of\_nitrogen\_produced}{mole\_number\_of\_hydrogen\_peroxide\_used} - 1 \qquad (6\text{-}8)$$

The total amount of nitrogen generated from the hydrogenation reaction was recorded and compared with $[H_2O_2]_0$ for different catalysts and different reactant concentrations. The results are presented below. All the data for HE are provided in the corresponding tables in Section 6.3..

The HE includes two parts, the efficiency at the interface and the efficiency in the organic phase. For these pressure-buildup experiments, the amount of hydrogen peroxide used is less than 10% of the amount of *C=C* present. Therefore, the latex is fresh all through the reaction process. As shown in Chapter 4, the HE of fresh latex during the semi-batch hydrogenation is 100%, which suggests that the efficiency in the organic phase is 100% for fresh latex. All the comparisons conducted here are based on this assumption. The measured HE on fresh latex is actually the efficiency at the interface.

6.4.1 : HE for different catalysts

Based on the analysis in Section 6.3, the catalysis of diimide production in latex can be classified into three types, interface catalysis with the promotion of boric acid (boric acid with/without added metal ions), interface catalysis without the promotion of boric acid (with/without added metal ions), and aqueous catalysis (solid metal ion catalyst in aqueous phase). In Table 6-3, the aqueous catalysis gives the lowest HE; the use of boric acid helps to improve HE; the addition of metal ion shows no effect upon HE.

This comparison of HE for different catalysts uncovered the first two competitions mentioned in Chapter 3. The first competition is that between the reaction of hydrazine and hydrogen peroxide in the aqueous part and that in the interface part. Complexed metal ions stay exclusively in the interfacial area with anionic surfactants. The reaction occurs exclusively at the interface, since the uncatalyzed reaction between hydrazine and hydrogen peroxide is much slower than the catalyzed one (refer to Chapter 5). On the other hand, when the catalysts are held back in the aqueous phase, the efficiency would be much lower as was the case with solid metal ion catalysts.

For the metal-ion-catalyzed hydrogenation of fresh latex as conducted in the pressure build-up experiments, the difference on HE is the result of the second competition. This competition is actually the competition between the release rate of diimide from the coordination site and the coordination rate of the second hydrogen peroxide molecule. In Table 6-3, the concentrations of

hydrazine and hydrogen peroxide are at the same level. Therefore, the HE difference would demonstrate the performance of different catalysts on the second competition.

The catalytic substance in situ in the NBR latex may have similar performance on the second competition when compared to cupric ion. However, this benefit was not observed in the semi-batch hydrogenation experiment. This is probably because the catalytic activity and/or the concentration of the catalytic substance are/is lower without adding cupric ion. The slow reaction between hydrazine and hydrogen peroxide compared to the addition rate of hydrogen peroxide would cause hydrogen peroxide to build up. The efficiency decreases as $[H_2O_2]$ increases.

The complexing of a strong ligand such as EDTA or gelatin improves the performance of cupric ion. The presence of large size ligands tends to hamper the coordination of the second H_2O_2 molecule and reduce the chance for diimide to coordinate with hydrogen peroxide molecule.

To summarize, in order to achieve high HE,

(1) the catalyst should stay at the interface exclusively;

(2) the catalyst should be highly active for the reaction between hydrazine and hydrogen peroxide; cupric ion is a good catalyst in this case.

6.4.2 : HE at different $[H_3BO_3]$

$[H_3BO_3]$ at the range of 0.08-0.15M is preferred to achieve high HE. At this concentration range, boric acid provided the best promotion effect and fastest diimide generation reaction is achieved.

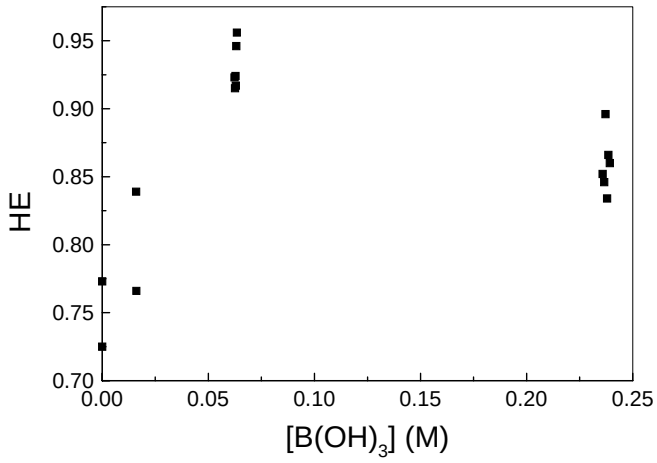

Figure 6-9: HE at different $[H_3BO_3]$ levels ($[H_2O_2]_0 \approx 0.025$ M, $[N_2H_4] = 2.2 \pm 0.1$ M, T=25.0°C)

6.4.3 : HE at different $[N_2H_4]$

Table 6-6 shows that HE is still at the same level when $[N_2H_4]$ goes up from 1.01 M to 5.17 M. However, it was observed in Chapter 2 that higher $[N_2H_4]$ tended to give higher HE. Actually, in that case, $[N_2H_4]$ shows effects upon HE through reducing $[H_2O_2]$. In the semi-batch hydrogenation experiment, higher $[N_2H_4]$ would keep $[H_2O_2]$ at a lower level and as a result HE is higher.

6.4.4 : HE at different $[H_2O_2]_0$

HE at different $[H_2O_2]_0$ was measured and summarized in Table 6-10.

It was observed that HE decreased as $[H_2O_2]_0$ increased. HE was actually 100% when $[H_2O_2]_0$ was less than 0.009M. The HE data are illustrated in Figure 6-10.

Table 6-10: HE at different $[H_2O_2]_0$ ($[N_2H_4]$=2.2M, $[H_3BO_3]$ = 0.060M, T=25.0ºC)

No.	**$[H_2O_2]_0$(M)**	**HE**
6-26	0.237	0.402
6-27	0.190	0.476
6-28	0.0728	0.701
6-29	0.0296	0.827
6-30	0.00861	1
6-31	0.004	1

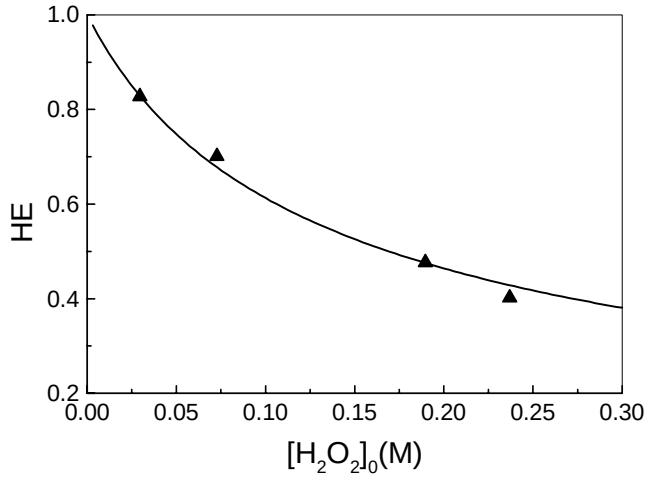

Figure 6-10: HE at different $[H_2O_2]_0$ ($[N_2H_4]$ = 2.2 M, $[H_3BO_3]$ = 0.060 M, T = 25.0ºC)

These results are in accord with the proposed mechanism in Chapter 3. The decrease in HE results from the competition of hydrogen peroxide for diimide. Because of interfacial catalysis, diimide is generated from the catalytic site at the interface, and has a strong tendency to diffuse into

the organic phase. Even so, the presence of hydrogen peroxide around the catalytic site has the potential to capture part of the diimide produced. Lower $[H_2O_2]$ would give diimide more chance to diffuse into the rubber phase and to achieve higher HE.

6.4.5 : HE at different temperatures

The results presented in Table 6-9 indicate that HE decreases as the reaction temperature increases. The effect is not as strong as that from increasing $[H_2O_2]_0$. When the reaction temperature increases from 23ºC to 87ºC, HD decreases from 87% to 67%. It is hard to explain the exact reason from this efficiency drop other than an increase in the undesirable reaction between hydrogen peroxide and diimide.

6.4.6 : HE at different solid contents

The solid content results presented in Table 6-8 are widely dispersed. However, it can be deduced that the solid content does not have any major effects upon HE.

6.4.7 : HE at different HD levels

In this experiment, the same pressure build-up experiment was repeated on the same batch of latex by adding the same amount of hydrogen peroxide into the latex when the first batch of hydrogen peroxide was totally consumed. HD increased slowly as more runs were conducted on the same latex. In the following runs, the latex was not fresh anymore, the measured HE would be the combination of HE_{org} and HE_{aqu}.

The results in Figure 6-11 and Figure 6-12 show that HE tends to decrease when HD is over 35%. Below 35% HD, the HE remains at the same level.

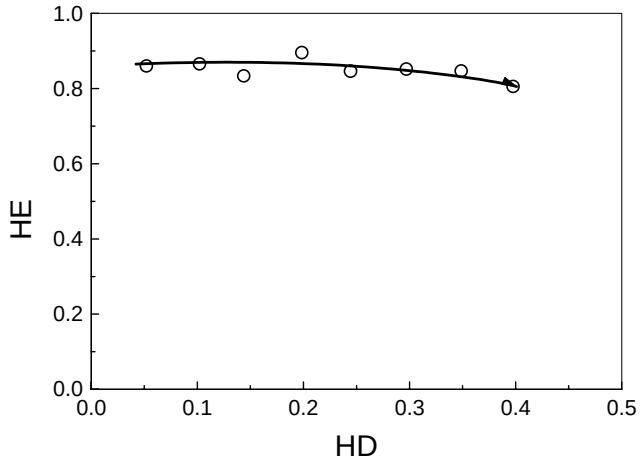

Figure 6-11: Decrease of HE at increasing HD ($[H_2O_2]_0 \approx 0.025M$, $[N_2H_4]=2.23\pm0.12M$, $[H_3BO_3]=0.24M$, T=25.0ºC)

When the HD became higher, HE decreased sharply (Figure 6-12). Basically, this phenomenon is quite similar to that for the semi-batch hydrogenation experiment.

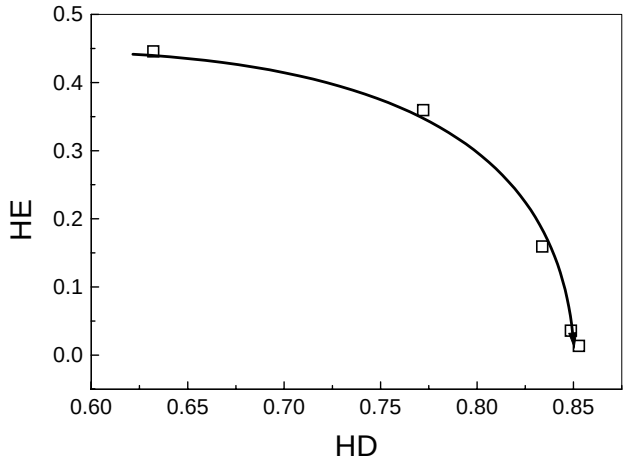

Figure 6-12: HE versus HD at high HD range ($[H_2O_2]_0 \approx 0.18M$, $[N_2H_4]=1.7\pm0.5M$, $[H_3BO_3]=0.20M$, T=25.0ºC)

6.4.8 : Summary

Based on the results of this investigation, it can be concluded that HE is mainly controlled by type of catalyst, $[H_2O_2]_0$, and HD. Solid content of the latex and the concentration level of hydrazine have little if any influence on HE. When high HE is desired, lower temperature, lower $[H_2O_2]_0$, and the use of boric acid as promoter are suggested. HE decreases significantly at higher HD.

6.5 : Comparison of the redox reaction in aqueous solution and in NBR latex

The presence of two phases in the latex system separates the diimide generation step from the diimide utilization step. This separation makes it possible for diimide to conduct hydrogenation. In order to achieve hydrogenation, diimide has to be generated at the interface and diffuse into the rubber phase immediately. Measures have to be in place to make it impossible for diimide to meet hydrogen peroxide.

The catalysts perform similarly for both systems except that catalysts in the latex system tend to be concealed by rubber from the reaction. For hydrogenation, the catalyst has to stay at the interface, be stable and selective.

Chapter 7
Hydrogenation of *C*=*C*s by Diimide

The reaction of diimide with *C*=*C*s is the central reaction in this latex hydrogenation process. However, it seems impossible to isolate this reaction and investigate it. In this chapter, the reaction rates of internal *C*=*C*s are compared with that of the vinyl group.

7.1 : Results from the literature

There are limited data regarding the reaction of diimide toward *C*=*C*s. Mango and Lenz [28] showed semi-quantitatively the relative rates of hydrogenation for *cis*-, *trans*- and vinyl butene units were in the order $k_{cis} \approx k_{trans} < k_{vinyl}$. However, the exact values of the ratios between these parameters were not available from Mango's study due to measurement error. Ratnayake, et al [27] showed $k_{vinyl}/k_{cis} = 5.8$ when the diimide hydrogenation rates of the vinyl group (end *C*=*C*) and the internal *cis*-*C*=*C* on C_{16}-C_{20} fatty acid chains were compared. However, this data may not be accountable for the hydrogenation of *C*=*C*s on polymer chains. The present work was carried out in an attempt to provide an accurate estimation of the reaction rates of different *C*=*C* toward diimide both in the homogeneous organic solution and in the heterogeneous latex system.

7.2 : Experimental

The apparatus used for the homogeneous hydrogenation experiments was similar to that used by Stephen F. Hahn [22]. *P*-TSH (>99.0%) was purchased from Aldrich Chemical Co. poly(acrylonitrile-co-butadiene) (NBR) with an acrylonitrile (AN) content of 38.5 wt% was provided by Bayer Inc. (Sarnia, Canada). Prior to carrying out hydrogenation experiments, 3.0g of NBR was dissolved in 300 mL of chlorobenzene and stored overnight. Upon complete dissolution of the NBR, the solution was purged with dry nitrogen and then heated. When the vessel began to reflux, 11.8g of TSH was added to the solution, which was then kept under a positive pressure of nitrogen and refluxed for 2 hours. Samples were taken at 15 minute intervals. The polymer samples were isolated by adding ethanol into the sample solutions, re-dissolving in acetone and re-precipitating by addition of ethanol. The washed samples were dried under vacuum at room temperature overnight and then dissolved into *D*-chloroform. These *D*-chloroform solutions of the sample polymers were subjected to ^{1}H-NMR and FT-IR. ^{1}H-NMR spectra were obtained using an Avance300 spectrometer. FTIR analyses were obtained from film cast on KBr windows using a Bio-Rad FTS 3000MX spectrometer.

The hydrogenation of NBR latex was conducted following the procedures described in Chapter 4. NBR latex, hydrazine hydrate (~99.0%), aqueous hydrogen peroxide (29.0~32.0 wt%) , and boric acid are from the same source as described in Chapter 4. Samples were taken from the reactor, precipitated by mixing with ethanol, washed using ethanol, and vacuum dried for 12 hours.

7.3 : Analysis methods

7.3.1 : The rationale for the kinetic analysis

NBR hydrogenation by TSH can be expressed as:

NBR+TSH → HNBR + *p*-toluenesulfinic acid (7-1)

Nang, et al [30] showed that the kinetics of reaction shown in (7-1) can be represented as

Rate of hydrogenation = rate constant [Polymer] [TSH] (7-2)

There are two steps for the overall reaction of (7-1), the decomposition of TSH to generate diimide and the hydrogenation of *C*=*C*s with diimide. The hydrogenation of the vinyl *C*=*C* and the internal *C*=*C* can be described by (7-3) and (7-4) respectively:

$N_2H_2 + R\text{-}CH{=}CH_2 \rightarrow N_2 + R\text{-}CH_2\text{-}CH_3$ (7-3)

$N_2H_2 + R_1\text{-}CH{=}CH\text{-}R_2 \rightarrow N_2 + R_1\text{-}CH_2\text{-}CH_2\text{-}R_2$ (7-4)

A well defined kinetic description of reaction (7-3) and (7-4) is not available in the literature. It is reasonable to assume that reaction (7-3) and (7-4) are elementary reactions as suggested in the references [30, 55, 56]. The two reactions involve the actual coordination step for the hydrogenation. Diimide is an active intermediate which coordinates with a *C*=*C* and releases two hydrogen atoms to the *C*=*C*. The rate law of reaction (7-3) and (7-4) can be expressed as

$$\frac{d[C=C]_{vinyl}}{dt} = -k_{vinyl}[N_2H_2][C=C]_{vinyl} \quad (7\text{-}5)$$

$$\frac{d[C=C]_{trans}}{dt} = -k_{trans}[N_2H_2][C=C]_{trans} \quad (7\text{-}6)$$

The fractional hydrogenation conversion for the vinyl group, X_{vinyl}, is defined as

$$X_{vinyl} = 1 - \frac{[C=C]_{vinyl}}{[C=C]_{vinyl0}} \quad (7\text{-}7)$$

A similar definition,

$$X_{trans} = 1 - \frac{[C=C]_{trans}}{[C=C]_{trans0}} \quad (7\text{-}8)$$

can be used for *trans*- *C*=*C* hydrogenation conversion. As diimide is a very active intermediate, it can be assumed that Pseudo-steady-state hypothesis be valid for the concentration of diimide in the system, then reaction (7-3) and (7-4) would become first-order reactions with respect to *C*=*C*.

On combining (7-5) with (7-7) and (7-6) with (7-8), the relations shown in (7-9) and (7-10) are obtained respectively.

$$\ln(1 - X_{vinyl}) = -k_{vinyl}[N_2H_2] \bullet t \quad (7\text{-}9)$$

$$\ln(1 - X_{trans}) = -k_{trans}[N_2H_2] \bullet t \quad (7\text{-}10)$$

(7-9) and (7-10) can be used to compare the hydrogenation rate of the vinyl group with that of the internal *C=C*.

7.3.2 : Measurement of *C=C* conversion by ^{1}H-NMR spectrum

The polymer chain of partially hydrogenated NBR includes four characteristic groups: internal -*C=C*-, vinyl -*C=C*H_2, saturated hydrocarbon structure, and nitrile. The structures of the four groups are illustrated in Scheme 1 together with the symbols for their average percentages in the molecule.

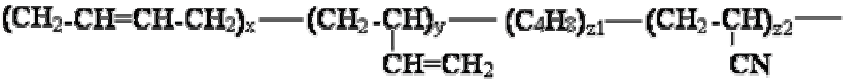

Scheme 1

To facilitate the analysis below, in the ^{1}H-NMR spectrum of NBR, the area between 5.2-5.9 ppm was defined as "a", which is correspondent to the proton of $R_1CH=$; the area between 4.9-5.2 ppm as "b", which is correspondent to the protons of $CH_2=$; the area between 0.8-2.8 ppm as "c", which is correspondent to all of the other protons[38]. Based on these assignments, the following relationships are obtained:

$$\frac{a}{a+b+c} = \frac{2x+y}{6x+6y+8z_1+3z_2} \quad (7\text{-}11)$$

$$\frac{b}{a+b+c} = \frac{2y}{6x+6y+8z_1+3z_2} \quad (7\text{-}12)$$

$$\frac{c}{a+b+c} = \frac{4x+3y+8z_1+3z_2}{6x+6y+8z_1+3z_2} \quad (7\text{-}13)$$

where x, y, z_1 and z_2 correspond to the subscripts in Scheme 1. For NBR, when the hydrogenation degree is zero, $z_1 = 0$, and then $x_{(HD=0)}$, $y_{(HD=0)}$ and z_2 can be calculated based on "a", "b" and "c" using (7-11), (7-12), (7-13). z_2 does not change during the hydrogenation. The percentage of each part in a partially-hydrogenated NBR can be calculated using the same method when z_2 is measured. A comparison of "x" or "y" of a partially-hydrogenated NBR with $x_{(HD=0)}$ or $y_{(HD=0)}$ gives conversion of the two types of *C=Cs*.

7.3.3 : Measurement of *C=C* conversion by FT-IR spectrum

The IR spectrum of partial hydrogenated NBR shows peaks at 970 cm^{-1} due to the 1, 4- *trans*-butadiene unit, 915 cm^{-1} due to the vinyl group, and 2236 cm^{-1} due to the nitrile group [38]. The conversion of *trans*- and vinyl groups can be calculated from equations (7-14) and (7-15).

$$x_{trans-} = \frac{S_{970}(sample)/S_{2236}(sample)}{S_{970}(raw\_NBR)/S_{2236}(raw\_NBR)} \tag{7-14}$$

$$x_{vinyl} = \frac{S_{915}(sample)/S_{2236}(sample)}{S_{915}(raw\_NBR)/S_{2236}(raw\_NBR)} \tag{7-15}$$

7.4 : Results and discussion

7.4.1 : Rate comparison of diimide hydrogenation in a homogeneous system

The reaction courses of vinyl and internal *C=C*s were presented in Table 7-1. For the NBR used in the experiment, the percentage of *cis*- *C=C* is quite low. Therefore, the rate for internal *C=C*s is actual the rate for *trans*- *C=C*.

First-order regression according to (7-9) and (7-10) was carried out for the hydrogenation of vinyl and that of *trans*-*C=C* (Figure 7-1 and Figure 7-2). Very good fitting of the data to the kinetics equations was observed as shown in Figure 7-1 and Figure 7-2 when NMR spectra were used to measure the conversions of *C=C*s. However, the estimation of hydrogenation conversion based on FT-IR spectra failed to limit the error below an acceptable level because of the overlap of peaks 970 and 915 cm^{-1}. A similar rate comparison conducted using the conversions calculated based on FTIR spectra did not fit the first-order regression very well. Therefore, the result based on ^{1}H-NMR was adopted to estimate the value of $\frac{k_{vinyl}}{k_{trans-}}$ (See in Table 7-1).

Table 7-1: Conversion of *C*=*C*s in NBR (132ºC, TSH/[*C*=*C*] = 2.0, chlorobenzene as the solvent)

t(min)	^{1}H-NMR			FT-IR		
	Conversion in total	x_{vinyl}	x_{trans}	Conversion in total	x_{vinyl}	x_{trans}
0	0.000	0.000	0	0.000	0	0
15	0.045	0.128	0.037	0.118	-0.029	0
30	0.208	0.515	0.175	0.211	0.218	0.102
45	0.415	0.602	0.396	0.403	0.708	0.361
60	0.598	0.870	0.569	0.572	0.915	0.565
75	0.715	0.932	0.693	0.691	0.995	0.704
90	0.786	1.000	0.763	0.787	1	0.805
105	0.846	1.000	0.829	0.831		

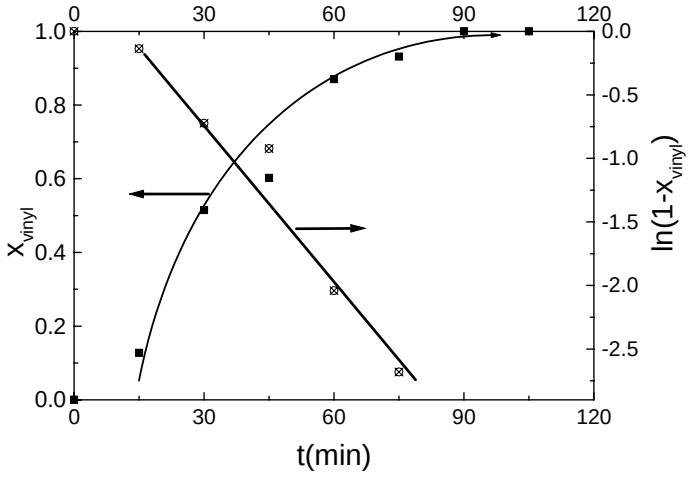

Figure 7-1: Hydrogenation course of vinyl group in NBR by diimide and its first-order fitting (132ºC, TSH/[*C*=*C*] = 2.0, chlorobenzene as the solvent)

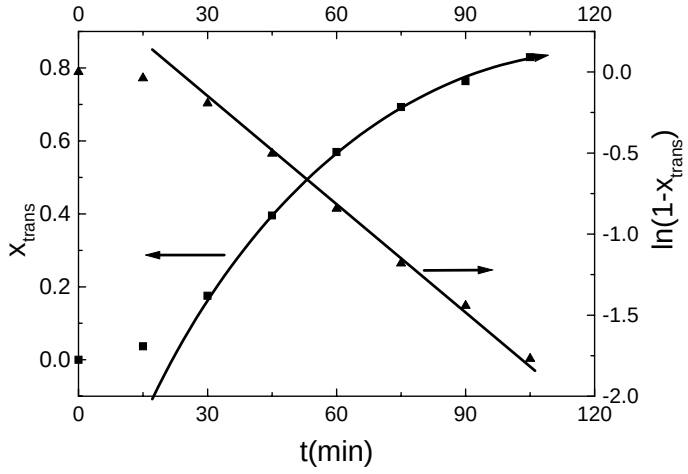

Figure 7-2: Hydrogenation course of *trans*- *C*=*C* group in NBR by diimide and its first-order fitting (132ºC, TSH/[*C*=*C*] = 2.0, chlorobenzene as the solvent)

Table 7-2: Rate ratio of *C*=*C*s to diimide in the homogeneous hydrogenation system

No.	$k_{vinyl}[N_2H_4]$ (s^{-1})	$k_{trans}[N_2H_4]$ (s^{-1})	$\frac{k_{vinyl}}{k_{trans-}}$ (95% confidence)
9-1	7.038×10^{-4}	3.253×10^{-4}	2.16 ± 1.01
9-2	8.257×10^{-4}	3.415×10^{-4}	2.42 ± 0.68

The results show that the hydrogenation rate of vinyl is therefore 2.29 times that of *trans*-*C*=*C*.

$$\frac{k_{vinyl}}{k_{trans-}} = 2.29 \qquad (7\text{-}16)$$

7.4.2 : Rate comparison of diimide hydrogenation in the latex system

The hydrogenation rates of different *C*=*C*s of NBR in a latex system were compared using the same method as detailed above. Hydrogen peroxide was added slowly into the reaction system to ensure no hydrogen peroxide buildup. The concentration of diimide would be stable over the entire process. The typical reaction courses of vinyl and internal *C*=*C*s were recorded in Table 7-3. The presence of *cis*-*C*=*C* is negligible also because the percentage of *cis*- *C*=*C* is quite low in the NBR latex used in the experiment. The rate for internal *C*=*C*s is used as an estimate of that of *trans*- *C*=*C*.

The reaction course of both the vinyl and the *trans*- *C*=*C* fit the first-order regression very well (Figure 7-3 and Figure 7-4). The calculated values of $\frac{k_{vinyl}}{k_{trans-}}$ are summarized in Table 7-4.

Table 7-3: Conversion of *C*=*C*s in NBR (40ºC, $[N_2H_4]/[C{=}C] = 3.0$, $[H_3BO_3]/[C{=}C] = 0.076$, $[N_2H_4]/[H_2O_2] = 1.0$, H_2O_2 (30.47% aqueous solution) added over 6.5 hours)

t (min)	^{1}H-NMR			FT-IR
	Total conversion	x_{trans}	x_{vinyl}	Total conversion
0	0	0	0	0
30	0.127	0.107	0.312	0.105
60	0.255	0.226	0.513	0.187
90	0.377	0.337	0.730	0.326
125	0.506	0.468	0.833	0.424
165	0.639	0.608	0.918	0.508
213	0.761	0.740	0.950	0.696
255	0.833	0.818	0.968	0.788
300	0.884	0.871	1.000	0.864
330	0.908	0.897	1.000	0.891
360	0.928	0.920	1.000	0.921

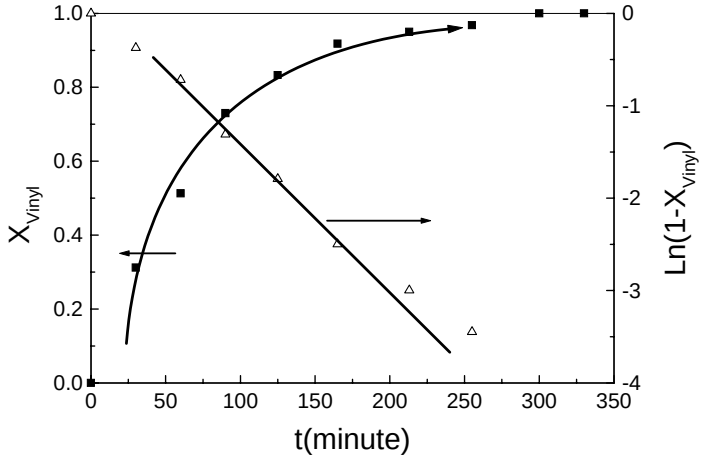

Figure 7-3: Hydrogenation course of vinyl group in NBR latex by diimide and its first-order fitting (40°C, $[N_2H_4]/[C=C] = 3.0$, $[H_3BO_3]/[C=C] = 0.076$, $[N_2H_4]/[H_2O_2] = 1.0$, H_2O_2 (30.47% aqueous solution) added over 6.5 hours)

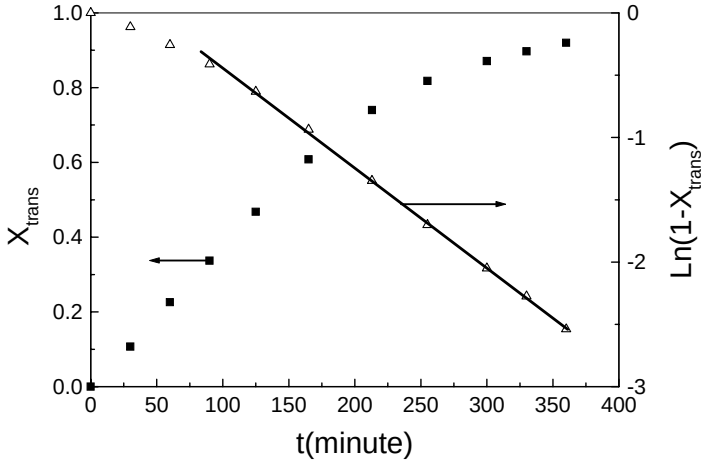

Figure 7-4: Hydrogenation course of *trans*- *C=C* group in NBR latex by diimide and its first-order fitting (40°C, $[N_2H_4]/[C=C] = 3.0$, $[H_3BO_3]/[C=C] = 0.076$, $[N_2H_4]/[H_2O_2] = 1.0$, H_2O_2 (30.47% aqueous solution) added over 6.5 hours)

Table 7-4: Hydrogenation rate ratio of vinyl to *trans-C=C* observed in the diimide hydrogenation of NBR latex

Exp. No.	7-3	7-4	7-5
$[N_2H_4]/[C=C]$	3.0	1.5	1.5
$[H_3BO_3]/[C=C]$	0.076	0.076	0.076
$[N_2H_4]/[H_2O_2]$	2.0	1.0	1.0
Addition time (hours)	6.5	6.5	11.2
$k_{vinyl}[N_2H_2]$ (s^{-1})	2.470×10^{-4}	1.678×10^{-4}	1.090×10^{-4}
$k_{trans}[N_2H_2]$ (s^{-1})	1.190×10^{-4}	7.687×10^{-5}	4.578×10^{-5}
$\frac{k_{vinyl}}{k_{trans-}}$ (95% confidence)	2.08± 0.34	2.18± 0.74	2.38± 0.42

7.5 : Summary

It was shown that different *C=C*s had different reaction activities towards diimide. The rate of diimide hydrogenation of vinyl group was compared to that of *trans- C=C* using ^{1}H-NMR and FTIR. The apparent rate ratio is $\frac{k_{vinyl}}{k_{trans-}} = 2.29$ in the homogeneous solution. The rate ratio as measured in the latex system with a average particle diameter of 72 nm is $\frac{k_{vinyl}}{k_{trans-}} = 2.38$ at $[N_2H_4]/[C=C]$ = 1.5, $[H_3BO_3]/[C=C]$ = 0.076, $[H_2O_2]/[N_2H_4]$= 1.0, H_2O_2 (15.24% aqueous solution) added over 11.2 hours.

However, the rate constant of the diimide hydrogenation can not be measured without measuring the concentration of the intermediate diimide.

7.6 : Analysis of the effect of diimide diffusion upon the diimide hydrogenation process

The reaction rate comparison of different *C=C*s aimed to distinguish the controlling mechanism of the process initially. It was expected that the interference of diffusion would diminish the rate difference between the parallel reactions. However, kinetics deduction suggests that diffusion would only interfere with non-first-order reactions.

The role of diimide diffusion could be shown in a simple reaction, in which bulky NBR was cut into small pieces (3mm×3mm). The NBR particles, surfactant SDS and boric acid were added into water. In this case, the mixture would be similar to a latex with much larger particle size. Diimide hydrogenation was conducted on the mixture following the semi-batch hydrogenation procedures as described in Chapter 4. When the reaction was terminated, NBR particles were taken out the reactor, washed and dissolved in acetone. When the particles were totally dissolved, the overall hydrogenation percentage could not be observed by FT-IR spectrum. However, when the particles were dissolved for only 2 minutes, the IR spectrum of the dissolved part showed a HD above 80%. Comparing the two IR spectra, one would believe that the diimide hydrogenation method could hydrogenate only the very thin layer of the particle surface. The hydrogenation degree overall is negligible. This experiment showed that diimide diffusion was the main resistance in the diimide hydrogenation of particles with a size of 3mm×3mm. Therefore, reducing of the latex particle size would help to improve hydrogenation efficiency. However, this experiment can not show how diimide diffusion affects the hydrogenation of NBR latex with a particle diameter of 72nm.

Chapter 8
Crosslinking mechanism of diimide hydrogenation reaction

Diimide from the thermal decomposition of *p*-TSH was utilized to hydrogenate unsaturated polymers dissolved in organic solvents [18-22]. Diimide from the reaction between hydrazine and hydrogen peroxide was used to hydrogenate unsaturated polymers in latex form [30-37]. However, the hydrogenated rubbers from the two methods are fully crosslinked, and have very poor mechanical properties. It is necessary to restrain the gel formation in the hydrogenation operation before the diimide hydrogenation route can be commercialized.

There is very little discussion in the literature regarding the gel-formation mechanism. Hong-Quan Xie, et al [37] suggested the use of inhibitors both in the rubber phase (as an example, *p*-tert-butylpyrocatechol) and in the aqueous phase (as an example, sodium N,N-dimethyldithiocarbonate) to reduce gel formation. A similar result was also presented by M. De Sarkar [38]. Johannes W. Belt, et al [33] found the use of amines, hydroxylamine, imines, azines, hydrazone, or oximes before, during or after hydrogenation might help to reduce gel content in the hydrogenated rubber. These practices suggest a radical crosslinking mechanism is assumed by the researchers. But, it was observed in G. L. Rempel, et al [46] that the beneficial effect of antioxidant addition was marginal [46].

The purpose of this study is to investigate the gel formation mechanism in diimide hydrogenated polymers. Specially designed reactions have been carried out to check the effects of all the possible reactions involved on the gel generation process.

8.1 : Experimental

The diimide hydrogenation process involves a redox reaction in the aqueous phase, hydrogenation in the organic phase, side reactions, and the mass-transfer of diimide within the organic phase; the reactant hydrogen peroxide is not stable, and the intermediate diimide is highly reactive. All these factors make the study of gel-formation difficult. In this study, an attempt was made to isolate the reactions involved in the diimide hydrogenation process. Systematic experiments were designed to mimic each radical generation situation in the diimide hydrogenation process.

The experiments were conducted in a 500-mL three-necked round-bottom flask equipped with an overhead agitator, a temperature-controlled water bath and a nitrogen inlet tube. Hydrazine hydrate (~99%) and hydrogen peroxide (29.0~32.0%) were purchased from VWR Scientific Products (West Chester, PA). Boric acid was provided by J. T. Baker Company Co.(Phillipsburg, N.J.); sodium dodecyl sulphate (~99%) and styrene (St; ~99%) inhibited by 10~15 ppm 4-*tert*-butylcatechol were purchased from Aldrich Chemical Company, Inc, (Milwaukee, WI); ferrous sulphate (ACS, ~99.0%) was provided by BDH Inc., (Toronto, Canada); formaldehyde sulfoxylate sodium (CH_3NaO_3S; ~97%) was purchased from Fluka Chemical (Buchs, Switzerland). Deionized water was used whenever water was required in the experiments. NBR latex was provided by LANXESS Inc. (Sarnia, Canada)

For emulsion polymerization experiments with St, 100.0g of deionized water and 0.100g of SDS were charged into a flask and were followed by the addition of 10.0g of St and different initiators. The initiation systems included hydrogen peroxide decomposition, the redox reaction between hydrazine and hydrogen peroxide, the redox reaction catalyzed by boric acid, and thermal

initiation. The contents were kept under 40.0 ± 0.1℃ for 8 h under nitrogen protection if not stated otherwise. The conversion of St into polystyrene was determined from the weight of the solid content after polymerization. For the crosslinking experiments with the NBR latex, 100.0g of NBR latex was used.

8.2 : Results and discussion

The hydrogenation reaction of unsaturated polymer latex with diimide can be expressed as follows:

$$N_2H_4 \; + \; H_2O_2 \; + \; -HC=CH- \longrightarrow N_2 + \; -H_2C-CH_2- \; + \; 2H_2O \qquad (8\text{-}1)$$

The reactants involved in this reaction system include hydrazine, hydrogen peroxide, and an unsaturated polymer. As the unsaturated polymer is in latex form, inherited from a previous emulsion polymerization process, some surfactant(s) exist in the system. Boric acid is some time used as a promoter [33]. Besides, some impurities also possibly exist. All of these chemicals possibly play some roles in gel formation.

Aside from the aformentioned individual chemicals, the roles that the following four possible reactions/sources play in gel formation need to be investigated: 1) the electron transfer of the redox reaction between hydrazine and hydrogen peroxide may generate radicals; 2) hydrogen peroxide may generate radicals via the Fenton's reaction[57](8-2); 3) oxygen from hydrogen peroxide decomposition may present strong oxidization ability together with the residual hydrogen peroxide [52](8-3); and 4) the side reaction of hydrogenation, in which diimide disproportionates[58], may generate radicals (8-4).

$$Fe^{2+} + H_2O_2 + H^+ \rightarrow Fe^{3+} + H_2O + \bullet OH \qquad (8\text{-}2)$$

$$Fe^{2+} + O_2 + H_2O_2 \rightarrow Fe^{2+}[O_2][H_2O_2] \qquad (8\text{-}3)$$

$$N_2H_2 + N_2H_2 \leftrightarrow N_2H_3\bullet + N_2H\bullet \qquad (8\text{-}4)$$

To investigate the effects of these chemicals on gel formation and the roles that the relevant reactions play in gel formation, we designed and carried out special experiments, and the results are detailed next.

8.2.1 : Effect of the individual chemicals on gel formation

Experiments were conducted to investigate the individual effect of hydrazine, boric acid or hydrogen peroxide through the heating of NBR latex together with the individual chemicals for 8.0hr at 40ºC. The results, summarized in **Table 8-1**, indicate that hydrazine, boric acid or hydrogen peroxide alone does not induce crosslinking in unsaturated rubber. Retaining the latex at 40-80 ºC for more than 40 hours did not increase the gel content in the rubber either.

Table 8-1: Effects of individual chemicals on gel formation during NBR hydrogenation

No.	Experimental systems	Operating conditions	Observed Phenomena
8-1	100.0 g of NBR latex + 4.0g of H_2O_2	8.0hr at 40ºC	No gel
8-2	100.0 g of NBR latex + 4.0g of N_2H_4	8.0hr at 40ºC	No gel
8-3	100.0 g of NBR latex +1.3g of H_3BO_3	8.0hr at 40ºC	No gel
8-4	100.0g of NBR latex	> 40 hr, 40ºC	No gel
8-5	100.0g of NBR latex	> 40 hr, 80ºC	No gel

8.2.2 : Analysis of the possibility of crosslinking from aqueous radicals

Radicals may be generated from the redox reaction between hydrazine and hydrogen peroxide, and hydrogen peroxide decomposition. These radicals are generated in the aqueous phase. Conventional emulsion polymerizations were conducted to determine whether aqueous radicals can cause crosslinking in the unsaturated polymer.

The thermal initiation of styrene polymerization is quite slow at 40° C (entry 8-9 in Table 8-2). The conversion under thermal initiation is negligible. The experiments shown in Table 8-2 indicate that both hydrogen peroxide decomposition and the reaction between hydrazine and hydrogen peroxide are capable of radical initiation. The resultant polystyrenes are all quite soluble with no physical strength, and this suggests a low molecular weight. These experiments demonstrate that the substances used in the diimide hydrogenation process are capable of generating radicals in the aqueous phase.

Table 8-2: Initiation of styrene polymerization by substances in diimide hydrogenation (reaction for 8.0hrs at 40.0ºC)

No.	Initiation system	Conversion	Polymer
8-6	15.0 g of N_2H_4 + 2.0 g of H_2O_2	≈10%	Quite soluble, low M_w
8-7	15.0 g of N_2H_4 + 2.0 g of H_2O_2 + 0.65 g of H_3BO_3	≈30%	Soluble in toluene
8-8	2.0 g of H_2O_2 + 0.65 g of H_3BO_3	≈3%	Quite soluble, low M_w
8-9	Thermal	0	

Table 8-1 shows that H_2O_2 alone cannot crosslink the NBR latex. NBR is still soluble in acetone after the NBR latex is heated with different amounts of H_2O_2 at 40°C for 24 hours. The radical from H_2O_2 is not capable of crosslinking NBR in the latex form even if the radical is capable of initiating polymerization. It has been deduced that the radicals from the reaction between N_2H_4 and H_2O_2 in the aqueous phase behave in the same way as those from H_2O_2 decomposition. On the other hand, when 2 mL of styrene was added into a mixture of NBR latex and H_2O_2 under 40ºC, gel formed in just 2 hours, and this rendered NBR insoluble in acetone. When we compare results from these experiments, it becomes obvious that aqueous radicals are hydrophilic and may initiate polymerization in the aqueous phase, but they have little chance to attack NBR chains that are hydrophobic and are separated from the aqueous phase by a bi-layer of surfactant molecules. During emulsion polymerization, the hydrophilic primary radicals are transformed into hydrophobic polymer radicals by chain propagation. The resultant hydrophobic radicals are then capable of causing crosslinking in the emulsion particles. This understanding leads to the conclusion that the radicals generated in the aqueous phase are not the cause of NBR crosslinking during hydrogenation in the absence of the chain propagation mechanism.

8.2.3 : Analysis of the possibility of crosslinking from oxygen

The crosslinking of saturated polymer in emulsion polymerizations by oxygen is extensively observed in practice [59]. The gel formation is believed to be related to oxygen residues in the emulsion system. Moreover, it has been shown that H_2O_2 and molecular oxygen together have superior oxidation strength [51]. Hydrogen peroxide may decompose to generate its own oxygen atmosphere in the diimide hydrogenation system.

Table 8-3 shows that oxygen alone or oxygen together with hydrogen peroxide (entry 14 and 15) cannot crosslink NBR polymer in latex particles. On the other hand, with the help of the monomer styrene, oxygen is capable of crosslinking the saturated polymer polystyrene (entry 10) and unsaturated NBR (entry 16). The difference between the two cases results from whether or not the radical can be transferred into the organic phase. The addition of the monomer styrene helps to transfer aqueous radicals into the hydrophobic polymer phase. Therefore, the super-oxidative radical from H_2O_2 and molecular oxygen is not the source for crosslinking observed in the diimide hydrogenation process because of the absence of a radical transfer mechanism.

Table 8-3: Experiments with oxygen crosslinking (reaction for 8.0hrs at 40.0ºC)

No.	Experimental details	Polymer
8-10	St emulsion polymerization; Initiator: 15.0 g of N_2H_4 + 2.0 g of H_2O_2, without degassing	Completely Cross-linked
8-11	St emulsion polymerization; Initiator: 15.0 g of N_2H_4 + 2.0 g of H_2O_2, degassing	Soluble
8-12	2.0 g of H_2O_2 + 100.0 g of NBR latex, without degassing	Soluble
8-13	2.0 g of H_2O_2 + 100.0 g of NBR latex, degassing	Soluble
8-14	2.0 g of H_2O_2 + 100.0 g of NBR latex, without degassing	Soluble
8-15	2.0 g of H_2O_2 + 100.0 g of NBR latex + little Fe^{2+} + CH_3NaO_3S , without degassing, 40ºC for 40 h	Soluble
8-16	2.0 g of H_2O_2 + 100.0 g of NBR latex + 2.0 g of St, degassing	Insoluble

8.2.4 : Analysis of the possibility of crosslinking from the side reactions of diimide hydrogenation

According this analysis, the primary radical for gel formation in the diimide hydrogenation process must be generated inside the unsaturated polymer phase in situ. Gel formation has been observed for both the diimide hydrogenation of unsaturated polymer latex [31-39] and the homogeneous diimide hydrogenation in organic solvents [27,28], and this suggest that crosslinking should be directly related to diimide. Diimide has been identified to be the intermediate of this hydrogenation route [55, 56]. The hydrogenation reaction involves the simultaneous transfer of two atoms from diimide to the unsaturated bonds. Diimide is highly selective for symmetrical double or triple bonds. Until now, there has been no discussion in the literature regarding possible side reactions occurring during the diimide hydrogenation reaction.

The diimide disproportionation as shown in (8-4), though not directly observed, has been shown to be an energy-favorable pathway for diimide consumption [58]. So far there is no feasible method for checking for the existence of radicals in situ in the rubber phase. The corresponding crosslinking bonds can not be identified by spectroscopic methods because of the very low concentration of such bonds. Nevertheless, the gel phenomena observed during the hydrogenation experiments support the radical generation process shown in (8-4).

Gel formation is not observed at low degrees of hydrogenation (defined as the conversion of *C*=*C*s; <60%). Meanwhile, diimide is 100% efficient as a hydrogen atom donor for hydrogenation (The efficiency of diimide at performing hydrogenation is defined as the hydrogenation efficiency) (refer to Chapter 4). As the degree of hydrogenation goes up, the hydrogenation efficiency goes down, and the gel content of the resultant polymer increases sharply. Slowing down the addition rate of hydrogen peroxide results in higher efficiency of diimide and has a beneficial effect upon gel reduction. This phenomenon corresponds to the assumed radical process. As the degree of hydrogenation increases, the hydrogenation reaction slows down, and the concentration of diimide increases accordingly. The increase in diimide concentration gives way to diimide consumption by way of (8-4). Consequently, radicals form, and crosslinking results.

8.3 : Summary

The gel formation during diimide hydrogenation process is a radical process. The radicals responsible for crosslinking are generated within the polymer phase. Although the radicals generated within the aqueous phase are capable of initiation, they are not the source of the radicals that cause the crosslinking within the latex particles under normal hydrogenation conditions. The use of radical scavengers in the aqueous phase of the latex does not help to reduce the gel content of the resultant polymer. It has been postulated that the diimide disproportionation reaction within the latex particles generates the primary radicals that causes crosslinking inside the polymer. When the concentration of the unsaturated bonds decreases as the hydrogenation proceeds, radicals are generated at an increasing rate. The addition of antioxidants to the polymer phase does show some beneficial effects for gel inhibition. However, the effect is marginal, as the large amount of radicals generated can not be scavenged efficiently.

Chapter 9
Simulation of diimide hydrogenation process

This research begins with process kinetics investigation. Specially designed experiments have been carried out in the previous chapters to investigate the process kinetics of this diimide hydrogenation system. Reaction kinetics were recorded. The two key experimental variables, HE and HD, were correlated to operating conditions. Process simulation based on the kinetic data may help to refine the understanding of this system, and also provide ideas to optimize this process.

As detailed in Chapter 3, there are four reactions and one mass transfer process in this system. The four reactions and the mass transfer process form three competing processes. In Chapter 4-7, the kinetic behavior of the four reactions was investigated. Reaction (3-2) is of first-order to $[N_2H_4]$ and $[H_2O_2]$ (Chapter 5). The kinetic equation is:

$$r_1 = k_1 f([Cat] \bullet [N_2H_4]) \bullet [H_2O_2] \tag{9-1}$$

The three reactions ((3-2) to (3-5)) are elementary reactions. The rate of hydrogenation according to (3-3) is

$$r_2 = k_2[C=C] \bullet [N_2H_2] = -\frac{d[C=C]}{dt} \tag{9-2}$$

The reaction (3-4) follows:

$$r_3 = k_3[N_2H_2] \bullet [H_2O_2] \tag{9-3}$$

The reaction (3-5) follows:

$$r_4 = k_4[N_2H_2]^2 \tag{9-4}$$

9.1 : Process simulation

This simulation has to take into account four reactions and one mass transfer process, to express the development of HD, HE, and crosslinking with the reaction time. In order to simplify the simulation, certain assumptions are made and listed here.

- It is assumed that there is only one type of *C*=*C*, i.e. all the *C*=*C*s inside have the same reaction activity. The NBR latex has a quite high percentage of *trans*-*C*=*C*, about 10% of vinyl group and a very small amount of *cis*-*C*=*C*. This assumption is justified therefore.
- It is assumed that all the particles inside the latex have the same radius of "R". The particle size distribution of typical latex is quite narrow. This assumption is generally accepted for latex.
- It is generally accepted that reaction (3-4) occurs at the inter-phase before diimide dissociates from the catalytic site. The catalytic sites concentrate at the interfacial area rather

than distribute over the aqueous part of the latex. Reaction (3-4) occurs exclusively at the interface.

The locations for the four reactions are illustrated in Figure 9-1. V_p is the total volume of NBR rubber particles, which is the reaction location for (3-3) and (3-5). V_s is the volume of interface. It is an interfacial layer in which the catalyst, aqueous-phase-borne hydrazine and hydrogen peroxide, and organic-phase-borne diimide can contact with each other. V_a is the volume of the aqueous phase. $[N_2H_4]$ and $[H_2O_2]$ are calculated based on V_a. It is also assumed that the concentration is equal for the aqueous phase and the interface for both hydrazine and hydrogen peroxide.

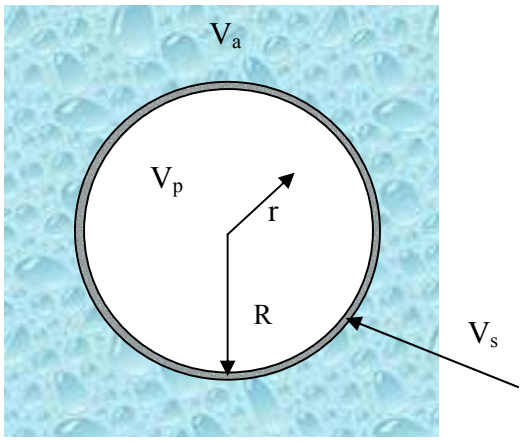

Figure 9-1: Diagram of a latex particle and reaction locations for diimide hydrogenation

At the interface, the balance over diimide gives

$$(\frac{dN_{N_2H_2}}{dt})_{r_1} = w_R \bullet 4\pi R^2 \bullet N + (\frac{dN_{N_2H_2}}{dt})_{r_3} + (\frac{dN_{N_2H_2}}{dt})_{r_4} \tag{9-5}$$

$$w_r = -D_{org}\frac{d[N_2H_2]}{dr} \text{ (Inward as negative), } w_R = -D_{org}(\frac{d[N_2H_2]}{dr})_{|r=R} \tag{9-6}$$

N is the total number of latex particles inside this system, and

$$N = \frac{V_p}{\frac{4}{3}\pi R^3} \tag{9-7}$$

(9-5) can be converted to

$$k_1 f([Cat],[N_2H_4]) \bullet [H_2O_2] = -D_{org} \bullet \frac{3}{R} \bullet \frac{V_p}{V_s} \bullet (\frac{d[N_2H_2]}{dr})_{|r=R} + k_3 \bullet [N_2H_2]_s \bullet [H_2O_2] + 2k_4 \bullet [N_2H_4]_s^2 \tag{9-8}$$

Inside the particle, mole balance over diimide in a differential region gives

$$-\frac{\partial(w_r \bullet r^2)}{\partial r} - r_2 \bullet r^2 - r_4 \bullet r^2 = \frac{\partial([N_2H_2] \bullet r^2)}{\partial t} \tag{9-9}$$

$$-r^{-2}\frac{\partial}{\partial r}(r^2 \bullet D_{org} \bullet \frac{\partial[N_2H_2]}{\partial r}) + k_2[C=C] \bullet [N_2H_2] + 2k_4[N_2H_2]^2 = -\frac{d[N_2H_2]}{dt} \quad (9\text{-}10)$$

The boundary conditions for (9-10) are given by (9-8) and (9-11).

$$\frac{d[N_2H_2]}{dr}_{|r=0} = 0 \quad (9\text{-}11)$$

The initial condition for (9-10) is

$$[N_2H_2]_{t=0} = 0 \quad (9\text{-}12)$$

The initial condition for (9-2) is:

$$[C=C]_{|t=0} = [C=C]_0 \quad (9\text{-}13)$$

The degree of hydrogenation is

$$HD(r,t) = 1 - \frac{[C=C]}{[C=C]_0}, \quad (9\text{-}14)$$

$$HD(t) = 1 - \int_0^R \frac{[C=C]}{[C=C]_0}\frac{3r^2}{R^3}dr \quad (9\text{-}15)$$

Hydrogenation efficiency of hydrogen peroxide includes two parts. The HE from the competition of reaction (3-4) is

$$HE_{aqu} = 1 - \frac{2k_3[N_2H_2]_{|r=R}}{k_1 f([N_2H_4],[Cat]) + k_3[N_2H_2]_{|r=R}} \quad (9\text{-}16)$$

The HE from the disproportionation of diimide is

$$HE_{org} = \int_0^R \frac{r_2}{r_2 + 2r_4}\frac{3r^2}{R^3}dr \quad (9\text{-}17)$$

The total efficiency is

$$HE = HE_{aqu} \bullet HE_{org} \quad (9\text{-}18)$$

Reaction (3-5) is the radical source. The major concern about crosslinking is at the interface. The ratio of reaction (3-5) to (3-2) at the interface can be used to evaluate the degree of crosslinking.

$$Crosslinking \propto \left.\frac{r_4}{r_2}\right|_{r=R} \quad (9\text{-}19)$$

The simulation begins with (9-2), (9-8), (9-10), (9-11), and (9-13). Based on the input of D_{org}, k_1f, k_2, k_3, k_4, and $[C=C]_0$, the simulation will produce the course of hydrogenation and crosslinking according to equations (9-14) through (9-19). However, the parameters D_{org}, k_2, k_3, k_4 are not available from the literature. The analytic solution of simplified cases carried out below may provide insights into these parameters.

9.2 : Simulation of reaction-controlled processes

When the diimide diffusion is much faster than the reaction (3-2), $[N_2H_2]$ would keep the same all over the particle; hydrogenation proceeds at the same rate all over the particle.

Because diimide is a highly reactive intermediate, its concentration in the system is quite low. The total amount of diimide in the system at any time is much less than that generated in the system. Therefore, PSSH (Pseudo Steady State Hypothesis) can be assumed for this system. Mole balance over diimide gives:

$$\frac{dN_{N_2H_2}}{dt} = \left(\frac{dN_{N_2H_2}}{dt}\right)_{r_1} - \left(\frac{dN_{N_2H_2}}{dt}\right)_{r_2} - \left(\frac{dN_{N_2H_2}}{dt}\right)_{r_3} - \left(\frac{dN_{N_2H_2}}{dt}\right)_{r_4} = 0 \tag{9-20}$$

i.e.:

$$r_1 \bullet V_s = r_2 \bullet V_p + r_3 \bullet V_s + 2r_4 \bullet V_p \tag{9-21}$$

Let

$$\gamma_1 = \frac{r_3 V_s}{r_2 V_p} = \frac{k_3 V_s}{k_2 V_p} \bullet \frac{[H_2O_2]}{[C=C]}, \tag{9-22}$$

$$\gamma_2 = \frac{r_4 V_p}{r_2 V_p} = \frac{k_4}{k_2} \bullet \frac{[N_2H_2]}{[C=C]} \tag{9-23}$$

Then,

$$[N_2H_2] = \frac{k_1 f V_s \bullet [H_2O_2]}{k_2 V_p [C=C]} \bullet \frac{1}{1+\gamma_1+2\gamma_2} \tag{9-24}$$

$$HE_{aqu}^{ins} = \frac{V_p \bullet (r_2 + 2r_4)}{2V_s \bullet r_3 + V_p \bullet (r_2 + r_4)} = \frac{1+2\gamma_2}{1+2\gamma_1+2\gamma_2} \tag{9-25}$$

$$HE_{org}^{ins} = \frac{r_2}{2r_4 + r_2} = \frac{1}{1+2\gamma_2} \tag{9-26}$$

9.2.1 : Simulation of the pressure-buildup experiment

In order to acquire estimates of these parameters for the reactions in this system, a specially designed experiment called “pressure buildup experiment” was conducted (see in the previous chapters). In the pressure-buildup experiment, the batch reaction of hydrazine and hydrogen peroxide was investigated in a closed container. The nitrogen generation course was recorded. Hydrazine and double bond were kept at a large excess. The concentrations of hydrazine and double bond were therefore assumed unchanged during the reaction. This process is controlled by reaction rather than mass transfer of diimide. And also, the percentage of reaction (3-5) is negligible when compared to reaction (3-3).

9.2.1.1 : Reaction course

The nitrogen production rate is

$$\frac{dN_{N_2}}{dt} = V_s r_1 = V_s \bullet k_1 f([Cat],[N_2H_4]) \bullet [H_2O_2] \tag{9-27}$$

The hydrogen peroxide consumption rate can be deduced from (9-24) by omitting r_4 item.

$$-\frac{d[H_2O_2]}{dt} = \frac{V_s}{V_a}(r_1 + r_3) = \frac{V_s}{V_a} k_1 f \bullet [H_2O_2] \bullet (1 + \frac{[H_2O_2]}{[H_2O_2] + a_0}) \tag{9-28}$$

with $a_0 = \dfrac{k_2[C=C]_0 V_p}{k_3 V_s}$

The concentration of hydrogen peroxide is always calculated over the total volume of the aqueous phase. The reaction actually occurs at the interface with a volume of V_s. Therefore, the V_s/V_a term should be added to this equation. Integrating (9-28) gives

$$[H_2O_2] = e^{-\frac{V_s}{V_a}k_1 ft}(b_0 \cdot e^{-\frac{V_s}{V_a}k_1 ft} + \sqrt{{b_0}^2 e^{-2\frac{V_s}{V_a}k_1 ft} + a_0 \bullet b_0}),$$

$$\text{with, } b_0 = \frac{[H_2O_2]_0^{\,2}}{2[H_2O_2]_0 + a_0} \tag{9-29}$$

Combining (9-29) with (9-27) and integrating (9-27) gives,

$$N_{N_2} = N_T - \frac{1}{2} V_a (b_0 \cdot e^{-\frac{V_s}{V_a}k_1 ft} \cdot b_1 + a_0 \cdot \ln(b_1) - \frac{a_0}{2} \cdot \ln(\frac{a_0}{b_0})),$$

$$\text{with } b_1 = e^{-\frac{V_s}{V_a}k_1 ft} + \sqrt{e^{-2\frac{V_s}{V_a}k_1 ft} + \frac{a_0}{b_0}} \tag{9-30}$$

$$N_T = \frac{1}{2} V_a \{[H_2O_2]_0 + \frac{a_0}{2} \ln(1 + \frac{2[H_2O_2]_0}{a_0})\} \quad (9\text{-}31)$$

(9-30) and (9-31) are quite complicate and it is not easy to use the two equations to collect the kinetics constant. Experiments showed that the pressure of nitrogen generated from the reaction looks like the first-order curve. The superficial first-order equation is:

$$P_{N_2} = P_{N_{2T}}(1 - e^{-k_m t}) \quad (9\text{-}32)$$

$$x = \frac{N_2}{N_T}, \quad \text{and} \quad \ln(1 - x) = -k_m t \quad (9\text{-}33)$$

Numerical methods are used to compare (9-30) with (9-32). As a first step, data of a_0, $[H_2O_2]_0$ and $\frac{V_s}{V_a} k_1 f$ are chosen based on the experimental ranges and put into (9-30). $[H_2O_2]$s at different time points are calculated using (9-30), and then the $[H_2O_2]$~ t data is regressed using (9-32) to get the k_m. The comparison results are summarized in Table 9-1. The input data of a_0 and $[H_2O_2]$ actually cover all the experimental ranges and $\frac{V_s}{V_a} k_1 f$ can be chosen arbitrarily since it is relevant to the independent variable t. One set of the comparison is shown in Figure 9-2. It is shown that the nitrogen generation curve departs from the first-order kinetics equation (9-32), however, the slope of the first-order fitting from the nitrogen generation curve (k_m) is a very good estimate of $\frac{V_s}{V_a} k_1 f$ (Table 9-1). Therefore, $k_m = \frac{V_s}{V_a} k_1 f$ is assumed in this study. This simplification makes the interpretation of the data easier.

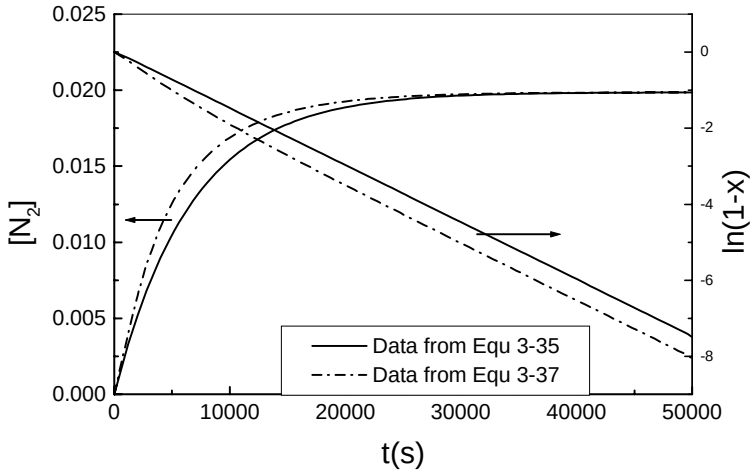

Figure 9-2: Comparison of nitrogen generation curve with the first-order approximation

9.2.1.2 : HE

In case of a batch reaction and for $[H_2O_2]_0$ much less than $[C=C]_0$, $[C=C]$ will not change. HD=0 is assumed. The average efficiency for hydrogen peroxide can be expressed as

$$HE_{aqu} = \frac{2N_T}{[H_2O_2]_0} - 1 = \frac{\ln(1+2\gamma_1^{t=0})}{2\gamma_1^{t=0}}, \quad \gamma_1^{t=0} = \frac{k_3}{k_2} \bullet \frac{V_s}{V_p} \bullet \frac{[H_2O_2]_0}{[C=C]_0} \tag{9-34}$$

This expression of HE_{aqu} fits the HE data in Chapter 6 (Figure 6-10) very well.

Table 9-1: Comparing (9-30) with (9-32) by numerical method

Data input for (9-30)			k_m from (9-32) (s^{-1})	$\frac{k_m - \frac{V_s}{V_a}k_1 f}{\frac{V_s}{V_a}k_1 f}$ (%)	Fitting relevance	HE (%)
a_0 (M)	$[H_2O_2]$	$\frac{V_s}{V_a}k_1 f$ (s^{-1})				
0.001	0.03 M	0.00015	0.0001557	3.80	0.9997	6.8
0.01			0.0001528	1.87	0.9999	32.4
0.1			0.0001513	0.87	0.9999	78.2
1			0.0001502	0	0.99999	97.0
10			0.0001500	0	0.99999	100
0.001*	0.3 M		0.0001674	11.60	0.998	1.1
0.01*			0.0001557	3.80	0.9997	6.8
0.1			0.0001528	1.87	0.9999	32.4
1			0.0001513	0.87	0.9999	78.2
10			0.0001502	0	0.99999	97.0

* Data of the low conversion range is not used for fitting when a_0=0.001 or 0.01

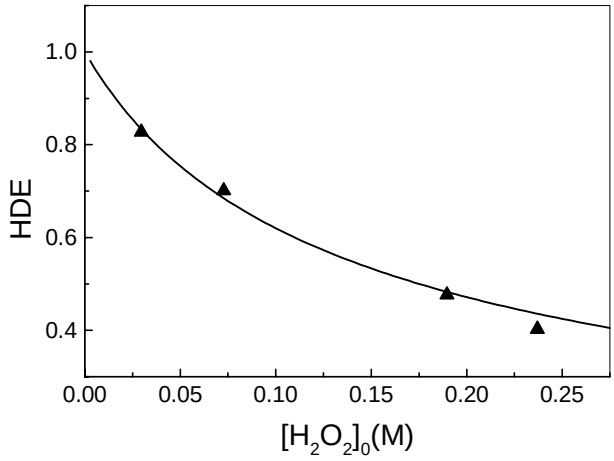

Figure 9-3: HE at different $[H_2O_2]_0$ ($[N_2H_4]$ ~ 2.2M, T=25.0°C, $[H_3BO_3]$ ~ 0.063M, solid content=3.8wt%)

Regression gives:

$$\frac{k_2}{k_3} \bullet \frac{V_p}{V_s} == 0.012 \pm 0.002M \ (95\% \ confidence) \qquad \textbf{(9-35)}$$

From this equation, the rate ratio of the hydrogenation to the side reaction of diimide at the interface can be estimated. Unfortunately, similar data are absent in the literature and therefore can not be compared. This ratio is quite small when compared to one, which means the in-situ $[H_2O_2]$ must be much lower than $[C=C]$ to make the hydrogenation reaction dominate over the side reaction from hydrogen peroxide competition. This ratio is different for different catalytic systems.

9.2.2 : Simulation of the semi-batch hydrogenation process

As suggested by M.S. El-aasser et al [36], the diimide hydrogenation of latex with small particle size (such as a diameter of 50 nm) was mainly a reaction controlled process. A homogeneous model was proposed for this case. On the other hand, the hydrogenation of latex with large particle size (such as a diameter of 230 nm) was a diffusion controlled process. The layer model was proposed for the diffusion controlled process.

In the semi-batch hydrogenation of latex with particle size of about 72 nm, it was observed that the hydrogenation efficiency was virtually 100% before HD reached 60% when boric acid was used as catalyst (Chapter 4), which means the disproportionation reaction (3-5) is negligible all through the major part of the hydrogenation process. The high efficiency suggests that the concentration of diimide is quite low and the hydrogenation reaction (3-3) is quite slow when compared with the diimide diffusion process. Therefore, the hydrogenation of latex with an average diameter of 72 nm is probably a reaction-controlled process before HD reaches 60%. This simulation begins with a reaction-controlled assumption. The resultant hydrogenation curve from this simulation will be compared to that from hydrogenation practice to check whether this assumption is supported.

The differential equations about [*C*=*C*], [N_2H_2] and [H_2O_2] are given by

$$\frac{d[C=C]}{dt} = -r_2 \tag{9-36a}$$

The initial condition is

$$[C=C]_{t=0} = [C=C]_0 \tag{9-36b}$$

$$\frac{d[N_2H_2]}{dt} = (r_1 - r_3)\frac{V_s}{V_p} - r_2 - 2r_4 \tag{9-37a}$$

The initial condition is

$$[N_2H_2]_{t=0} = 0 \tag{9-37b}$$

$$\frac{d[H_2O_2]}{dt} = \frac{q_a - V_s(r_1 + r_3) - q_v[H_2O_2]}{(V_0 + q_v t)} \tag{9-38a}$$

q_a is defined as the H_2O_2 addition rate in mole/second; q_v is defined as the addition rate of H_2O_2 aqueous solution in liter/second;

The initial condition is

$$[H_2O_2]_{t=0} = 0 \tag{9-38b}$$

The actual simulation is based on a semibatch hydrogenation process with the assumption of reaction control. The reaction is conducted on 100 mL of NBR latex with 15.0 wt% solid content using 17.4 hydrazine hydrate (2.0 times of *C*=*C*) and 1.3 g of boric acid consist of the reaction medium. 29.6 g of hydrogen peroxide aqueous solution (30.0%) is added over a period of 10 hours.

This simulation aims to check the effects of values of these parameters upon the HD curve. Values of k_2, k_3 and k_4 are related to diimide concentration level. During this simulation, k_2 is preset at 0.1 $(sM)^{-1}$. k_3 is estimated from (9-35) with some adjustment to accommodate the difference with [H_3BO_3]. k_4 is then changed over a range to compare the HD curves. When k_2 and k_3 are increased by a factor of 10 and k_4 is increased by a factor of 100, the simulation will be exactly the same. [N_2H_2] will be just one tenth of that with k_2=0.1 $(sM)^{-1}$.

The Matlab M file is compiled in Appendix C.

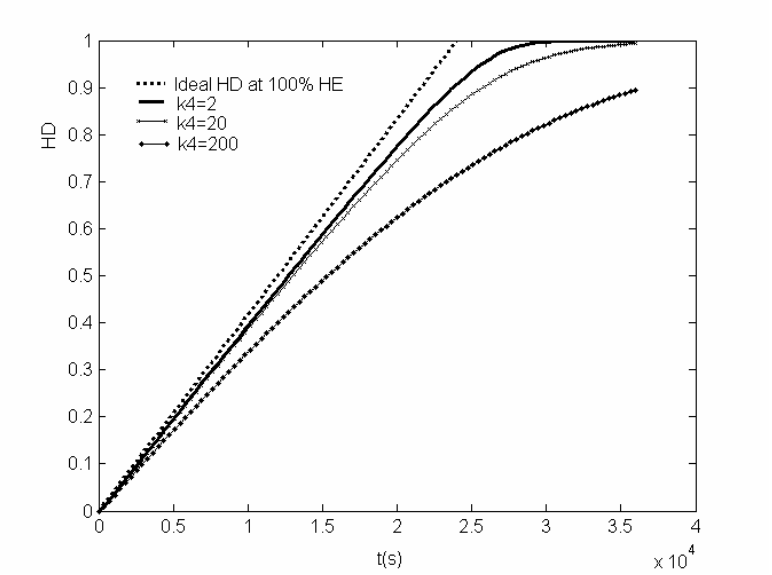

Figure 9-4: Simulation of HD curve at different k_4 values (k_2=0.1 $(sM)^{-1}$, k_3=1.47 $(sM)^{-1}$, V_p=0.015L, V_s=0.0015L, k_4 in $(sM)^{-1}$)

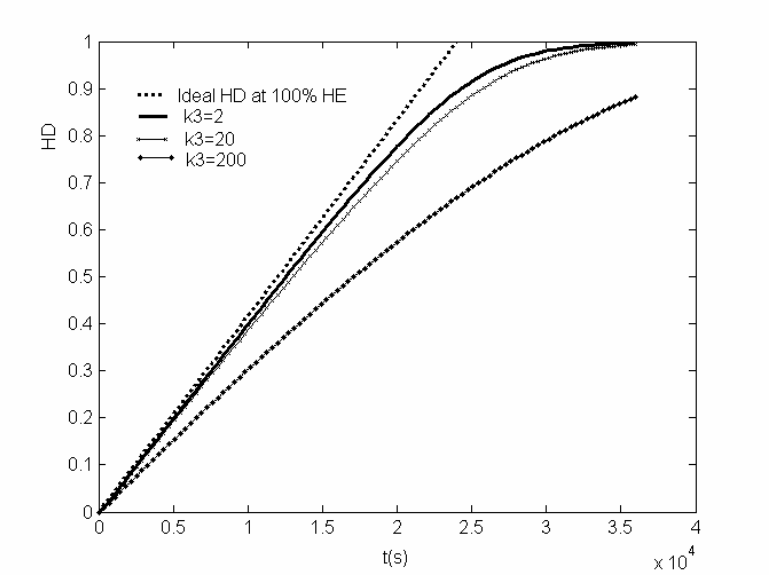

Figure 9-5: Simulation of HD curve at different k_3 values (k_2=0.1 $(sM)^{-1}$, k_4=1.8 $(sM)^{-1}$, V_p=0.015L, V_s=0.0015L, k_3 in $(sM)^{-1}$)

Figure 9-4 and Figure 9-5 clearly show that the increase in side reactions r_3 or r_4 would result in the decrease in hydrogenation efficiency. Based on this simulation, both k_3 and k_4 should be smaller than 20 when k_2 is set at 0.1 $(sM)^{-1}$. This estimation is based on the results detailed in Chapter 5: HE_{org} is close to 100% before HD reaches 35% (Section 5.4.4); HE_{aqu} is close to 100% when $[H_2O_2]$ is below 0.009 M (Section 5.4.7).

It was shown by Figure 9-4 and Figure 9-5 that HD can reach 98% and above when the hydrogenation efficiency is close to 100% at low HD range (such as the case of $k_3 < 20$ $(sM)^{-1}$, $k_4 < 20$ $(sM)^{-1}$). However, as shown in Chapter 2, HD can not reach 98% even if the HE at low HD range is close to 100%. HE decreases sharply at high HD range (Refer to Figure 5-12). When HD reaches above 85%, HE is close to zero. This difference between simulation curves shown above with actual HD curves in Chapter 4 would suggest that **pure reaction –control mechanism can not be assumed for the latex with an average particle size of 72nm.** Mass transfer interference would increase diimide build-up. The second order side reaction r_4 would be accelerated significantly and dominate over r_2. The hydrogenation of residual *C*=*C*s can only be achieved at a very low efficiency. A long tail of the hydrogenation curve would be observed as the result. The hydrogenation experiments on latex with different particle sizes by M.S. El-Aasser [36] have shown that higher HD can be achieved on latex with smaller particle size, which suggests that the hydrogenation on latex with a particle diameter of 230nm is interfered by diimide diffusion. The simulation carried out here shows that diimide mass transfer is a problem even for the latex with a particle diameter of 72nm.

This simulation also tells that in order to achieve high efficiency at low HD range till 60%, k_3 has to be smaller than 20 $(sM)^{-1}$, k_4 has to be smaller than 20 $(sM)^{-1}$ (when k_2 is set at 0.1 $(sM)^{-1}$).

9.3 : Simulation of diffusion-interfered hydrogenation process

9.3.1 : Parameter presetting and simulation

In this section, a comprehensive simulation of the diimide hydrogenation process is carried out, in which the role of diimide mass transfer is also taken into consideration. Equations (9-2), (9-8), (9-10), (9-11), (9-13), (9-14) through (9-19) is used for the simulation.

The diffusivity of diimide in NBR rubber is given the value of $5\times10^{-13} m^2/s$ based on the general magnitude of diffusivity in solid [59].

(9-35) is used as a limitation when the values for k_2 and k_3 are preset. Simulations in 9.2 show that values $k_3<20$ $(sM)^{-1}$, $k_4<20$ $(sM)^{-1}$ fit to the actual hydrogenation curves well when k_2 is set at 0.1 $(sM)^{-1}$. Increasing k_2 and k_3 by ten times and increasing k_4 by 100 times would result in the decrease of $[N_2H_2]$ by ten times. By this way, the role of diffusion can be demonstrated. This limitation on the relative magnitude for k_2, k_3 and k_4 ensures high HE at low HD range.

The system described in 9.2.2 is also used here. In this semi-batch process, $[N_2H_4]$ decreases from 2.9 M at the beginning to 0.9 M in the end. To make the simulation easier, an average $[N_2H_4]$ is taken. The concentration effect of hydrazine is combined into the rate parameter k_1f. Following by this simplification, a steady state for $[H_2O_2]$ can be assumed. The solution of (9-39) shows that $[H_2O_2]$ reaches the steady state at 0.0181M in just 1800 seconds (just 5.0% of the total reaction time). See in Figure 9-6. In the actual hydrogenation reaction, $[N_2H_4]$ decreases and $[H_2O_2]$ increases to compensate each other and to make sure that no accumulation of hydrogen peroxide happens.

$$\frac{d[H_2O_2]}{dt} = \frac{qC_{H_2O_2} - V_s k_1 f [H_2O_2]}{V_0 + qt}, \quad C_{H_2O_2} : [H_2O_2]\ of\ the\ addition\ solution \qquad (9\text{-}39)$$

$$q : flow\ rate\ of\ the\ addition\ solution$$

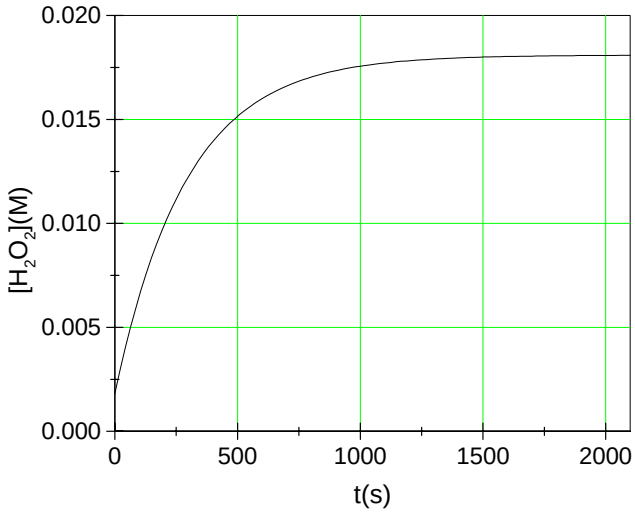

Figure 9-6: $[H_2O_2]$ dynamics for the semi-batch hydrogenation process described in section 9.2.2

The well known scientific computing software Matlab was used to conduct this simulation. The M-file is compiled in Appendix D. Values for R, k_2, k_3 and k_4 are modified to achieve different situations for this process.

When $k_2=2\times10^3$ $(sM)^{-1}$; $k_3=2\times10^5$ $(sM)^{-1}$; and $k_4=3.2\times10^{10}$ $(sM)^{-1}$, mass transfer of diimide shows significant effects upon this process. See in Figure 9-7 and Figure 9-8. The final distribution of *C*=*C* in Figure 9-8 shows that the outer layer of the latex particle is fully hydrogenated, while [*C*=*C*] in the internal layers is still quite high. The final HD reaches 0.8468 in this example.

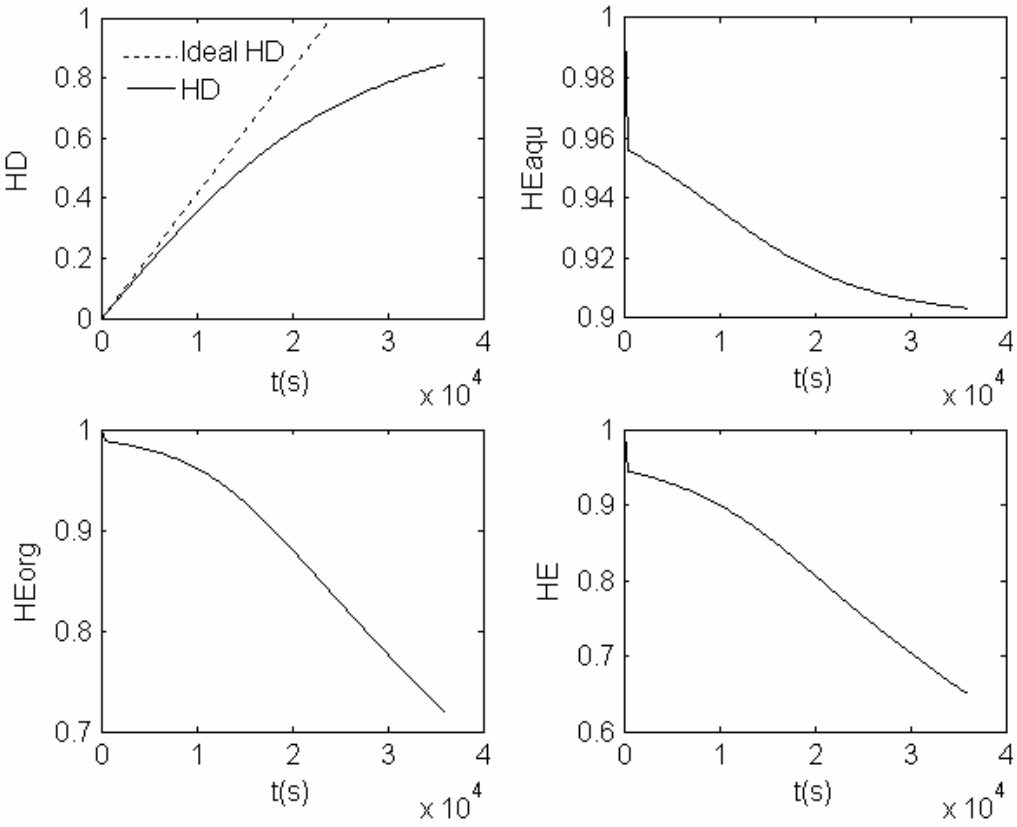

Figure 9-7: HD, HE, HE_{aqu}, and HE_{org} curve for the case with $k_2=2\times10^3$ $(sM)^{-1}$; $k_3=2\times10^5$ $(sM)^{-1}$; and $k_4=3.2\times10^{10}$ $(sM)^{-1}$

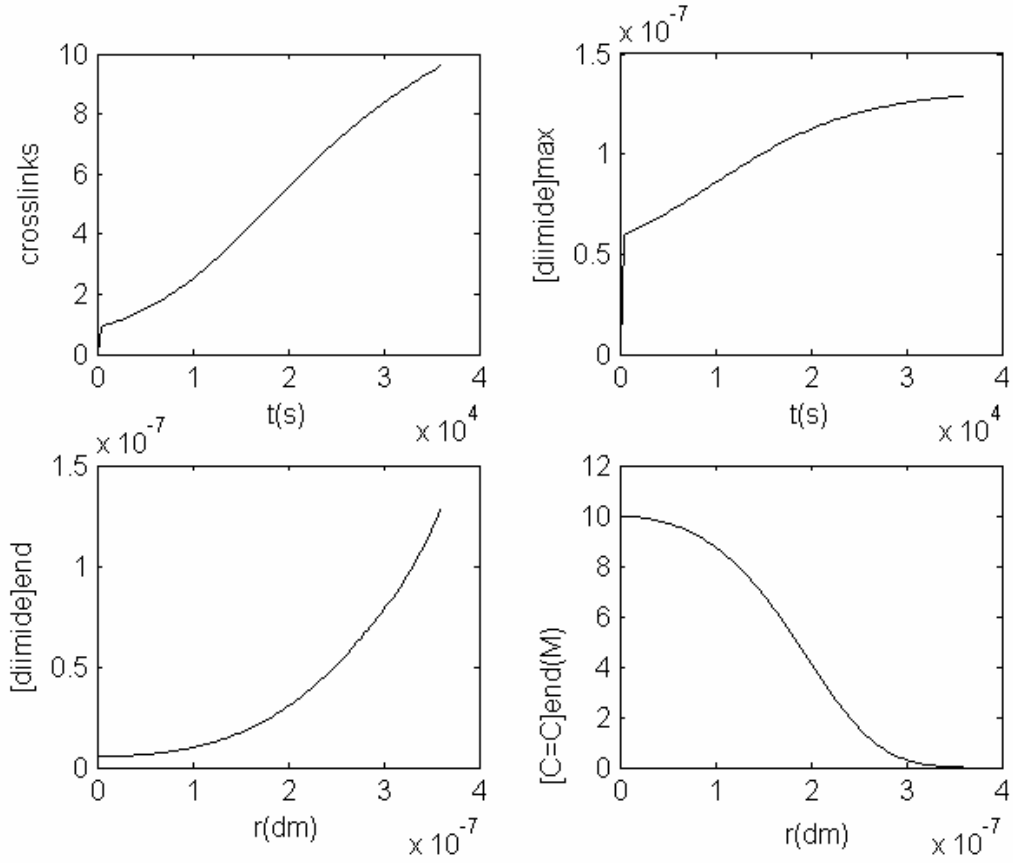

Figure 9-8: Development of crosslinking, $[N_2H_2]$ at the surface, $[N_2H_2]$ distribution in the particle, and the residual *C=C* distribution curves for the case with $k_2=2\times10^3$ $(sM)^{-1}$; $k_3=2\times10^5$ $(sM)^{-1}$; and $k_4=3.2\times10^{10}$ $(sM)^{-1}$

On the other hand, when $k_2=20$ $(sM)^{-1}$, $k_3=4000$ $(sM)^{-1}$, and $k_4=3.2\times10^6$ $(sM)^{-1}$, mass transfer of diimide is not a problem at all. Hydrogenation proceeds homogeneously in the particle (See in Figure 9-9 and Figure 9-10). HD reaches 0.9571in the final.

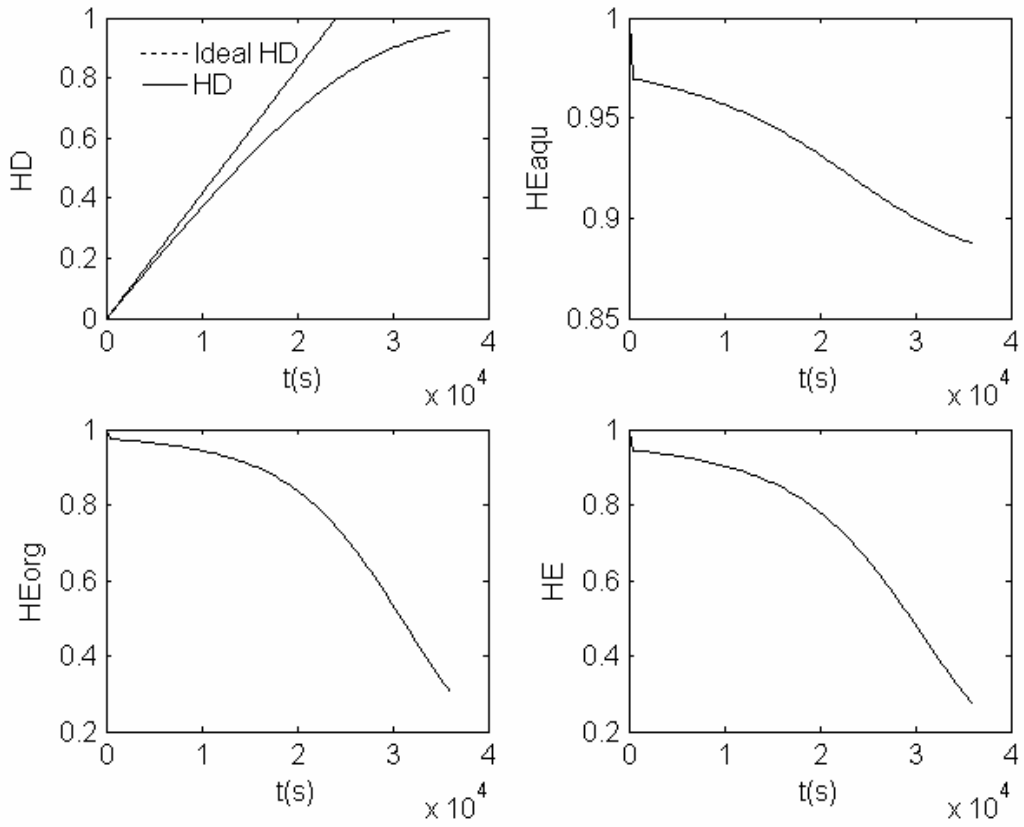

Figure 9-9: HD, HE, HE_{aqu}, and HE_{org} curve for the case with k_2=20 $(sM)^{-1}$, k_3 = 4000 $(sM)^{-1}$, and k_4=3.2×10^6 $(sM)^{-1}$

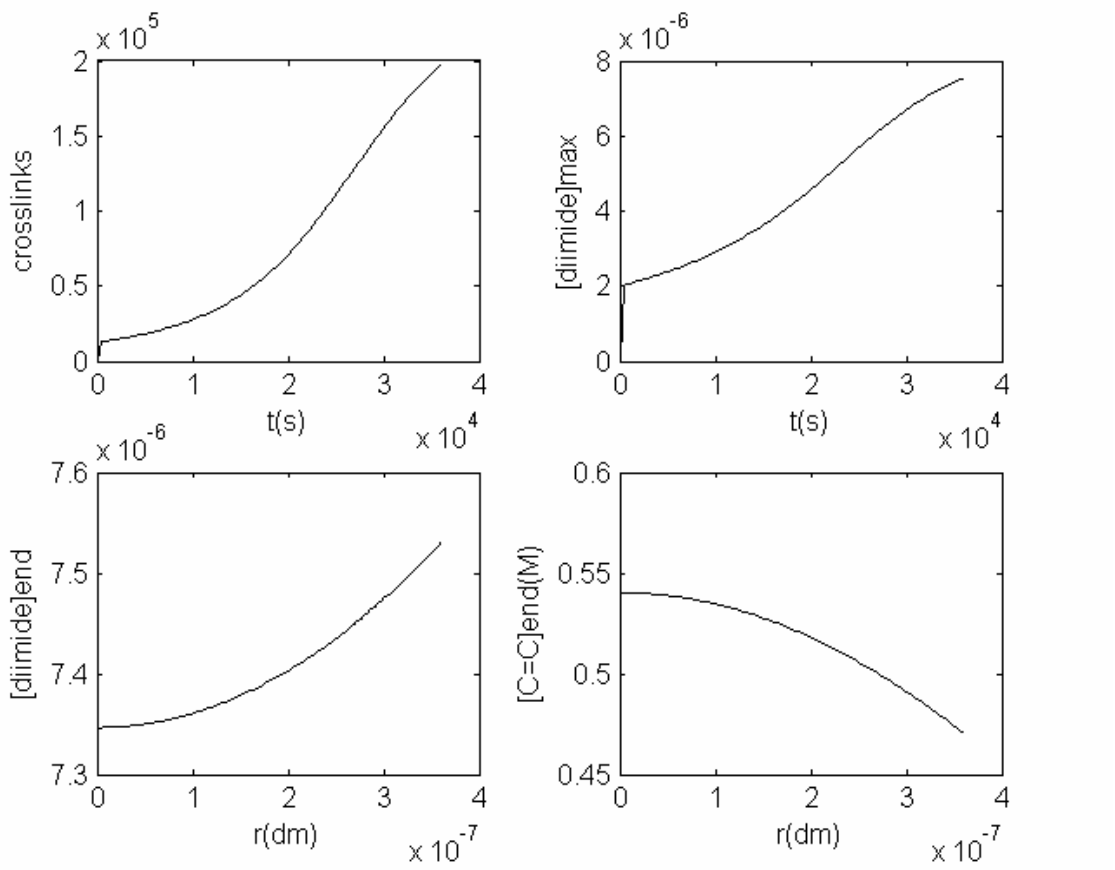

Figure 9-10: The development of crosslinking, $[N_2H_2]$ at the surface, $[N_2H_2]$ distribution in the particle, and the residual *C=C* distribution curves for the case with k_2=20 $(sM)^{-1}$, k_3=4000 $(sM)^{-1}$, and $k_4=3.2\times10^6$ $(sM)^{-1}$

In order to further narrow down the value ranges for the three rate constants, the hydrogenation data from M.S. El-Aasser, et al [36] on latex with different particle sizes are taken into consideration. Based on their experiments, the hydrogenation of latex with a particle diameter of 230nm is controlled by diimide mass transfer, while that on latex with a particle diameter of 50nm is not. By setting k_2 = 800 $(sM)^{-1}$, $k_3=1.6\times10^5$ $(sM)^{-1}$. and $k_4=5.12\times10^9$ $(sM)^{-1}$, the simulation results on latex with different particle sizes fit well to the observation by M.S. El-Aasser, et al [36] (Refer to Figure 9-11 through Figure 9-16). The final HD is 0.6174 for 230 nm latex, 0.9324 for 72 nm latex and 0.9531 for 50nm latex.

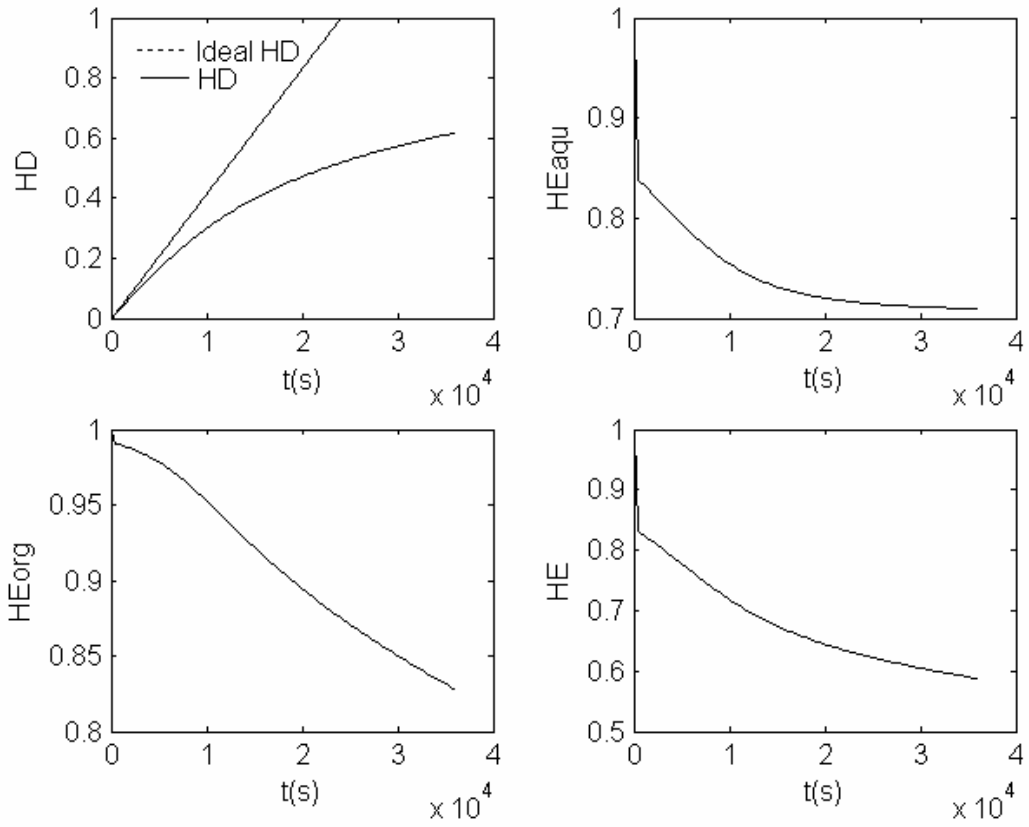

Figure 9-11: HD, HE, HE_{aqu}, and HE_{org} curves for the case with k_2=800 $(sM)^{-1}$, k_3=1.6×10^5 $(sM)^{-1}$, k_4=5.12×10^9 $(sM)^{-1}$, and R=115 nm

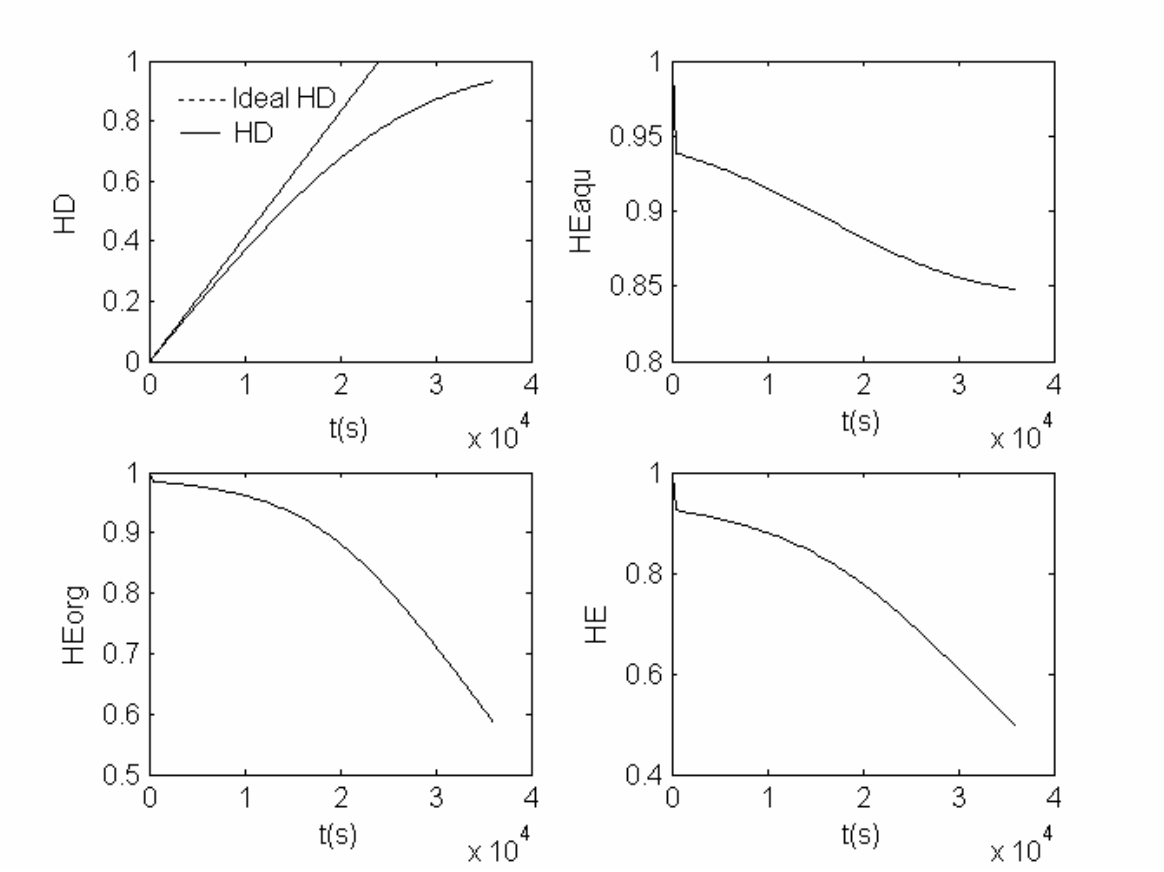

Figure 9-12: HD, HE, HE_{aqu}, and HE_{org} curves for the case with k_2=800 $(sM)^{-1}$, k_3=1.6×10^5 $(sM)^{-1}$, k_4=5.12×10^9 $(sM)^{-1}$, and R=36 nm

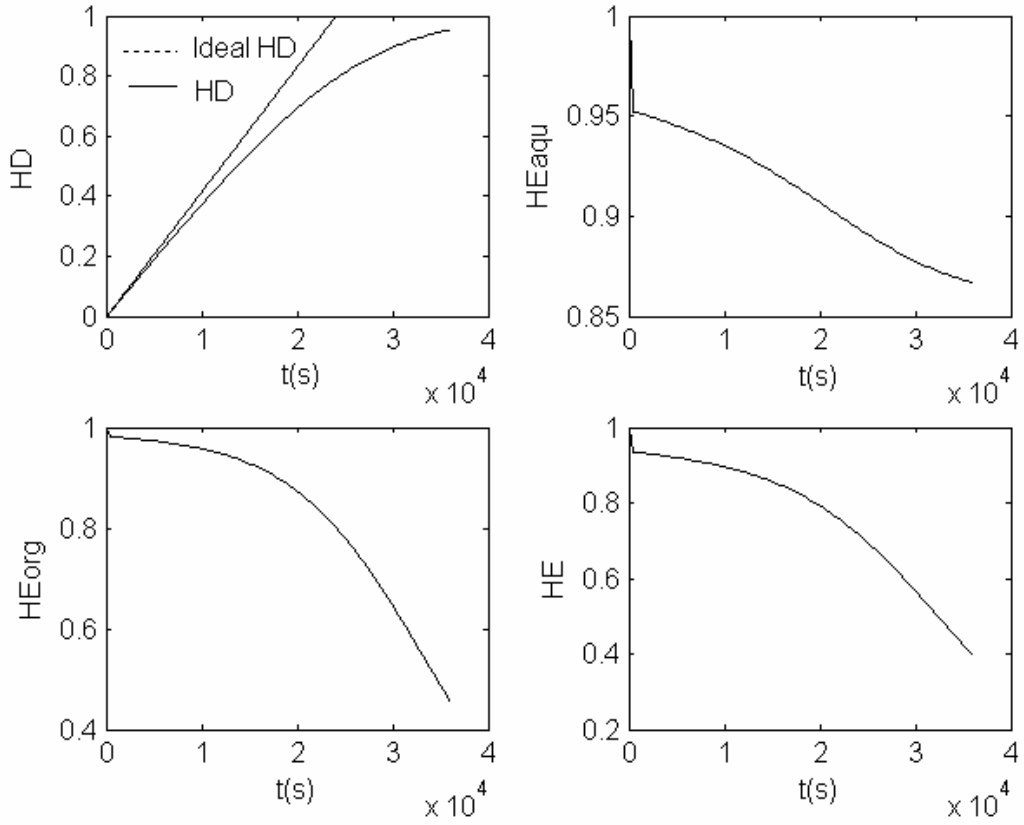

Figure 9-13: HD, HE, HE_{aqu}, and HE_{org} curves for the case with k_2=800 $(sM)^{-1}$, k_3=1.6×10^5 $(sM)^{-1}$, k_4=5.12×10^9 $(sM)^{-1}$, and R=25 nm

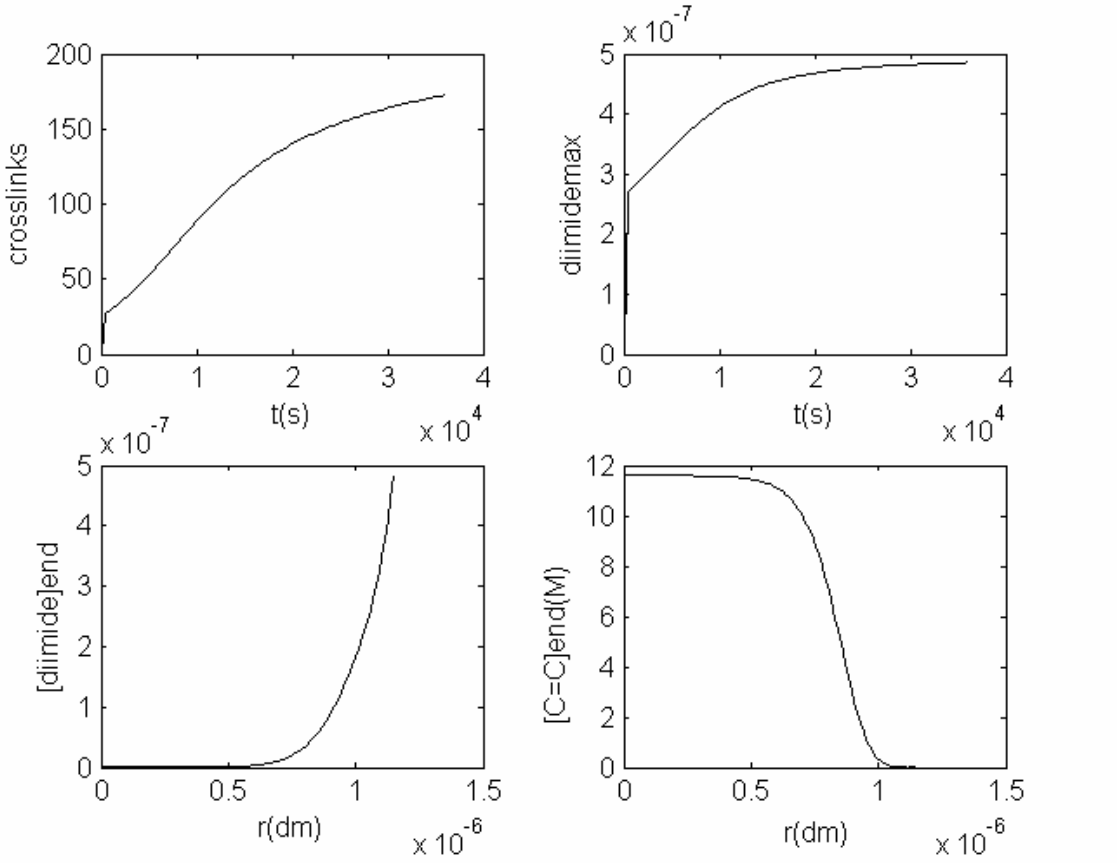

Figure 9-14: Development of crosslinking, $[N_2H_2]$ at the surface, $[N_2H_2]$ distribution in the particle, and the residual *C=C* distribution curves for the case with $k_2 = 800\ (sM)^{-1}$, $k_3 = 1.6\times10^5\ (sM)^{-1}$, $k_4 = 5.12\times10^9\ (sM)^{-1}$, and R = 115 nm

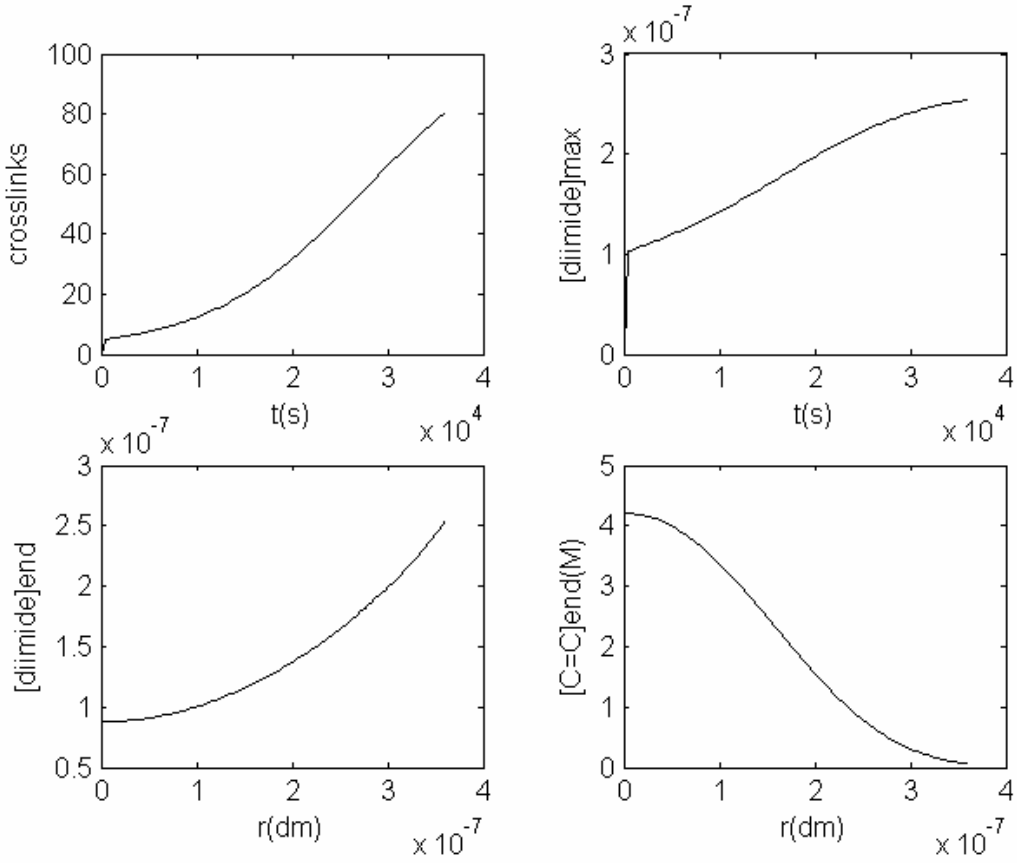

Figure 9-15: Development of crosslinking, $[N_2H_2]$ at the surface, $[N_2H_2]$ distribution in the particle, and the residual *C=C* distribution curves for the case with $k_2 = 800\ (sM)^{-1}$, $k_3 = 1.6\times10^5\ (sM)^{-1}$, $k_4 = 5.12\times10^9\ (sM)^{-1}$, and R=36 nm

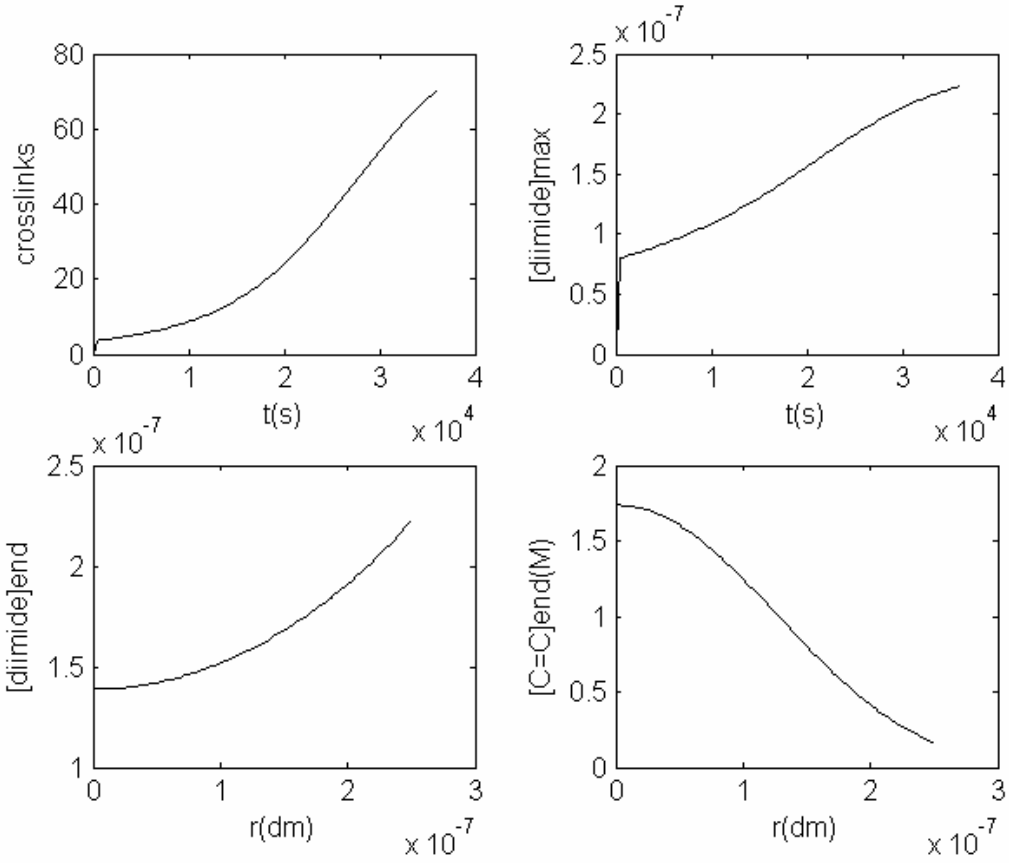

Figure 9-16: Development of crosslinking, $[N_2H_2]$ at the surface, $[N_2H_2]$ distribution in the particle, and the residual *C=C* distribution curves for the case with $k_2 = 800\ (sM)^{-1}$, $k_3 = 1.6\times10^5\ (sM)^{-1}$, $k_4 = 5.12\times10^9\ (sM)^{-1}$, and R=25 nm

9.3.2 : Limitation of this simulation

In this simulation, a steady state is assumed for the reactions outside the latex particle. However, $[N_2H_4]$ would decrease as the reaction proceeds; $[H_2O_2]$ would increase at the same time. The changes would result in a decreased supply of diimide as hydrogenation proceeds. An ideal simulation can divide the whole reaction time into a number of sections, such as 100 parts. The steady state can be assumed for each part of this process. The PDE solver used in Section 9.3.1 is used for each part of this process. The results from the PDE solver can be combined with the ODE solver used in Section 9.2.2 to provide the boundary conditions and initial conditions for the next time slot. This computation is conducted on each part of this process to collect data of the whole process. This improved simulation would be able to provide more accurate description of the late part of this process.

Because crosslinking increases together with hydrogenation, the relaxation of rubber molecule chains may be restrained at the high HD range. The rate constant for hydrogenation may

decrease as a result and the diffusivity of diimide in the crosslinked rubber may also decrease. Nevertheless, it is very difficult to evaluate these effects.

9.4 Summary

This comprehensive simulation of the semi-batch hydrogenation process reveals the relative rates of the four reactions. **It is felt that k_2=800 $(sM)^{-1}$, k_3=1.6×10^5 $(sM)^{-1}$, k_4=5.12×10^9 $(sM)^{-1}$ are reasonable estimations for these rate constants provided that $\frac{V_s}{V_p} = 0.1$ and $D_{org}\ of\ diimide = 5 \bullet 10^{-13} m^2 / s$ are assumed.** This estimation has taken into consideration the three key observed experimental phenomena:

- High HE is observed at the low HD range;
- Hydrogenation becomes quite slow when HD reaches above 90%;
- Hydrogenation of latex with a particle diameter of 230 nm is a totally mass-transfer controlled process. When the diameter is 50 nm, mass transfer of diimide is not a problem.

It is concluded from this simulation that diimide diffusion interferes with the hydrogenation reaction for the latex with an average particle diameter of 72 nm. Just because of the mass transfer limitation, it is very difficult to reach above 95% of HD. Therefore, it is suggested that specially-designed core-shell latex with an inert core and a NBR shell should be used for the diimide hydrogenation process. The core with a diameter of 40 nm would only account for 17% of the total volume. By using a core-shell latex, both the low efficiency problem and the crosslinking problem can be eased significantly.

It is also shown that radical generation in the organic phase is always part of this system. Crosslinking increases with HD. Therefore, the NBR latex should have relatively low molecular weight to allow for some degree of crosslink formation. The hydrogenated rubber would still be processable after limited crosslink formation.

Chapter 10
Gel formation reduction

This investigation has revealed that the diimide hydrogenation process can be optimized to an efficient level to achieve 80% of hydrogenation of NBR latex. Virtually 100% efficiency of hydrogen peroxide utilization and insignificant gel formation can be achieved simultaneously up to this stage. However, when HD goes up further, two problems: explosive gel formation and low hydrogenation efficiency, are observed. This research has identified that the two problems are related to the disproportionation reaction of diimide. Both problems are associated with the slowing-down of the hydrogenation reaction and the building-up of diimide within high HD range. Hydrogenated NBR is totally gelled when HD goes above 90%. Overcoming these problems is the main challenge in developing a commercial hydrogenation process.

Above 95% of HD is required for a practically useful HNBR. Significant improvement in the thermal and oxidative stability of polymers can only be realized when the residual double bond content (RDB) is below 5%. See in Figure 10-1.

On the other hand, gel formation must be controlled at a very low level. By principle, one crosslink bond per polymer molecule on average would be able to crosslink all the molecules into a three-dimension network. Because rubbery polymers normally have quite high degree of polymerization (DP), one bond per polymer molecule on average is actually a very low concentration of crosslink bonds in the polymer. Therefore, highly efficient gel inhibition has to be in place for a practical and useful hydrogenation process.

The cost analysis in Appendix E shows that the total manufacture cost for the diimide hydrogenation process is just 55% of that of the conventional solution hydrogenation process. If the diimide method can achieve above 95% of HD without gel formation, it would provide a great breakthrough for the production of HNBR. Based on preliminary experimental results, the possible methods to refine this process and the future research directions will be discussed in this chapter.

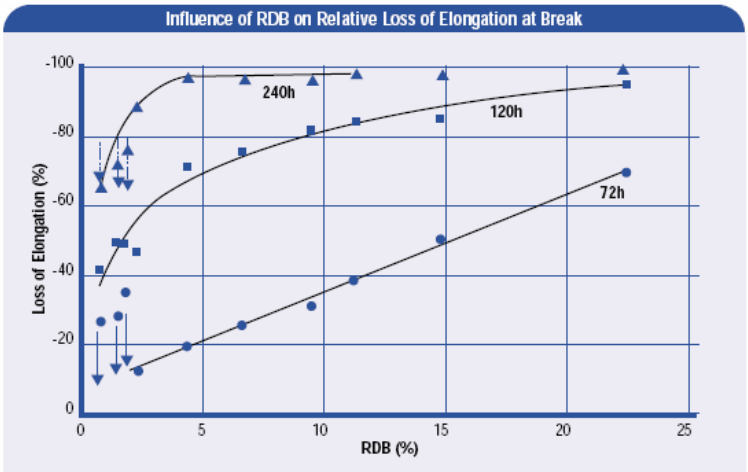

Figure 10-1: Aging of Therban in air at 160°C: influence of RDB on relative loss of elongation at break [61]

10.1 : Effects of antioxidants upon gel formation

The use of antioxidants is the common method considered for gel inhibition. Hong-Quan Xie, et al [37] suggested using sodium N, N-dimethyldithiocarbonate and *p-tert*-butylpyrocatechol as the inhibitors in order to reduce gel formation. It was believed that the combination of an aqueous antioxidant with a rubber-phase antioxidant helped to reduce gel formation. Wang Jianguo et al [35] used amines and quinines, such as phenol, *o*-hydroquinol, *p*-hydroquinol, benzoquinone, aniline, *o*-phenylenediamine, *p*-phenylenediamine, as an anti-gel-agent. Johannes Wilhelmus Belt, et al [62] also included diamines, hydroxylamine, oximes as effective additives to reduce gel formation.

However, when all these data were carefully analyzed, it was found that the HD achieved was at relatively low level in all these experiments. At this stage of hydrogenation, gel formation had not become a problem for this process even in the absence of such inhibitors. The partially saturated rubber samples were generally quite soluble in suitable solvents. These experiments failed to demonstrate the effectiveness of antioxidants for crosslink inhibition at high HD range. For the hydrogenation process, there is another gel formation problem. Gel content of the hydrogenated NBRs would increase significantly after being taken out from the latex. This phenomenon is well documented already in the literature [63]. The mechanism for this type of gel formation is different from that responsible for gel formation during diimide hydrogenation. Autoxidation and photo-oxidation contribute to the increase of gel content when the sample is taken out of the latex [64](Figure 10-2). Antioxidants are designed to capture/break down radicals from these reactions shown in Figure 10-2. Radicals are generated quite slowly under normal conditions. Antioxidants would be able to capture 100% of these radicals. Backbones are protected as the result. But in the diimide hydrogenation process, a major part of diimide generated during the second half of this reaction transfers to radicals, which may attack backbones to initiate crosslinking. When radicals are generated in a large amount, antioxidants would not be able to capture all of them. Gel formation would therefore be inevitable.

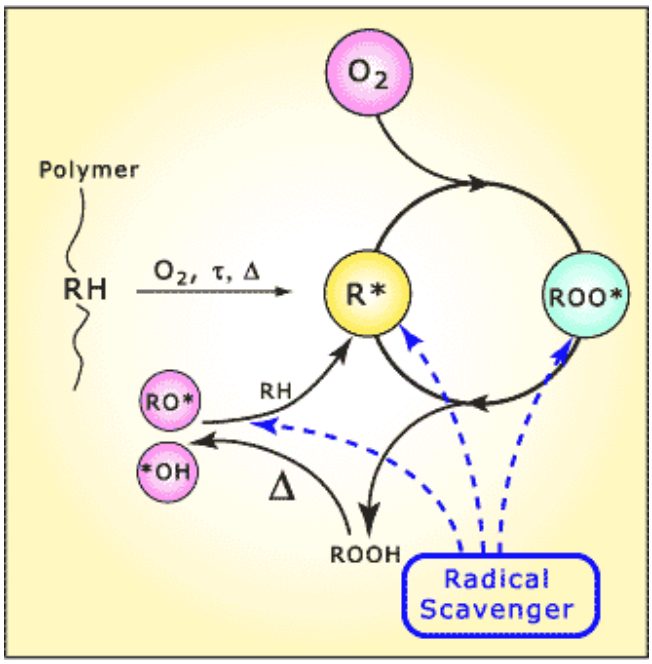

Figure 10-2: General accepted degradation scheme for polymers, originally developed for natural rubber [64]

In order to quench a large amount of radicals, it is necessary to find a highly reactive chemical agent which can be provided in a large amount in the rubber phase; is quite small in size to ease the diffusion process, and can deactivate the radicals. Based on this idea, methanethiol was tried. However, it was found that methanethiol is highly reactive toward hydrogen peroxide. The reaction between methanethiol and hydrogen peroxide is strongly preferred over that between hydrazine and hydrogen peroxide. Diimide hydrogenation simply can not be carried out in the presence of methanethiol. Therefore, using methanethiol during diimide hydrogenation is not the solution. Other possible chemicals are still under study.

To summarize, simply adding antioxidants into the latex can not solve the gel formation problem during the diimide hydrogenation process. However, antioxidants should be added into hydrogenated latex before coagulation.

10.2 : Two-step hydrogenation

A feasible method is still not available to solve the problems incurred with the diimide method. In the literature, proposals have been presented to reduce gel content. One method used ozone to break down crosslinking bonds and to further increase the saturation of the resultant rubber [45]. The other tried to make use of the partially hydrogenated rubber by compounding [44]. However, good mechanical properties of the rubbers obtained from the two methods were significantly reduced.

During this investigation, it was noticed that thiol molecules can also be used to saturate *C*=*C*s. It was expected that thiol may be used to saturate the 20% of *C*=*C*s left from the diimide method. High degree of hydrogenation can then be achieved by diimide hydrogenation followed by thiol addition. Therefore, thiol addition to *C*=*C*s was investigated to check the feasibility.

10.2.1 : Summary of research on thiol addition in the literature

10.2.1.1 : Thiol addition reactions

The addition of thiols to olefinic double bonds has been known since 1905. The thiol addition can be carried out in a solution or in latex form of unsaturated polymers. An organic-phase-borne initiator, such as AIBN, is used to initiate the reaction. The reaction can be conveniently carried out at 30~60ºC. The reaction normally takes tens of hours to obtain high conversions [67-73].

For thiol addition, the free radical mechanism is preferred over the acid-or base-catalyzed mechanism. It is generally accepted that an initiator is needed for the initiation step. The secondary radicals from thiols add onto olefinic double bonds to generate polymeric radicals, which then transfer to thiols to terminate the process. However, there is possibility of termination reactions involving two polymeric radicals, which would form crosslink bonds between polymer backbones.

The free radical chain reactions are listed below [65]. The preliminary radical is generated from

$$I \rightarrow 2R\bullet \qquad (10\text{-}1)$$

The chain transfer to methanethiol produces methanethiol radical.

$$R\bullet + MeSH \rightarrow MeS\bullet \qquad (10\text{-}2)$$

Thiol addition is achieved by

$$MeS\bullet + C = C \rightarrow P\bullet \qquad (10\text{-}3)$$

Radicals are transferred or terminated by

$$MeS\bullet + MeS\bullet \rightarrow MeS - SMe \qquad (10\text{-}4)$$

$$P\bullet + MeSH \rightarrow P + MeS\bullet \qquad (10\text{-}5)$$

$$MeS\bullet + P\bullet \rightarrow P \qquad (10\text{-}6)$$

Crosslink bonds are formed by

$$P\bullet + P\bullet \rightarrow Crosslink \qquad (10\text{-}7)$$

The major concerns with this process are the thiol addition rate and the crosslink formation rate. Reaction (10-3) is probably reversible, which makes the thiol addition rate very slow. High concentration of methanethiol would increase the rate of reaction (10-3), and at the same time, suppress the combination reaction of two polymeric radicals through reaction (10-7). Crosslink

formation would be inhibited as a result. The results in the literature showed that crosslinking was not a problem during thiol addition. Chain cleavage, on the other hand, might present problems especially when oxygen was not excluded from the system.

Methanethiol as the first member of the thiol series possesses higher reactivity and possibly faster movement. The high reactivity of methanethiol may help to ease the problems of crosslinking and chain cleavage. "When prepared in the absence of oxygen, the number-average molecular weight of the product appears to be that calculated from the original molecular weight of the polymer, plus the quantity of added thiol."[66] "The addition reaction can be carried to essentially complete saturation by the use of appropriate initiators"[66]

10.2.1.2 : Thiol saturated rubber

The saturated rubber by methanethiol addition possesses good aging property, heat resistance, and ozone resistance. Adducts with saturation levels up to 85% could be cured by the same procedure used for the base polymers. Activated or a butyl-curing system was required for higher saturation levels [66].

10.2.2 : Thiol addition experiment

10.2.2.1 : Thiol addition of SBS

In this experiment, a mixture of 1.0g SBS, 60.0 mL toluene, and 0.05g AIBN (recrystallized) was kept at 50.0ºC in a degassed reactor under 24.5 psi of a methanethiol atmosphere for 3100 minutes. The pressure of methanethiol in the reactor was recorded using a pressure transducer. It was found that the pressure dropped by 1.5 psi during the reaction and flattened beyond 3000 minutes of reaction. The resultant thiol-saturated SBS has quite high conversion and is quite soluble in acetone. The peak for *trans*-*C*=*C* (970 cm^{-1}) in the FT-IR spectrum of thiol-saturated SBS disappears and a new peak at 950 cm^{-1} appears (Figure 10-3). The conversion is close to 100% as measured by ^{1}H NMR spectrum.

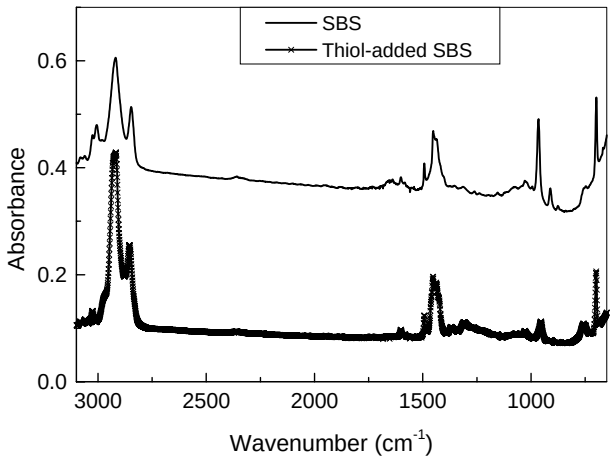

Figure 10-3: FT-IR Spectra of SBS and thiol-saturated SBS

10.2.2.2 : Thiol addition of NBR

Thiol addition experiments were conducted on NBR following the same procedures described above for SBS. Lower conversion was generally observed for NBR as measured by the ratio of *trans* *C=C* peak at 970 cm^{-1} to nitrile group at 2230 cm^{-1} (See in Figure 10-4).

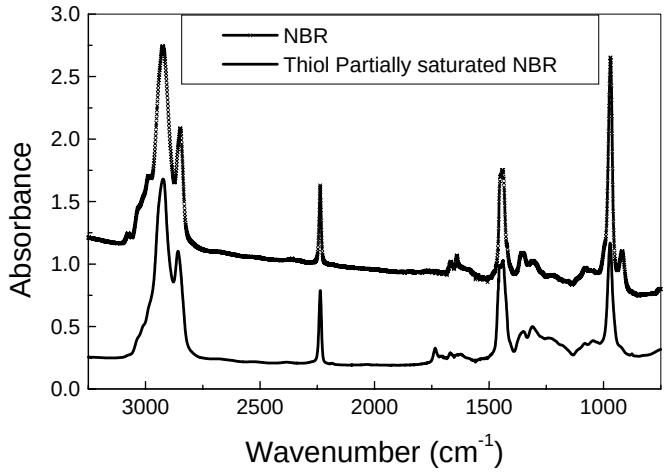

Figure 10-4: FT-IR spectra of NBR and thiol partially saturated NBR

The results are summarized in Table 10-1. Increasing the pressure of methanethiol (D-14 in Table 10-1) accelerated the thiol addition rate. 80% saturation was achieved. Supplement of the initiator (D-15 in Table 10-1) did not generate higher conversion. The saturation level increased very

slowly (may even stop) when [*C*=*C*] dropped below 3.0 M. No matter what may be the mechanism, this phenomenon is quite similar to the diimide hydrogenation.

The reaction on fresh NBR latex generated similar results (NBR latex was used instead of SBS or NBR). The mixture of 6.8g NBR latex, 50.0ml water, and 0.05g AIBN (recrystallized) was kept at 50.0ºC in a degassed reactor under 32.5 psi of methanethiol atmosphere for 2000 minutes (D-8 in Table 10-1). The resultant thiol-saturated NBR had a conversion of around 80%. The resultant rubber was quite soluble in acetone. The solution was clear and homogeneous when it was taken out the reaction. The rubbers were still soluble after precipitation, drying and dissolution. However, the rubber would gel after staying in air or in vacuum for one hour. It is believed that the problem is caused by the residual active sites in the polymer and/or the initiator AIBN. FT-IR spectra show the presence of a carbonyl group, which suggests the interaction with oxygen during the degradation/crosslinking process. Addition of radical scavengers before precipitation (as an example, benzoquinone was tried) could not suppress the crosslinking process. Gel was still observed after the solution was kept in air for 8 hours.

Table 10-1: Thiol addition experiments

Rubber	Exp. No	[I] (mg/mL)	P_0 (psi)	t(hr)	Conversion
SBS	D-5	0.83	24.5	52	~100%
NBR	D-7	0.42	19.0	2.5	~5%
	D-7re	1.0	16.2	93	~60%
	D-12	1.0	23.8	77	~40%
	D-13	4.0	26.5	55	~40%
	D-14a	2.8	Large excess	50	~80%
	D-14b	3.3		50	~74%
	D-15a	3.0+3.0	Large excess	75	~80%
	D-15b	3.8+1.8		70	~80%
NBR latex[1]	D-8	49.0	32.5	33	~80%
NBR latex[2]	D-9	51.9	35	56	~10%
	D-10	51.6	40.7	73	~10%
	D-11	54.2	47	100	~10%

1: Thiol addition of fresh NBR latex;

2: Thiol addition of partially-saturated NBR latex. 83.0% of the *C*=*C*s inside the latex has been saturated by diimide before thiol addition.

10.2.3 : Thiol addition of diimide-partially-saturated NBR latex

In this experiment, the fresh NBR latex was hydrogenated to a certain degree of saturation and the resultant latex was further saturated by methanethiol. At the first step, a conventional diimide hydrogenation reaction was carried out. 100.0g NBR latex together with 1.3g boric acid and 12.6g hydrazine hydrate was kept at 40.0ºC. 24.0 mL hydrogen peroxide aqueous solution (1.25 times of *C*=*C*s) was added into the mixture over 7 hours. The final conversion was 83.0% by FT-IR. The

rubber was hardly soluble (can be dispersed, can't be dissolved). In the second step, 9.0g of the resultant NBR latex was mixed with 50.0ml water and 0.05g AIBN (recrystallized), and was kept at 50.0ºC in a degassed reactor under 35.0 psi of methanethiol atmosphere. The pressure dropped by 3.3 psi during the reaction. The reaction was terminated after 3000 minutes. The resultant thiol-saturated NBR had a conversion of around 91.0%. The resultant rubber is totally gelled.

The presence of air did not benefit the thiol addition reaction of partially diimide-saturated NBR latex. With (D-9 in Table 10-1) or without (D-10 in Table 10-1) air, the saturation of *trans*-*C=C* increased by ~10% in both cases upon the diimide-partially-saturated NBR latex. However, the presence of air might bring some side reactions to this system. With air, the resultant rubber had a green color; appearing like a degraded and crosslinked rubber; without air, the rubber had a very light green color, appearing like partially crosslinked rubber.

The extent of thiol addition was quite limited even if the reactants were kept under 50.0ºC for 6000 minutes (D-11 in Table 10-1).

10.2.4 : Analysis

Due to safety concerns over the use of methanethiol, this investigation has been suspended. However, this work has revealed that SBS can be totally saturated by thiol addition; NBR has not been fully saturated by thiol addition. What contributed to this difference in reaction activity between SBS and NBR is still not understood. The difficulty in the thiol addition of NBR may not be a reaction rate problem. The chain structure of NBR might contribute to this difficulty. The block copolymer SBS should have much lower glass transition temperature (T_g) for the butadiene block, which is actually polyethylene. See in Table 10-2. The T_g for polyethylene is much lower than NBR or HNBR. The chain movement in HNBR would be restrained. The presence of thiol suspending group makes the movement even more restrained. The limited motion of the thiol-added NBR backbone would make the reaction very difficult to proceed further. This factor may also contribute to the difficulty in raising conversion for the diimide process.

Table 10-2: Glass transition temperature of polymers

polymer	T_g(ºC)	Source
NBR (Kryn3850)	-27.67	Experiments in this lab
Hydrogenated NBR(96.6%) from Bayer latex	-29.01	
cis-polybutadiene	-102	Ref. 74
Trans-polybutadiene	-58	
Polyethylene	-125	

As for the future of thiol addition to diimide hydrogenation, both the positive part and the negative part have to be considered. The combination of diimide hydrogenation with thiol addition

would probably provide a novel route of saturating polymers in latex form. Difficulties still exist at optimizing the reaction conditions. However, the thiol addition is the result of the competition between several radical reactions. Radical reactions on rubbers would deteriorate the mechanical properties of the elastomer. The strong smell and toxicity of thiols also present a major problem.

10.3 : Recommendations

It has been mentioned in Chapter 9 that core-shell latex may be the solution to the problems encountered with the diimide system. The hydrogenation of the shell layer of NBR would be facilitated because of a reduction of diffusion distance. Therefore, **the synthesis of core-shell NBR latex with suitable core material and its hydrogenation is of interest for further research**. It has been mentioned in chapter 9 that the shell should be no more than 16nm in thickness. The core is only 17% of the total particle volume in this case when the particle diameter is still 72nm. It is expected that the blending in of the core material will not deteriorate the physical properties of this rubber.

Even it this work failed to find a radical scavenger for the gel formation during diimide hydrogenation, this direction is still worth thinking. It is expected that the special radical scavenger can be used in a large amount, probably in a gas form. It can scavenge a large amount of radicals.

On the other hand, compounding method and recipe research should emphasize on making use of HNBR with a certain level of gel content.

Appendix A

Nomenclature

- $a_0 = \frac{k_2}{k_3} \bullet \frac{V_p}{V_s}[C = C]_0$
- $b_0 = \frac{[H_2O_2]_0^{\ 2}}{2[H_2O_2]_0 + a_0}$
- BKF: a common antioxidants used in elastomers, 2,2' methylene-bis (4-methyl 6 tertiary butyl phenol)
- CN: Nitrile group
- C_{OL}: operation labor cost
- C_{RM}: raw material costs
- C_{UT}: utility cost
- C_{WT}: waste treatment cost
- diw: deionized water
- D: diameter of a particle
- Dorg: the diffusivity of diimide in NBR rubber
- DP: degree of polymerization
- EDTA: ethylenediaminetetraacetic acid
- f: the combining effect of catalyst concentration and hydrazine concentration upon the reaction between hydrazine and hydrogen peroxide
- FCI: fixed capital investment
- FT-IR: Fourier transform infrared spectrum
- HD: degree of hydrogenation, also the conversion of C_4H_6 unit in NBR to C_4H_8
- HE: hydrogenation efficiency, to measure the portion of hydrogen peroxide used for the purpose of polymer hydrogenation
- HE_{aqu} : hydrogenation efficiency in the aqueous phase of NBR latex, used to evaluate the effect of the side reactions in the aqueous phase and at the interface upon hydrogenation efficiency

- HE_{org} : hydrogenation efficiency in the organic phase of NBR latex, used to evaluate the effect of the side reactions in the organic phase upon hydrogenation efficiency
- HNBR: hydrogenated acrylonitrile-butadiene rubber
- k_1: rate constant for r_1
- k_2: rate constant for r_2
- k_3: rate constant for r_3
- $k_{4:}$ rate constant for r_4
- k_m: The apparent rate constant of the reaction between hydrazine and hydrogen peroxide, which includes rate constant, the effects of catalyst and hydrazine concentration
- k_{trans}: the rate constant for the reaction between *trans* *C*=*C* and diimide
- k_{vinyl}: the rate constant for the reaction between vinyl *C*=*C* and diimide
- M: concentration unit, mole/liter
- MCB: chlorobenzene
- N: the total number of NBR particles in the reaction medium
- NBR: acrylonitrile-butadiene rubber
- n_{N2}: the amount of nitrogen produced from a reaction by mole at time t
- n_{N2T}: the total amount of nitrogen produced from a reaction by mole
- P: pressure
- PBD: polybutadiene
- P_{N2}: the pressure of nitrogen at time t;
- P_{N2T}: the highest pressure of nitrogen reached by a reaction
- *p*-TSH: *p*-toluenesulfonylhydrizide
- R: the average radius of latex particles
- RDB: residual double bond content
- r_1: reaction rate for the reaction between hydrazine and hydrogen peroxide
- r_2: reaction rate for the reaction of diimide with *C*=*C*
- r_3: reaction rate for the reaction between hydrogen peroxide with diimide
- r_4: reaction rate for the disproportionation of diimide

- r_{H2O2de}: reaction rate of hydrogen peroxide decomposition
- $r_{N2H4de:}$ reaction rate of hydrazine decomposition
- r_{redox}: reaction rate of the reaction between hydrazine and hydrogen peroxide in aqueous solution
- SBR: poly(styrene-co-butadiene)
- SBS: styrene-butadiene-styrene block copolymer
- SDS: a common anionic surfactant, Sodium n-dodecyl sulfate
- Subscript:
    - 0: the value at t=0
    - t: the value at time point "t"
- $t_{1/2}$: half time of a first-order reaction with respect to a reactant
- t: time
- T: temperature
- Tg: glass transition temperature
- Va: total volume of the aqueous phase in which hydrogen peroxide and hydrazine distribute
- V_p: total volume of rubber phase in the latex
- V_s: total volume of the interface which is the location for interfacial reactions
- wt%: weight percentage of a component in a mixture
- ΔT: the temperature difference for a water-cooling device

Appendix B

Matlab program-simulation of a semibatch hydrogenation process with the assumption of reaction control

```
function semibatch

%simulation of a semibatch hydrogenation process with the assumption of
%reaction control;
%100ml of NBR latex, 15.0% solid content;
%17.4 hydrazine hydrate (2.0 times of C=C), 1.3 g of boric acid;
%29.6g of hydrogen peroxide aqueous solution (30.0%) added over a period of
%10 hours;

global k1f k2 k3 k4 Vp Vs
%
%given values for the parameters;
%
k1f=0.5;
k2=0.1;
k3=20;
k4=20;
Vs=0.0015;
Vp=0.015;
Tspan=linspace(0,36000,100);
%
%ODE solver
%
[t,y]=ode45(@reactioncontrolfun, Tspan, [11.6 0 0]);
doubleC= y(:,1);
diimide=y(:,2);
peroxide=y(:,3);
HD=1-doubleC/11.6;
for j=1:100,
```

```
    R1(j)=k1f*peroxide(j);
    R2(j)=k2*doubleC(j)*diimide(j);
    R3(j)=k3*peroxide(j)*diimide(j);
    R4(j)=k4*diimide(j)*diimide(j);
    HEaqu(j)=1-2*R3(j)/(R1(j)+2*R3(j));
    HEorg(j)=R2(j)/(R2(j)+R4(j));
end
%
figure (1)
subplot(3,2,1); plot(t,HD)
hold on;
plot (t,7.25e-6*t/0.174)
ylabel('HD')
subplot(3,2,2); plot(t,doubleC)
ylabel('doubleC')
subplot(3,2,3); plot(t,diimide)
ylabel('diimide')
subplot(3,2,4); plot(t,peroxide)
ylabel('peroxide')
subplot(3,2,5); plot(t,HEaqu)
ylabel('HEaqu')
subplot(3,2,6); plot(t,HEorg)
ylabel('HEorg')
%
%define input functions
%
function dy=reactioncontrolfun(t,y)

global k1f k2 k3 k4 Vp Vs

dy=zeros (3,1);

r1=k1f*y(3);
r2=k2*y(1)*y(2);
```

```
r3=k3*y(3)*y(2);
r4=k4*y(2)*y(2);

dy(1)=-r2;
dy(2)=(r1-r3)*Vs/Vp-r2-2*r4;
dy(3)=(7.25E-06-Vs*(r1+r3)-7.47E-7*y(3))/(0.117+7.47E-7*t);
```

Appendix C

Matlab program-Simulation of the diimide hydrogenation of NBR latex

```
function lin1
%
%constant and input data
%
global R D k1f H2O2 k2 k3 k4 Vs Vp ST C0 tT
R=36*10^(-8);
D=5*10^(-11);
k1f=0.5;
H2O2=0.01;
k2=2000;
k3=400000;
k4=16E9;
ST=3/R*15E-3;
Vs=0.0015;
Vp=0.015;
C0=11.6;
tT=10*3600;
%
%time and space spans
%
m=2;
r=linspace(0,R,100);
t=linspace(0,tT,100);
%
%PDE solver
%
sol=pdepe(m, @lin1pdefun, @lin1ic, @lin1bc, r, t);
diimide=sol(:,:,1);
doubleC=sol(:,:,2);
doubleCend=sol(100,:,2);
diimideR=sol(:,100,1);
doubleCR=sol(:,100,2);
%
for j=1:100,
   HD(j)=1-3/(R^3)/C0*trapz(r,(r.^2).*sol(j,:,2));
end
HD(50)
HD(100)

HEa=1-k3*diimideR./(k2*diimideR+k1f);
```

```
for j=1:100,
   HEo(j)=1/R*trapz(r,k2*sol(j,:,2)./(k2*sol(j,:,2)+k4*sol(j,:,1)));
   Crosslink(j)=trapz(r,sol(j,:,1).^2)*10^22;
end


HE=HEa'.*HEo;
%
figure (1)
subplot(2,2,1); plot(t,HD)
xlabel('t')
ylabel('HD')
hold on;
plot (t,k1f*Vs*H2O2/C0/Vp*t)
hold off;
subplot(2,2,2); plot(t,HEa)
xlabel('t')
ylabel('HEaqu')
subplot(2,2,3); plot(t,HEo)
xlabel('t')
ylabel('HEorg')
subplot(2,2,4); plot(t,HE)
xlabel('t')
ylabel('HE')


figure(2)
subplot(2,2,1); plot(t,Crosslink)
xlabel('t')
ylabel('crosslinks')
subplot(2,2,2); plot(t,diimideR)
xlabel('t')
ylabel('diimidemax')
subplot(2,2,3);plot(r,sol(:,100,1))
xlabel('r')
ylabel('[diimide]end')
subplot(2,2,4); plot(r,sol(:,100,2))
xlabel('r')
ylabel('[C=C]end')
   %
%output
%
figure (3)
surf(r,t,u1)
title('diimide')
```

```
xlabel('r')
ylabel('t')
%
figure (4)
surf(r,t,u2)
title('double bond')
xlabel('r')
ylabel('t')
%
%define input functions
%
function [c,f,s]=lin1pdefun(r,t,u,dudr)
global R D k1f H2O2 k2 k3 k4 Vs Vp ST C0 tT
c=[1 1]';
f=[D 0]'.*dudr;
s=[-k2*u(1)*u(2)-2*k4*u(1)^2 -k2*u(1)*u(2)]';
%
function u0=lin1ic(r)
global R D k1f H2O2 k2 k3 k4 Vs ST C0 tT
u0=[0 C0]';
%
function [pl, ql, pr, qr]=lin1bc(rl,ul,rr,ur,t)
global R D k1f H2O2 k2 k3 k4 Vs Vp ST C0 tT
pr=[k1f*H2O2-k3*ul(1)*H2O2 0]';
qr=[-ST/Vs 1]';
pl=[0 0]';
ql=[1/D 1]';
```

Appendix D
Comparison of manufacturing costs of two hydrogenation processes

The cost analysis is based on the method provided in Reference [60]. Data from this reference, when suitable, were also used in this analysis.

D.1: Homogeneous solution hydrogenation process

D.1.1: Process description

This homogeneous solution hydrogenation process is designed to manufacture 2000 tons of HNBR annually. Specially designed NBR latex is used as the feed stock for this process. This NBR latex is synthesized by low-temperature emulsion polymerization technology with a relatively lower conversion of monomers and a lower average molecular weight of polymer when compared with conventional NBR latex. The designed solid content is 15.0%.

The overall process for hydrogenation in solution includes five units.

1) Latex coagulation. NBR latex is coagulated by adding sulfuric acid to lower the pH value below 3.0. A 3 m^3 horizontal reactor with agitation is used to conduct this operation. The resultant slurry is fed into a dewatering extruder followed by a drying extruder. Dried NBR is formed into bales beyond the drying extruder die. This coagulation process breaks down NBR from latex at the rate of 1.67 ton/h. NBR rubber is recovered at the rate of 0.25 ton/h.

2) Dissolution. NBR bales are dissolved into chlorobenzene to prepare a homogeneous solution for hydrogenation. This step is a batch-mode operation. Two 30 m^3 reactors with agitation are used to conduct this operation. The dissolution operation takes twelve hours for one batch; the discharge of NBR solution takes twelve hours also.

3) Hydrogenation. Two reactors with the volume of 10 m^3 each are used for hydrogenation. Heat removal and gas-liquid contact are the two major concerns for the design of these reactors. Hydrogen is used as the drive gas for discharging the hydrogenated solution. One batch of hydrogenation takes four hours including loading reactant, reaction and discharge. The hydrogenated solution is charged into a reactor, in which the rhodium catalyst will be ionized to facilitate catalyst separation.

4) Catalyst recovery. An anion exchanger column is used to separate the ionic rhodium complex from the organic solution. Rhodium is then recovered by washed fully-loaded column using NaCl aqueous solution.

5) Solvent stripping. MCB is stripped using a flash vaporization followed by a falling-film devolatilization process. The major part of MCB is recovered by the flash vaporization process. MCB is condensed for reuse. HNBR is formed and packaged. (An alternative method would use ethanol to precipitate HNBR out of chlorobenzene. The ratio of ethanol: chlorobenzene =5:1. The solvent mixture can then be separated using a distillation column.)

The process flow diagram and the flow summary are provided in the following sections.

D.1.2: Estimating manufacturing costs

The manufacturing costs are estimated item by item as shown below.

Table D- 1: Calculation of raw materials costs (C_{RM}) of the solution hydrogenation process

C_{RM}*(#1)	Chemical	Flow rate (ton/year)	Unit cost** ($/ton)	Cost ($/year)
Raw materials	NBR latex	1.33×10^4	325	4.33×10^6
	MCB	11.4	1000	1.14×10^4
	Rh	4120g	38.7 $/g	1.59×10^5
	PPh_3	0.524	84000	4.40×10^4
	H_2	75.2	11000	8.27×10^5
	diw	2000	1.0	2.00×10^3
	Aqu H_2SO_4	264	6.0	1.58×10^3
	Catalyst regeneration	185kg	200$/kg	3.70×10^4
Total				5.37×10^6

*Calculation of C_{RM} (Homogeneous hydrogenation): 1.0% of MCB is consumed by the process; 20.0% of Rhodium and 100% of PPh_3 is left inside the product. The regeneration of Wilkinson's catalyst costs $200/kg.

** Because of the lack of an authoritative data source, such as *Chemical Marketing Reporter*, the prices provided are the averaged results based on internet information.

The datum $ 41/1000 m^3 is used to estimate waste water treatment cost (C_{WT}).

Table D- 2: Estimation of C_{UT} (The cost of electricity is $0.06/kwh, the heater efficiency is 90%) of the solution hydrogenation process

C_{UT}*(#1)	Item	consumption (kJ/year)	Unit cost** ($/kJ)	Cost ($/year)
Electricity-heating	NBR*	7.82×10^{8}	1.67×10^{-5}	1.31×10^{4}
	MCB**	1.87×10^{9}	1.67×10^{-5}	3.12×10^{4}
Electricity-agitation		1.44×10^{10}	1.67×10^{-5}	2.40×10^{5}
Cooling water***	NBR	1.03×10^{9}	1.58×10^{-4}	1.63×10^{5}
	MCB	1.70×10^{9}	1.58×10^{-4}	2.69×10^{5}
Total				7.16×10^{5}

*NBR, HNBR: Cp: 2.01J/g/K (25ºC, 1atm);

**MCB: t_b: 131.71 ºC (1atm); density: 1.1058 g/ml (20ºC); vaporization enthalpy: 35.19 kJ/mol (t_b), 40.97 kJ/mol (25ºC); Cp: 150.1J/mol/K (25ºC, 1atm).

***: Cooling water: Based on ΔT=10ºC; cost of cooling water: $6.62/ton

Table D- 3: Calculation of operation labor cost (C_{OL}) of the solution hydrogenation process

Equipment Type	Number of Equipment	Operators per shift per equipment	Operators per shift
compressor	1	0.15	0.15
Exchanger	1	0.10	0.10
Heater	1	0.50	0.50
Reactor	7	0.50	3.50
Tower	2	0.35	0.70
Extruder	1	1.0	1.0
Total			5.95

C_{OL} =4.5×6.0×$46800=$1.26\times10^{6}$ $/year

Fixed capital investment (FCI) is estimated based on the data of Bayer's HNBR facility in Germany. The capacity is 3000 tons/year; the FCI is $70 million.

FCI=$70 million × $(3000/2000)^{0.7}$ = $52.7 million

Table D- 4: Estimating manufacturing cost- Solution hydrogenation process

Cost Item	Cost estimate	Calculation guideline
1. Direct manufacturing costs		
A: Raw materials	5.37×10^6	C_{RM}
B: Waste treatment	558	C_{WT}
C: Utilities	7.16×10^5	C_{UT}
D: Operating labor	1.26×10^6	C_{OL}
E: Direct supervisory and clerical labor	2.27×10^5	$0.18C_{OL}$
F: Maintenance and repairs	3.16×10^6	0.06FCI
G: Operating supplies	4.74×10^5	0.009FCI
H: Laboratory charges	1.90×10^5	$0.15C_{OL}$
I: Patents and Royalties	0	
Total Direct manufacturing costs	1.13×10^7	
2. Fixed manufacturing costs	Cost estimate	Calculation guideline
A: Depreciation	5.27×10^6	0.1FCI
B: Local Taxed and Insurance	1.58×10^6	0.03FCI
C: Plant overhead costs	2.78×10^6	$0.708C_{OL}$+0.036FCI
Total Fixed manufacturing costs	9.63×10^6	
3. General manufacturing expenses	Cost estimate	Calculation guideline
A: Administration costs	6.97×10^5	$0.177C_{OL}$+0.009FCI
B: Distribution and selling costs	2.95×10^6	0.11COM
C: R & D	1.34×10^6	0.05COM
Total General manufacturing costs	4.99×10^6	
TOTAL COSTS	2.60×10^7	$C_{RM}+C_{WT}+C_{UT}+2.215C_{OL}$ +0.19COM+0.246FCI

D.2: Diimide hydrogenation process

D.2.1: Process description

1) Hydrogenation. NBR latex (solid content: 15.0%), together with hydrazine and catalyst, is added into a reactor with a volume of 30 m^3. 80.0% wt of aqueous solution of hydrazine is used for hydrazine. Hydrogen peroxide aqueous solution (30.0%) is added continuously for 9 hours. After reacting for one more hour, the content is discharged into a storage tank.

2) Latex coagulation. The latex coagulation step is the same as that for the homogeneous hydrogenation process.

3) Hydrazine removal. When HNBR latex is used as the product, hydrazine must be removed. Ozone may be used to react with the residual hydrazine.

The process flow diagram and the flow summary are provided in the following sections.

D.2.2: Estimating manufacturing costs

Table D- 5: Calculation of raw materials costs (C_{RM}) of the diimide hydrogenation process

C_{RM}(#2)	Chemical	Flow rate (ton/year)	Unit cost ($/ton)	Cost ($/year)
Raw materials	NBR latex	1.33×10^{4}	325	4.32×10^{6}
	N_2H_4(80%)	1813	1500	2.72×10^{6}
	H_2O_2(30%)	7133	200	1.43×10^{6}
	H_3BO_3	200	600	1.20×10^{5}
	diw	2000	1.0	2.00×10^{3}
	Aq. H_2SO_4	264	6.0	1.58×10^{3}
Total				8.59×10^{6}

The operation labor cost is calculated as

C_{OL} =4.5×2.0×$46800=$4.21\times10^{5}$ $/year

The FCI is estimated to be 3 million at the maximum.

Table D- 6: Estimation of utility costs (C_{UT}) of the diimide hydrogenation process

C_{UT} (#2)	Item	Consumption (kJ/year)	Unit cost** ($/kJ)	Cost ($/year)
Electricity-heating	NBR	3.82×10^{8}	1.67×10^{-5}	6.38×10^{3}
Electricity-agitation		1.44×10^{9}	1.67×10^{-5}	2.40×10^{4}
Cooling water	NBR	4.8×10^{8}	1.58×10^{-4}	7.58×10^{4}
Total				1.06×10^{5}

Table D- 7: Estimating manufacturing cost- diimide hydrogenation process

Cost Item	Cost estimate	Calculation guideline
1. Direct manufacturing costs		
A: Raw materials	8.59×10^6	C_{RM}
B: Waste treatment	768	C_{WT}
C: Utilities	1.06×10^5	C_{UT}
D: Operating labor	4.21×10^5	C_{OL}
E: Direct supervisory and clerical labor	7.58×10^4	$0.18C_{OL}$
F: Maintenance and repairs	1.80×10^5	0.06FCI
G: Operating supplies	2.70×10^4	0.009FCI
H: Laboratory charges	6.32×10^4	$0.15C_{OL}$
I: Patents and Royalties	3.83×10^5	0.03COM
Total Direct manufacturing costs	9.85×10^6	
2. Fixed manufacturing costs		
A: Depreciation	3.00×10^5	0.1FCI
B: Local Taxed and Insurance	9.0×10^4	0.03FCI
C: Plant overhead costs	4.06×10^5	$0.708C_{OL}+0.036$FCI
Total Fixed manufacturing costs	7.96×10^5	
3. General manufacturing expenses		
A: Administration costs	1.02×10^5	$0.177C_{OL}+0.009$FCI
B: Distribution and selling costs	2.95×10^6	0.23COM
C: R & D	6.38×10^5	0.05COM
Total General manufacturing costs	3.69×10^6	
TOTAL COSTS	1.43×10^7	$C_{RM}+C_{WT}+C_{UT}+2.215C_{OL}+0.19COM+0.246$FCI

D.3: Comparison

Table D- 8: Comparison of manufacturing costs of the two processes

Cost Item	Solution process	Diimide process
1. Direct manufacturing costs	1.13×10^7	9.85×10^6
2. Fixed manufacturing costs	9.63×10^6	7.96×10^5
3. General manufacturing expenses	4.99×10^6	3.69×10^6
TOTAL COSTS	2.60×10^7	1.43×10^7

It is clearly demonstrated the diimide process has much lower FCI (3 million versus 52.7 million for the 2000 ton/year plant). The cost for every item listed above is lower for the diimide process. The much higher operation costs (Operating labor, Maintenance and repairs) give rise to higher direct manufacturing costs for the solution process; the much higher FCI gives rise to the much

higher fixed manufacturing costs. The total cost of the diimide hydrogenation process is only 55% of that of the solution hydrogenation process.

This comparison of total manufacturing costs shows the diimide process is quite attractive when economics are considered even if the costs for raw materials are higher than that of the solution process. If the gel problem can be solved, the diimide process will have a promising future.

D.4: Process flow diagrams of the two processes

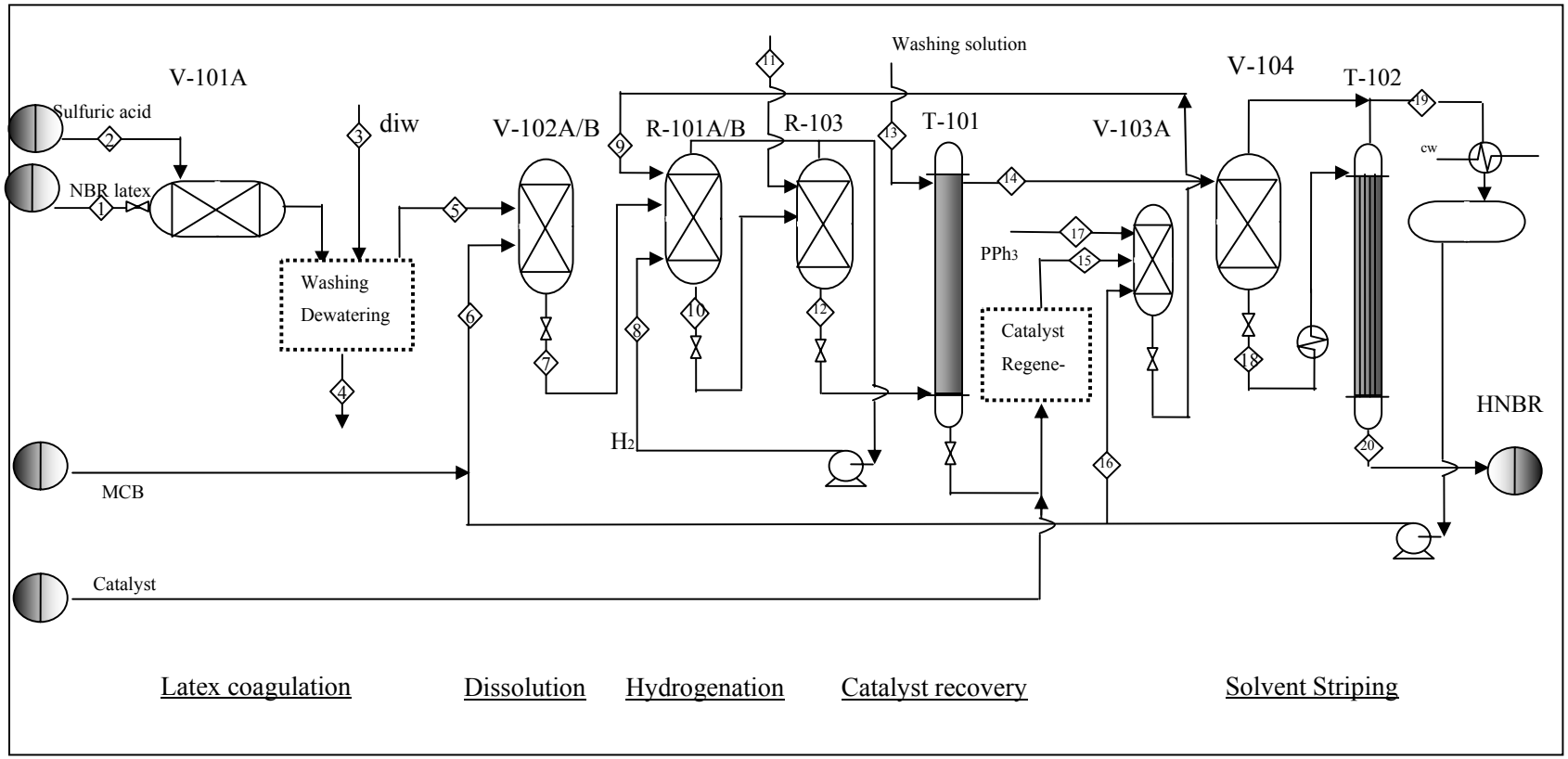

Figure D-1: PFD of the solution hydrogenation process

Table D- 9: Flow summary table for the solution hydrogenation process

#	Operation mode	Tempe-rature (ºC)	Press-ure (psi)	Vapor frac-tion	Mass flow (ton/h)	Component mole flow (kmol/h)							
						Water	NBR	HNBR	H_2	MCB	Rh catalyst	PPh_3	others
1	Continuous	25		0	1.67	78.7	4.7						
2	Continuous	25		0	0.033	1.8							Sulfuric acid: 0.002
3	Continuous	25	high	0	0.25	13.9							
4	Continuous			0	1.70	94.4							
5	Batch 1/12			0	3.0		56.6						
6	Batch 1/12	120	70	0	15.3					137			
7	Batch 0.5/4	130	70	0	12.2		37.7			91.1			
8	Continuous		1500	1	0.006		2.9						
9	Batch 0.5/4			0	1.13					10.1	2e-4	2e-3	
10	Batch 0.5/4			0	13.3			37.8		101.2	2e-4	2e-3	
12	Continuous	130		0	1.67			4.7		12.6	2.5e-5	2.5e-4	
14	Continuous	130		0	1.67			4.7		12.6	5e-6	2.5e-4	
18													
19	Continuous	120		0	1.42					12.6			
20	Continuous			0	0.25			4.7			5e-6	2.5e-4	

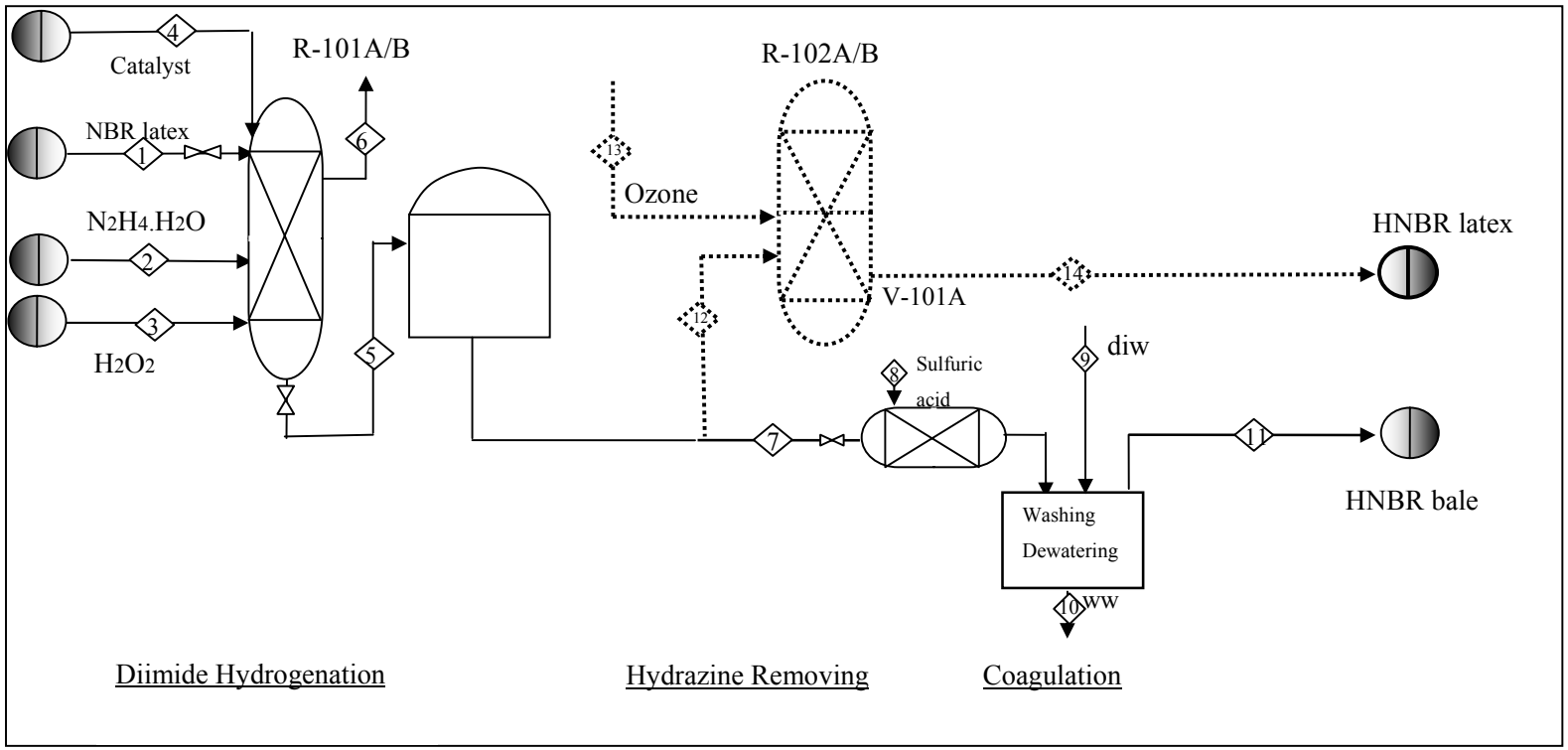

Figure D-2: PFD of the diimide hydrogenation process

Table D- 10: Flow summary table for the diimide hydrogenation process

#	Operation mode	T (°C)	P (psi)	g*	Mass flow (ton/h)	Component mole flow (kmol/h)							
						Water	NBR	HNBR	N_2H_4	N_2	H_2O_2	H_3BO_3	others
1	Batch 1/12	25		0	20.0	944.4	56.6						
2	Batch 1/12	25		0	2.72	30.2			67.9				
3	Semi-Batch 10/12	25		0	1.07	41.6					9.43		
4	Batch1/12	25		0	0.3							4.84	
5	Batch 1/12	40		0	30.72	1518.4	5.66	50.94				4.84	
6	Semi-batch 10/12	40		1	0.19					6.79			
7	Continuous	40		0	2.56	126.5	0.47	4.23					
8	Continuous	25		0	0.033	1.8							Sulfuric acid: 0.002
9	Continuous	25	high	0	0.25	13.9							
10	Continuous			0	2.34	128.3							
11	Continuous						0.47	4.23					
12													
13													
14													

* g: vapor fraction

Bibliography

1. General search of commercial products from internet
2. Manual for the rubber industry, 2nd addition, Bayer Inc.
3. Parent, J. Scott; McManus, Neil T.; Rempel, Garry L. , Journal of Applied Polymer Science, v 79, n 9, Feb, 2001, p 1618-1626
4. Mohammadi, N.A.; Rempel, G.L.; Journal of Molecular Catalysis, v 50, n 3, Apr 6, 1989, p 259-275
5. Guo, X.-Y.; Rempel, G.L.; Journal of Applied Polymer Science, v 65, n 4, Jul 25, 1997, p 667-675
6. Parent, J. Scott; McManus, Neil T.; Rempel, Garry L. , Industrial & Engineering Chemistry Research, v 37, n 11, Nov, 1998, p 4253-4261
7. Parent, J. Scott; McManus, Neil T.; Rempel, Garry L.; Industrial & Engineering Chemistry Research, v 35, n 12, Dec, 1996, p 4417-4423
8. Guo, Xiangyao; Rempel, G.L.; Journal of Molecular Catalysis, v 63, n 3, Dec 15, 1990, p 279-298S.
9. Bhattacharjee, Susmita; Rajagopalan, Padmavathy; Bhowmick, Anil K.; Avasthi, Bhola Nath; Journal of Applied Polymer Science, v 49, n 11, Sep 15, 1993, p 1971-1977
10. Rempel, Garry L.; American Chemical Society, Polymer Preprints, Division of Polymer Chemistry, v 41, n 2, Aug, 2000, p 1507-1508
11. Guo, X.-Y.; Rempel, G.L. ; Journal of Applied Polymer Science, v 65, n 4, Jul 25, 1997, p 667-675
12. Kubo, Y. ; International Chemical Engineering, v 33, n 1, Jan, 1993, p 113-123
13. Singh, U.K.; Vannice, M.A.; Applied Catalysis A: General, v 213, n 1, May 14, 2001, p 1-24
14. Guo, Xiangyao; Scott, P.J.; Rempel, G.L.; Journal of Molecular Catalysis, v 72, n 2, Mar 1, 1992, p 193-208
15. Chang, Jen-Ray; Huang, Shi-Ming; Industrial & Engineering Chemistry Research, v 37, 1998, p 1220-1227; Bhattacharjee, Susmita; Rajagopalan, Padmavathy; Journal of Applied Polymer Science, v 49, 1993, p 1971-1977
16. Basic Elastomer Technology, Chapter 10, Edited by Krishna C. Baranwal and Howard L. Stephens (1st edition).

17. Xinwang Lin, G. L. Rempel, Internal Report on Biphasic Catalysis, University of Waterloo, Feb. 2002

18. Lawson G. Wideman, United States Patent 4,452,950 (1984), assigned to The Goodyear Tire & Rubber Company (Akron, OH)

19. Hunig, S.; Muller, H.R.; Thier, W.; Angew. Chem. Int. Ed. Engl, v 4, n 4, 1965, p 271-280

20. Tamelen,E.E. Van; Dewey, R.S.; Lease, M.F.; Pirkle, W.H.; J. Am. Chem. Soc., v 83, 1961, p 4302

21. Sellmann, Dieter; Brandl, Alfred; Endell, Ralf; Angew. Chem. Intern. Ed. Engl, v 12, n 12, 1973, 1019

22. Hahn, Stephen, F. ; Journal of Polymer Science, Part A: Polymer Chemistry, v 30, n 3, Mar 15, 1992, p 397-408

23. Dewey, R. S.; Tamelen, E. E. van; J. Am. Chem. Soc.; v 83, n 17, 1961, p 3729-3729

24. Gangadhar, A.; Chandrasekhara Rao, T.; Subbarao, R.; Lakshminarayana, G. ; Journal of the American Oil Chemists' Society, v 66, n 10, Oct, 1989, p 1507-1508

25. Pasto, Daniel J.; Chipman, Daniel M.; Journal of the American Chemical Society, v 101, n 9, Apr 25, 1979, p 2290-2296

26. Garbisch, Edgar W.; Schildcrout, Jr. Steven M.; B. Patterson, Dennis; Sprecher; Carol M.; J. Am. Chem. Soc.v 87, n 13, 1965, p 2932-2944

27. Ratnayake, W. M. N.; Grossert, J.S.; Aclman, R.G.; JAOCS, v 67, 1990, p 940-946

28. Mango, L.A.; Lenz, R.W.; Die Makromolekulare chemie v 163,1973, p 13-36

29. Harwood, E. James; B. Russell, David; J. A. Verthe, John; Zymonas, Joseph; Die Makromolekulare chemie v 163, 1973, p 1-12

30. Tran Dai Nang; Katabe, Yasuo; Minoura, Yuji; Polymer, v 17, n 2, Feb, 1976, p 117-120

31. Parker, Dane K.; Roberts, Robert F.; Schiessl, Henry W. Rubber Chemistry and Technology, v 67, n 2, May-Jun, 1994, p 288-298

32. Schiessl; Henry W.; Migliaro, Jr.; Francis W., United States Patent 5,057,601 (1991), assigned to Olin Corporation (Cheshire, CT)

33. Belt; Johannes W.; Vermeulen; Jacobus A. A.; Kostermann; Mike, United States Patent 6,521,694 (2003) , WO 00/09576 (2000), United States Patent 6,552,132 (2003), WO 00/09568 (2004); Assigned to DSM N.V. (Heerlen, NL)

34. Zhang, Jie; Zhou, Shuqin; Yao, Ming, Hecheng Xiangjiao Gongye/China Synthetic Rubber Industry, v 26, n 2, March, 2003, p 78-80

35. Wang, Jianguo; Zhou, Shuqin; Zhang, Jie, Hecheng Xiangjiao Gongye/China Synthetic Rubber Industry, v 26, n 3, May, 2003, p 141-143; China Patent CN 1472232A

36. He, Y.; Daniels, E.S.; Klein, A.; El-Aasser, M.S. Journal of Applied Polymer Science, v 64, n 10, Jun 6, 1997, p 2047-2056

37. Xie, H.-Q.; Li, X.-D.; Liu, X.-Y.; Guo, J.-S. Journal of Applied Polymer Science, v 83, n 6, Feb 7, 2002, p 1375-1384

38. De Sarkar, M.; De, P.P.; Bhowmick, A.K. Polymer, v 41, n 3, Nov, 2000, p 907-915; De Sarkar, Mousumi; De, Prajna P.; Bhowmick, Anil K. Journal of Applied Polymer Science, v 66, n 6, Nov 7, 1997, p 1151-1162

39. Li, Xiaodong; Xie, Hongquan , Hecheng Xiangjiao Gongye/China Synthetic Rubber Industry, v 25, n 5, September, 2002, p 282-285

40. Parker, Dane K., Annual Technical Conference - ANTEC, Conference Proceedings, v 3, 1995, p 4083-4087

41. Parker; Dane K.; Ruthenburg; David M. United States Patent 5,442,009 (1995), assigned to The Goodyear Tire & Rubber Company (Akron, OH)

42. Belt; Johannes W.; Driessen, Marcus M.; WO 01/55223 A1 (2001), assigned to DSM N.V. (Heerlen, NL)

43. S. Zhou, H. Bai, J. Wang, Journal of Applied Polymer Science, v 91, n 4, Feb. 2004, p 2072–2078

44. Q. Pan, G. L. Rempel, Macromolecular Rapid Communications, v 25, n 8, April 2004, p 843-847

45. Tachiev, G.; Roth, J.A.; Bowers, A.R.; International Journal of Chemical Kinetics, v 32, n 1, Jan, 2000, p 24-35

46. Lin, Xinwang; Pan, Qinmin; Rempel, Garry L. Applied Catalysis A: General, v 276, n 1-2, Nov 25, 2004, p 123-128

47. H. Erlenmeyer, C. Flierl, H. Sigel, J. Am. Chem. Soc.; v 91, n 5, 1968, p 1065–1071

48. P. Graham, Donald; J. Am. Chem. Soc.; v 52, n 8, 1930, p 3035-3045

49. Sigel, Helmut; Flierl, Claus; Griesser, Rolf; J. Am. Chem. Soc.; v 91, n 5, 1969, p 1061-1064

50. Sigel, Helmut; Wyss, Kurt; Fischer, Beda E.; Prijs, Bernhard; Inorg. Chem.; v 18, n 5, 1979, p 1354-1358

51. Schmidt, Eckart W.; Hydrazine and its derivatives : preparation, properties, applications, Wiley-Interscience, New York, 2001

52. Donald T. Sawyer, Coord. Chem. Rev., v165, 1997, p 297-313

53. Higginson, W. C. E., D. Sutton, P. Wright, Journal of the chemical society. v 1953, 1953, p 1380-1386

54. Lin, Xingwang; Pan, Qinmin; Rempel, Garry L. Applied Catalysis A: General, v 263, n 1, May 28, 2004, p 27-32

55. E. J. Corey, D. J. Pasto, W. L. Mock; J. Am. Chem. Soc.; v 83, n 13, 1961, p 2957-2958

56. E. E. Van Tamelen, R. S. Dewey, M. F. Lease, W. H. Pirkle; Am. Chem. Soc.; v 83, n 20, 1961, p 4302-4302

57. Haber, F. ; Weiss, J.; Proc. R. Soc A, 1934, 147, 332

58. Daniel J. Pasto, J. Am. Chem. Soc.; v 101, n 23, 1979, p 6852-6857

59. Hans R. Kricheldorf, Handbook of polymer synthesis, edited by Hans R. Kricheldorf. New York; Marcel Dekker, 1992.

60. H. Scott Fogler, Elements of Chemical Reaction Engineering, Second edition. 1999

61. Richard Turton, Richard C. Ballie, Wallace B. Whiting and Joseph A. Shaeiwitz; Analysis, synthesis, and design of chemical process" 1998, published by Prentice Hall PTR

62. Technical information bulletin about Therban (Lanxess Global), website: Http: // www.therban.com

63. Belt; Johannes W.; Aagaard; Olav M., USP 6,756,451 (2004), assigned to DSM IP Assets B.V.

64. James E. Mark, Burak Erman, Frederick R. Eirich, Science and Technology of rubber, 2nd edition, published by Academic Press, 1994

65. Technical information about antioxidants from Ciba Chemical's Antioxidants Centre. Website: http://www.specialchem4polymers.com

66. Chemical reactions of polymers, edited by E. M. Fettes, Interscience Publishers, 1964;

67. Pierson, R.M.; Gibbs, W.E.; Meyer, G.E.; Naples, F. J.; Rubber Chemistry and Technology, v 31, 1958, p 213-242;

68. Serniuk, G.E.; Banes, F.W.; and Swaney, M.W.; J. Am. Chem. Soc. v70, n 5, 1948, p 1804-1808;

69. Kharasch, M.S.; Nudenberg, W.; and Mantell, G. J.; Journal of Organic chemistry, v 16, n 4, 1951, p 524-532

70. Hubbard, K. Lise; Finch, James A.; Darling, Graham D.; Reaction & functional polymers, v40, 1999, p 61-90

71. Romani, Francesco; Passaglic, Elisa; Aglietto, Mauro; Ruggeri, Giacomo; Macromol. Chem. Phys.; v 200, 1999, p 524-530

72. Boileau, Sylvie; Mazeaud-Henri, Brigitte, Blackborow, Richard; European polymer journal, v 39, 2003, p 1395-1404

73. Anton, P.; Laschewsky, A.; Europhen polymer journal, v 31, n 4, 1995, p 387-394

74. F. Schapman, F.; Couvercelle, J.P.; Bunel, C.; Polymer, v 39, n 20, 1998, p 4955-4962

75. CRC handbook of chemistry and physics, 85 edition, 2004-2005, published by CRC Press